2014

# Conducting polymer nanowires for multi-analyte chemiresistive sensing

Edward Song
*Louisiana State University and Agricultural and Mechanical College*

# CONDUCTING POLYMER NANOWIRES FOR MULTI-ANALYTE CHEMIRESISTIVE SENSING

A Dissertation

Submitted to the Graduate Faculty of the
Louisiana State University and
Agricultural and Mechanical College
in partial fulfillment of the
requirements for the degree of
Doctor of Philosophy

in

The School of Electrical Engineering and Computer Science

by
Edward Song
B.Sc., Queen's University, Canada, 2004
M.Sc., University of Alberta, Canada, 2007
August 2014

# Acknowledgements

First, I would like to express my deep appreciation to my advisor Dr. Jin-Woo Choi for his guidance and suggestions throughout the course of this research work. I am very grateful to have him as a mentor, and his professionalism in teaching and research is very much appreciated.

I would also like to thank my committee members Dr. Sunggook Park, Dr. Robin McCarley, Dr. Georgios Veronis, Dr. Kidong Park, and Dr. Peter Kelle for taking their time and effort to review my work and to provide positive feedback and suggestions that have greatly improved the quality of my work.

I would like to extend my appreciation to the cleanroom staff members at the Center for Advanced Materials and Devices for their assistance in microfabrication and SEM imaging.

I wish to give my special thanks to my friends and colleagues: Chao-Xuan Liu, Jeonghwan Kim, Kyung-Nam Kang, Junseo Choi, and the members of the BioMEMS and Bioelectronics Lab for many helpful discussions about the research work and for making my time at LSU more memorable.

Finally, I am grateful to have such a wonderful family: my grandmother, mom, dad, my brother and sister-in-law, and my fiancé Hana for their endless prayer and support. I would not be where I am today without them, and for that, I dedicate this thesis to my family.

# Table of Contents

# List of Tables

# List of Figures

# Abstract

A conducting polymer nanowire-based chemiresistive sensor array was developed for the liquid-phase multi-analyte detection. The ability to distinguish and quantify multiple chemical species with a single sensory device can be useful in many areas including food industry, pollution control, biosensors, and explosives detection. A polyaniline nanowire is a good candidate for use as a chemiresistive sensing material due to its large resistivity change and ease of synthesis. However the two most important issues in chemiresistive sensors are the reproducibility in sensing and the selectivity in chemical species.

For improving the reproducibility in polyaniline-based chemiresistive sensing, a self-calibration mechanism was proposed. This method utilizes two unique properties of polyaniline: one is the rate of the conductivity decay upon repeated cycling of the electrochemical potential, and the other is the position of the second redox potential, both of which are pH-dependent. These two properties were minimally affected by the polyaniline's inherent limitations, i.e. hysteresis and degradation, and therefore were effective in obtaining repeatable measurements.

In order to enhance the selectivity, a catalyst-based selective detection was proposed. This method is based on the concept that the catalytic reaction between the species and the catalysts causes a local pH change near the polyaniline nanowire network which changes the resistance of the polymer.

Finally, a sensor array consisting of polyaniline nanowire-based chemiresistors with each sensing element modified with a unique catalyst was implemented for multi-analyte sensing of ascorbic acid, dopamine, and hydrogen peroxide. Principal component algorithm was applied for the classification and semi-quantification of the chemical species.

# 1. Introduction

## 1.1. Motivation

Accurate detection and quantification of chemical and biological species are of great importance in many areas including health care, environmental monitoring, and recently, defense against biological warfare. In addition to being highly sensitive and selective, an effective sensor must have a simple and rapid detection method, and be able to perform parallel detection of multiple target analyte [1]. Nanomaterial-based sensors seem to be promising in this regard and have received great attention in recent years due to many unique properties that nanoscale materials offer. The main advantages of nanoscale materials include high surface-to-volume ratio leading to fast reaction speed and sensitivity, ease of miniaturization, reduced power consumption, and low cost as a result of small volume of required reagents. Therefore, the main focus of this thesis is the development of a nanomaterial-based sensor array for simultaneous detection of multiple chemical species.

Chemiresistive sensors, which measure the change in the conductivity or the resistivity of the sensing material as a result of its interaction with the chemical species of interest, have the benefit of being simple in configuration as well as being easily miniaturized to give high density and high throughput sensor arrays. Furthermore, signal processing is also relatively simple since only the resistance of the sensing material needs to be measured.

In chemiresistive sensing, a 1-dimensional nanomaterial-based sensing platform can achieve high sensitivity, fast response, massively parallel as well as easy miniaturization in sensor development. In particular, nanotubes, nanowires, or nanorods are ideal for this configuration for the following reasons [2]: First of all, the small cross-sectional area of the nanowires maximizes the current response along the axial direction of the wires creating large

conductance change. Secondly, the large surface area of the nanowires improves the sensitivity of the nanowire-based sensor by increasing the chance of the target analyte contacting the surface of the nanowires. Thirdly, the direct conversion of the chemical change into electrical signal greatly simplifies the device configuration. And lastly, the nanoscale of the sensing material enables for the development of high density, high throughput, and individually addressable sensor arrays for simultaneous multi-analyte detection. Therefore, the primary objective of this research is to develop a nanowire-based chemiresistive sensor array for the simultaneous multi-species detection.

Because of the advantages that the 1-dimensional nanowires provide in chemical sensing, as outlined earlier, many different types of nanowires have been investigated as chemiresistive materials such as carbon nanotubes [3]–[5], silicon nanowires [1], [6], [7], platinum and gold nanowires, and metal oxide nanowires [8]. However, there are several difficulties in utilizing such nanowires in sensor development. First, the fabrication of these nanowires are complex often requiring elevated temperatures in a well-controlled environment [9]. Second, the inability to grow these nanowires in a site-specific location has limited its application as a mass producible sensing device. Third, these nanowires physically placed on the electrodes require an extra processing step in order to reduce any contact resistance which may have adverse effect in measuring the conduction current through the wires. Hence, an alternative nanowire material that retains the electronic properties of the metal while minimizing or eliminating the disadvantages inherent in the metal- and oxide-based nanowires is needed.

Conducting polymer nanowires (CPNWs) have recently emerged as an attractive alternative to metal and semiconducting nanowires as chemiresistive material for their large conductivity change, flexibility, and ease of synthesis [10], [11]. Furthermore, the CPNWs can be synthesized

site-specifically at the desired location [11]–[15]. Using an electrochemical growth method, the CPNWs can be directly synthesized on the surface of a metal electrode of various types, which ensures secure contact between the polymer nanowires and the electrode thereby minimizing contact resistance. In 1977, the discovery of the first organic polymer, polyacetylene, which showed metallic conductivity, has opened up possibilities for the development of a new class of materials known as conjugated polymers or conducting polymers [16]. In 2000, the Nobel Prize for Chemistry was awarded to the three scientists who discovered polyacetylene (Alan G. MacDiarmid, Hideki Shirakawa, and Alan J. Heeger) "for the discovery and development of conducting polymers." Since then, a surge of research effort has been directed toward the development, synthesis, and characterization of new types of conducting polymer materials. As a result many different kinds of conducting polymers have been discovered and synthesized. Some of the most well-known examples of conducting polymers are polyaniline, polypyrrole, polythiophene, poly(3,4-ethylenedioxythiophene) (PEDOT).

Among the existing conducting polymers, polyaniline is one such organic polymer which has been known for over 150 years but was not known to possess electrical conductivity until it was revisited in the 1980s to discover its electron conducting nature. In addition, polyaniline is one of the most widely used conducting polymers due to its environmental stability [17], [18] both in air and moisture, reversible redox chemistry, and simple acid/base doping/dedoping chemistry. Furthermore, polyaniline is unique among conducting polymers in that it possesses a natural tendency to be synthesized in a 1-dimensional nanofiber-like morphology. Therefore, it has emerged as an excellent candidate to be used as a material for various nanoscale applications particularly in chemical and biological sensors [19]–[21]. Due to its large pH-responsive conductivity change by several orders of magnitude, polyaniline nanowire is well-suited as a

nanoscale chemiresistive sensing material. Hence, polyaniline was chosen in this work for the implementation of a nanowire-based chemiresistive sensor array with multi-analyte detection capability.

## 1.2. Objectives

The general objective of this thesis is the development of a polyaniline nanowire-based chemiresistor for chemical and biological sensing applications. However, there are several inherent limitations associated with polyaniline and a polyaniline-based sensing technology, with two main issues among them being: (1) irreproducibility in conductivity measurements and (2) the lack of selectivity in chemical sensing. This work attempts to address these two issues by suggesting possible solutions. In the following subsections, specific objectives of this research are stated.

### 1.2.1. Synthesis and Characterization of Polyaniline Nanowires

The first task is the electrochemical synthesis of the polyaniline nanowires. This involves the fabrication of the electrode where the polymer is to be grown as well as setting up the electrochemical cell system. A potentiostat circuit that controls the potential of the working electrode must be built, and an analog-to-digital converter module is needed for sending input voltages to the potentiostat and for measuring the current values for data processing. Once the system hardware is setup, a polyaniline nanowires can be synthesized. Scanning electron microscopy is also used for the morphology study.

After the device is fabricated, the current-voltage characterization is to be investigated. Since the conductivity of polyaniline is highly dependent on the pH of the environment and the redox state of the polymer, by varying both the pH and the electrochemical potential of the polymer, the operating region of the device can be defined. Other material properties that require

further characterization and investigation include sensor reproducibility, hysteresis, and conductivity degradation.

### 1.2.2. Self-Calibration of the Polyaniline Nanowire-Based Chemiresistive Sensor

Polyaniline is known to show degradation and hysteresis in its conduction current, which are common issues with most other chemiresistive sensors. The possible causes for conductivity degradation and hysteresis are irreversible damage in the chemical structure due to hydrolysis and structural deformation as a result of the oxidation and reduction of the polymer, respectively [22]. As a consequence, polyaniline-based chemiresistors suffer from the lack of repeatability in measurements rendering them unreliable. Therefore, the development of a polyaniline nanowire-based sensor with reproducible and hysteresis-free conductance measurement is an important objective of this research. Here, a novel self-calibration and current measurement scheme is proposed in order to obtain a reproducible and low hysteresis conductance measurement even in the presence of the degradation and hysteresis phenomena.

### 1.2.3. Nanoparticle-Functionalized Polyaniline Nanowires

One common issue with chemiresistive sensors is the lack of selectivity, and polyaniline-based chemiresistors, as one might expect, are vulnerable to this limitation. Since polyaniline is mostly pH-responsive, selective detection of other chemical species using a polyaniline-based chemiresistor is difficult. In order to enhance the selectivity of the polyaniline-based chemiresistor, the polymer must be modified so that the conductance of polyaniline changes upon interaction with a specific chemical species of interest. Here, a nanoparticle-based catalyst approach is proposed which, upon modification of polyaniline nanowires by attaching nanoparticles, a catalytic reaction at the surfaces of the nanoparticles will cause a local pH change near the polyaniline and subsequently influence the conductivity of the polymeric

chemiresistor. Various catalytic nanoparticles are tested to examine whether they respond to specific types of target species. Once the nanoparticles demonstrate clear evidence that selectivity can be enhanced by the polyaniline-nanoparticle combination, the next step is to search and identify the nanoparticles that show the best performance as well as finding the corresponding chemical species that respond well to the individual catalyst.

### 1.2.4. Development of a Sensor Array for Multi-Analyte Detection Capability

Once a set of possible catalytic nanoparticles and the corresponding analyte have been chosen, an array of polyaniline nanowire-based chemiresistors with each sensing element having been modified with different types of catalysts to uniquely respond to specific target analyte can be envisioned. Realization of such sensor array allows for a simultaneous detection of multiple target species by analyzing the conductance reading from the individual sensing components. An array of n x n sensing elements, which generates $n^n$ different measurements in parallel, requires a data processing algorithm that combines these individual signals to extract information about the sample composition. As a demonstration for multi-analyte sensing, a principal component analysis method, which is the most common and basic multivariate analysis technique, is applied to attempt to classify and quantify each individual analyte in the sample solution.

## 1.3. Dissertation Outline

Chapter 2 gives an overview and background information on polyaniline nanowires, discussing in detail the properties, method of synthesis, literature survey, and current limitations. Chapter 3 focuses on the fabrication, synthesis, and characterization of a polyaniline nanowire-based chemiresistive sensor. Chapter 4 discusses the development of a self-calibrating mechanism for the polyaniline nanowire-based pH sensor which yields reproducible conductance measurement while minimizing hysteresis in the conduction current. Chapter 5 describes the

catalyst-based chemical sensing with polyaniline nanowires for the selective detection of target species. Chapter 6 deals with the development and the implementation of the polyaniline nanowire-based sensor array for simultaneous multi-analyte classification and quantification.

# 2. Background

## 2.1. Introduction

Prior to the development and implementation of a chemiresistive sensing device based on polyaniline nanowires, a comprehensive understanding of polyaniline nanowires including the basic properties, method of synthesis, and a literature survey on the latest developments is required. In this chapter, the basic chemical structures, redox properties, electronic conduction, method of synthesis are described. Then, a literature review on recently reported polyaniline nanowire-based chemiresistive sensors is summarized. Finally, current limitations, challenges, and future prospect are discussed. The contents of this chapter is taken from the previously published review article titled "Conducting polymer nanowire and its applications in chemiresistive sensing," published in 2013 in *Nanomaterials* [23].

## 2.2. Overview of Polyaniline Nanowires

Polyaniline is one of the oldest known conducting polymer materials [24] and has been extensively reviewed [25]–[29]. It is the most studied conducting polymer closely followed by polypyrrole [30]. First discovered in the 19$^{th}$ century, polyaniline was originally known as "aniline black" [26], [27]. It was later found to be electrically conductive in nature and many researchers began to closely examine the properties of this material. Polyaniline was initially grown as thin films but later discovered that, under certain conditions, they can be grown in the form of an interweaved nanowire network. It has been reported that polyaniline has an intrinsic nature to grow in one dimension [31], which is not the case for other types of conducting polymers such as polypyrrole or polythiophene. Its unique ability to easily form 1-dimensional nanostructures, including wires, rods, tubes, and ribbons presents many advantages in nanoscale

devices [32]. Polyaniline has been studied for use in a wide range of applications including chemical sensors, battery electrodes [33], supercapacitors [34], fuel cells [35], display devices [36], separation membranes [37] and anticorrosion coatings [38].

### 2.2.1. Chemical Structure and Electrochemical Properties

The two factors that influence the chemical structure of polyaniline are the redox state of the polymer and the doping level. Polyaniline has three distinguishable redox states, namely the fully reduced leucoemeraldine state, the half-oxidized emeraldine state, and the fully oxidized pernigraniline state, with virtually an infinite number of possible redox states existing in between. Therefore, in principle, polyaniline can exist in a continuum of oxidation and reduction states ranging from a completely reduced to a completely oxidized form. A general chemical structure of polyaniline is shown in Figure 2.1(a) where the polymer chain consists of two types of repeating units, the reduced unit (b) and the oxidized unit (c).

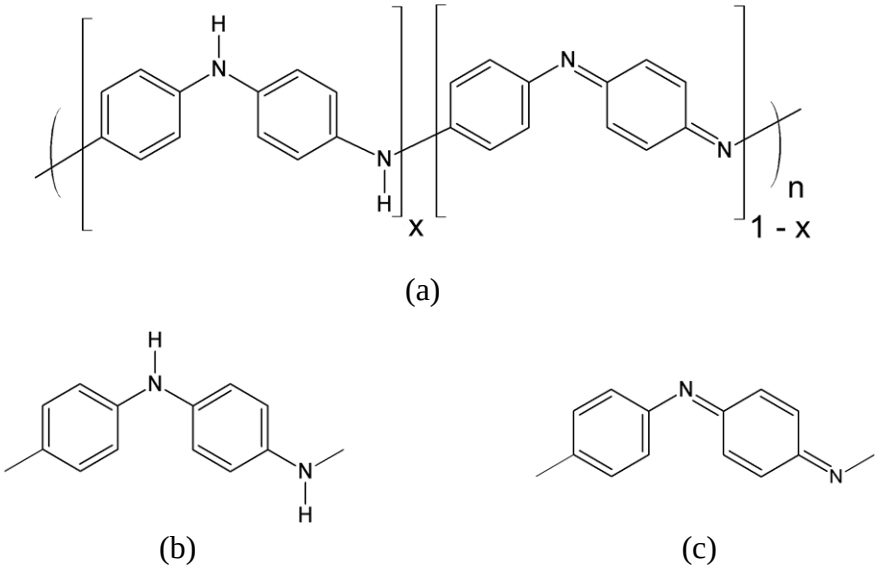


Figure 2.1. A general chemical structure of polyaniline and its repeating units: (a) a general chemical structure of polyaniline; (b) reduced repeating unit, and (c) oxidized repeating unit.

The degree of oxidation is described by the variable *x*, whose value is between 0 and 1, that represents the fraction of the two repeating units. In other words, leucoemeraldine, emeraldine, and pernigraniline refers to the chemical formula where $x$ = 1, 0.5, and 0, respectively. The reduced repeating unit contains only the amine nitrogen atoms whereas the oxidized repeating unit is made up of only the imine nitrogen atoms. Neutral polyaniline is known as a base whereas the protonated polyaniline with positive charges on the backbone structure is called a salt. The three different redox states of polyanilines in their base form and the corresponding salts are illustrated in Figure 2.2.

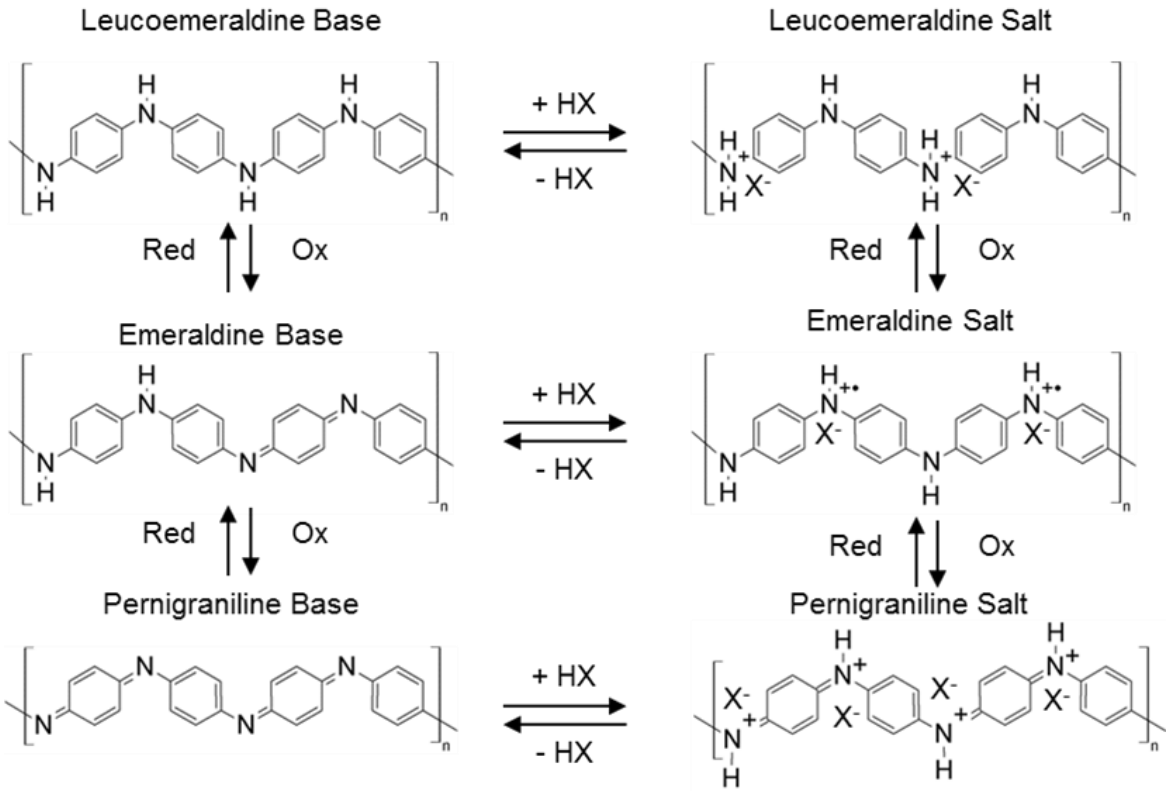


Figure 2.2. The three main electrochemical redox states and the corresponding doped forms of polyaniline.

The protonation of polyaniline, or more commonly referred to as doping, can occur in two ways. One is the addition of protons from the surroundings to the imine nitrogen atoms to form positively charged nitrogen atoms through acid treatment. The other is the removal of an electron from amine nitrogen to form the same positively charged nitrogen by oxidation of leucoemeraldine to emeraldine. Under these two scenarios, the delocalized radical cations are formed at the nitrogen sites, and these radical cations can travel along the conjugated backbone structure to give its conductive nature [39], [40]. The degree of protonation strongly depends on the oxidation state of polyaniline and the pH of the aqueous solution in which the polymer is immersed.

The electrochemical behavior and the redox states of polyaniline are commonly studied using a cyclic voltammetry (CV) technique [28], [41], [42]. A typical cyclic voltammogram polyaniline is shown in Figure 2.3. The CV curve shows two sets of distinct redox activity as indicated by the two pairs of anodic and cathodic current peaks. The first set of redox couple (peaks 1 and 1`) is associated with the conversion of the fully reduced leucoemeraldine base to the partially oxidized emeraldine, and the second set of redox current peaks (peaks 2 and 2') pertains to the conversion of emeraldine to the fully oxidized pernigraniline form. The potential of the first redox couple is largely independent of the pH whereas the potential for the second redox couple is strongly dependent on the pH value. This indicates that protons are involved in the second redox couple while the first redox couple does not require protons as part of the reaction. Another point to note is that polyaniline is more easily oxidized in less acidic solutions, and this can be experimentally verified where the peaks 2 and 2' shift to the left as the pH increases. A linear relationship has been observed between the peak height of the redox current

and the scan rate in a solution containing aniline and sulfuric acid, which is indicative of an electron transfer limited process [43].

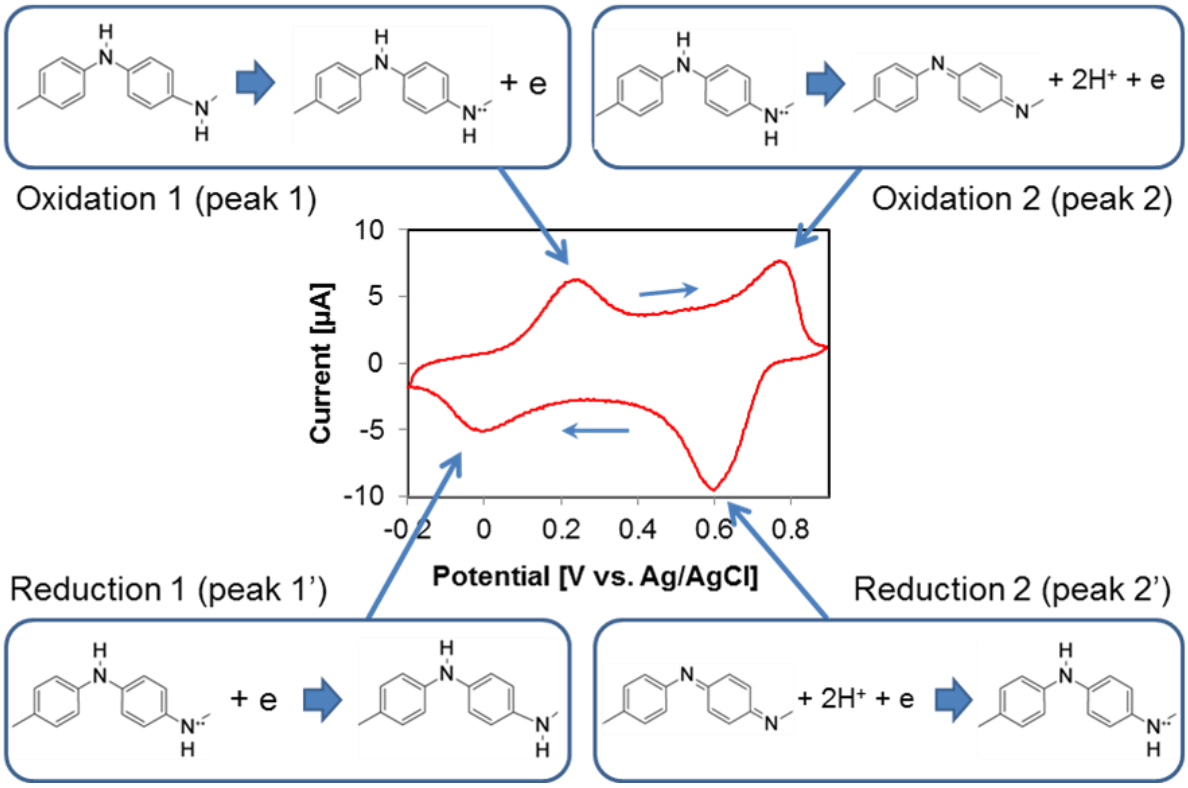


Figure 2.3. A typical cyclic voltammogram of polyaniline in HCl (pH 1) showing two sets of redox couples. The direction of potential scan is shown with the arrows.

Using the CV data, the electrochemistry and the structural formula for polyaniline as it goes through the redox process can be interpreted [28], [44]. Since the peak position of the first redox process in the CV plot is largely independent of pH, no proton is involved in the reaction. Hence, the reduction reaction can be described as the following:

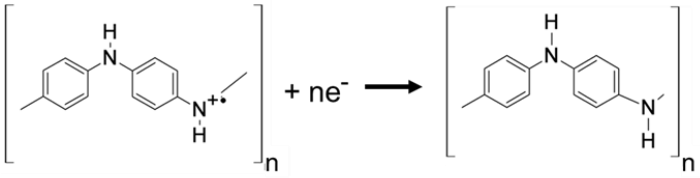

However, the peak position of the second redox process is highly dependent upon the pH of the solution. The second oxidation peak and its corresponding reduction peak tend to move to more negative values at a rate of approximately 120 mV per pH as the pH is increased [28]. Since the peak position moves as a function of the proton concentration in the solution, it can be expected that protons are involved the reaction as shown below:

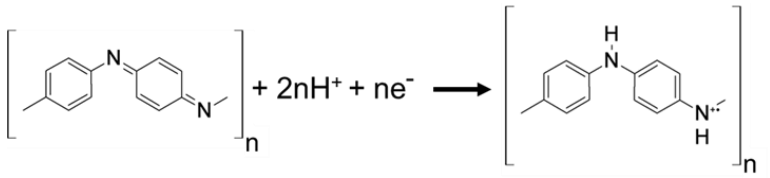


The doping mechanism of polyaniline is also unique among other conducting polymers. Most conducting polymers undergo a redox doping process during which the number of electrons associated with the polymer backbone changes. However, polyaniline can be doped through a non-redox process where the number of electrons in the polymer backbone structure remains unchanged [45], which makes the doping process simpler. As mentioned earlier, there are two different doping mechanisms for polyaniline: one is a non-redox doping process through acid treatment, and the other is a redox process by oxidation of leucoemeraldine to emeraldine. Upon proton doping, radical cations are formed at the nitrogen atoms and these charge carriers are believed to be responsible for the electronic conduction in polyaniline [46]. Hence, the majority charge carriers in polyaniline are holes. The next section gives a general description of the electrical conduction properties of the polyaniline.

### 2.2.2. Electronic Conduction

Since the delocalized and positively charged free radicals are the main source of conduction in polyaniline, it can be expected to show maximum conductivity when the number of radical cations in the polymer chains is maximized. This is in agreement with the fact that both

leucoemeraldine and pernigraniline, neither of which have free radicals in their backbone structure, are completely insulating. Hence, the conduction current versus the electrochemical potential relationship shows a bell-shaped curve as illustrated in Figure 2.4.

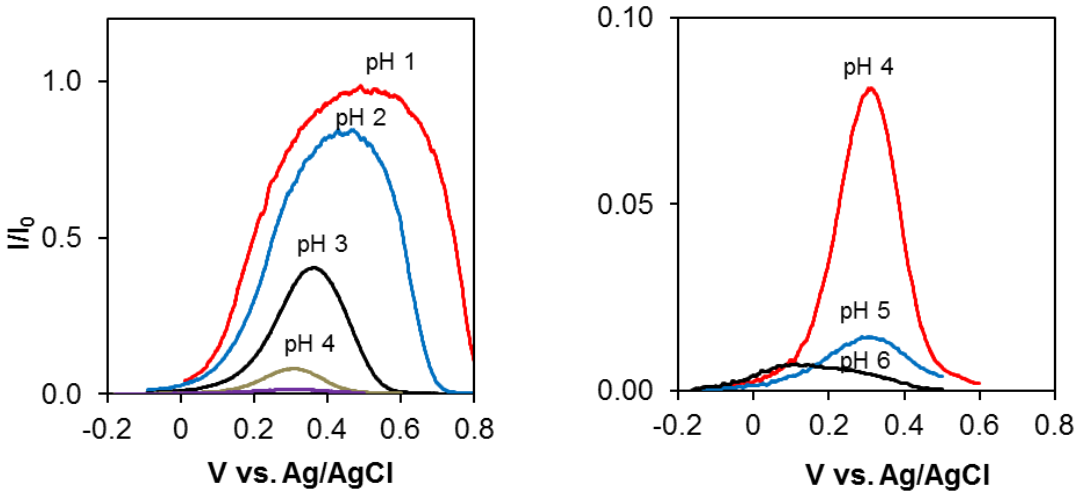


Figure 2.4. Conductance current versus potential of polyaniline in various pH solutions: (a) pH range 1–4 and (b) pH range 4–6. $I_0$ indicates maximum current observed.

The graph also confirms that the most conductive form of polyaniline is the fully protonated, half-oxidized emeraldine salt form, and the conductivity decreases as the polymer is deprotonated or the oxidation state changes toward either a fully oxidized or a fully reduced state. Over-oxidation of polyaniline by applying a potential beyond +0.6 V vs. Ag/AgCl should be avoided because it causes the irreversible formation of quinonediimine structures which are electrochemically inactive [44], [47], [22].

Although a true mechanism of electron transport is still under debate, several theories have been proposed to explain the electronic conduction of polyaniline. It is generally accepted that polyaniline nanowires consist of pockets of conductive grains embedded in insulating region as illustrated in Figure 2.5(a) [48]. Since the conductive grains are separated by an insulating

medium, electrons must gain sufficient energy to be able to overcome the insulating barrier and 'hop' into the nearest neighboring conductive grain. Some models also take into consideration the electronic conduction through internanotubular contact as illustrated in Figure 2.5(b).

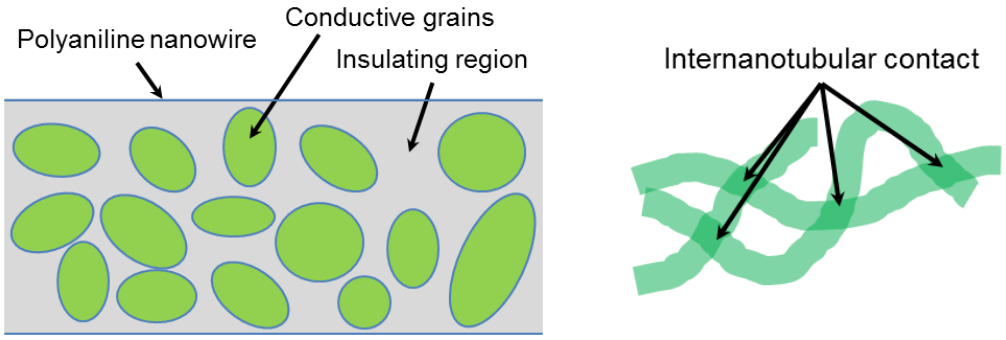


Figure 2.5. The electronic conduction path of the polyaniline nanowires: (a) internanotubular contacts between polyaniline nanowires and (b) conductive granular region encapsulated in the insulating region of the nanowire.

To further elucidate this phenomenon, different models to describe the electron transport in polyaniline nanowires have been proposed, including granular-rod model [49], 3-dimensional variable range hopping (3D VRH) [50], [51], 1D VRH with interchain coupling [52], Efros-Schklovskii (E-S) hopping conduction [53], and charging energy limited tunneling (CELT) [54].

### 2.2.3. Synthesis Methods

The two most common techniques for synthesizing 1-dimensional polyaniline nanowires are chemical synthesis and electrochemical polymerization. Although other methods such as electrospinning [55], enzyme assisted growth [56], and DNA template-based synthesis [57] exist, emphasis is placed on the chemical and the electrochemical methods. The true mechanism of the formation of polyaniline nanowires has not been fully elucidated [58]–[60]. However, many

reports have suggested the probable growth mechanisms based on their experimental results [26], [41], [61], [62].

**Chemical Synthesis**

The classical chemical synthesis involves the direct oxidation of aniline monomers by chemical oxidants [26]. Polyaniline nanofibers can be synthesized by mixing aniline monomers with a strong oxidizing agent in an acidic environment [63], [64]. The most commonly used oxidant in chemical synthesis is ammonium peroxydisulfate (APS) [65]. Depending on the growth condition, the chemical synthesis can yield various shapes and forms of polyaniline nanostructures including irregularly shaped agglomerates, granular particles, and elongated nanofibers. It has been experimentally observed that, during the early stage of polymerization, only 1-dimensional nanofibers were formed due to the homogeneous nucleation of polyaniline molecules. However, as further polymerization proceeds, preferential growth on previously formed nanowires due to heterogeneous nucleation occurs, resulting in irregularly shaped particles. Therefore, suppression of this 'secondary growth' that takes place during the later stage of polymerization is likely to be the key to growing directional nanowires.

Two novel synthesis methods that yield highly directional polyaniline nanowires with controllable diameters have been suggested: the first method is interfacial polymerization [66], [67], and the second method is rapid mixing technique [64], [68]. In the interfacial synthesis method, the polyaniline polymerization only occurs at the boundary of two immiscible organic/aqueous solutions. The synthesized polyaniline nanowires at the interface of the two solutions will migrate into the bulk of the aqueous phase, thereby avoiding further polymerization. Figure 2.6 illustrates the early, the intermediate, and the final stages of the interfacial polymerization process.

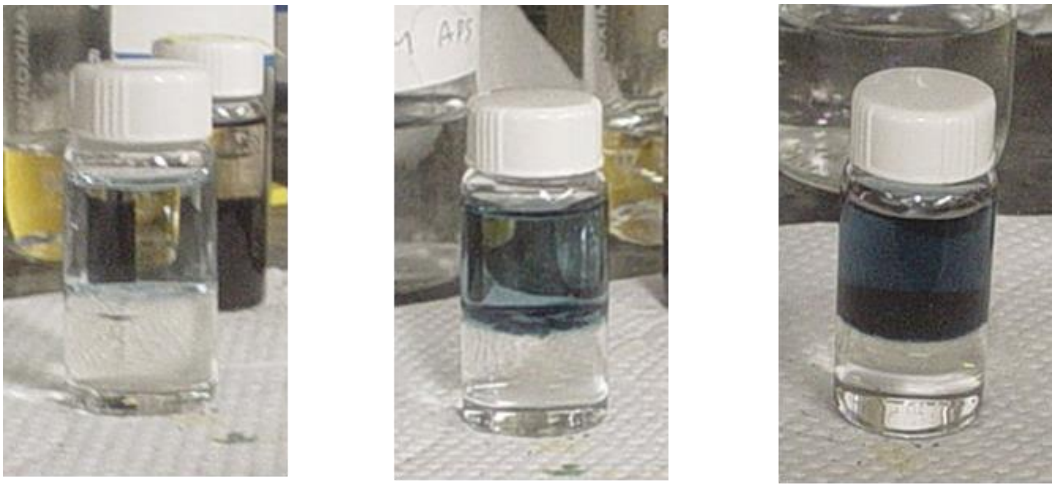

(a) (b) (c)

Figure 2.6. Interfacial polymerization process with 0.32 M of aniline in chloroform (bottom layer) interfacing 0.08 M of ammonium peroxydisulfate (top layer): (a) 1 min; (b) 5 mins, and (c) 10 mins of the reaction time after the reaction started.

The disadvantage of this technique is that the yield of nanofiber formation is generally too low for production in a large scale. To overcome this problem, a rapid mixing technique has been suggested. By quickly mixing aniline monomers with an appropriate portion of the oxidant at room temperature or higher, one can obtain large quantities of highly directional polyaniline nanofibers. The diameter of the nanowires is dependent on the type of acid used in the polymerization process. The average diameter of nanowires synthesized with HCl is approximately 30 nm while those obtained with camphorsulfonic acid (CSA) are roughly 50 nm, and $HClO_4$ yielded an average diameter of 120 nm [66].

Since the nanofiber morphology of polyaniline can be intrinsically grown, templates are not necessary for 1-dimensional polyaniline synthesis although there have been reports that use porous templates for the synthesis of nanowires [69], [70].

**Electrochemical Synthesis**

Polyaniline can be synthesized by anodic oxidation of aniline monomers through an inert electrode [26]. The electropolymerization of polyaniline nanowires can be categorized into 3 types: potentiostatic, galvanostatic, and potentiodynamic growth.

**i) Potentiostatic Growth:** In the potentiostatic growth method, polyaniline nanowires can be formed by applying a constant oxidative potential to the anode of the electrochemical cell, which causes a polymerization of aniline on the surface of the anode. Polyaniline can be grown on a variety of metallic surfaces including platinum, gold, stainless steel [71], iron, copper, zinc, indium tin oxide (ITO), graphite, and glassy carbon among many others [27]. The electrolyte solution is generally a mixture of a strong acid (such as 1 M $H_2SO_4$, HCl, or $HClO_4$) and aniline monomer with a concentration in the neighborhood of 0.05 M [71]. The potential under which polyaniline nanowires can be grown is between 0.7 V and 0.8 V vs. Ag/AgCl [71]. The oxidation of the aniline monomers occurs at around 0.7 V. These oxidized species are thought to be in radical forms that quickly become *p*-aminodiphenylamine dimer. The formed dimers are much more easily oxidized than aniline monomers (around 0.2 V), and can be further oxidized to form longer chains of polyaniline. Therefore, once these dimers are formed, polymerization of aniline can proceed even at potentials lower than 0.7 V vs. Ag/AgCl as long as the electrode surface is preliminarily covered with small amounts of polyaniline [72]. A typical polyaniline nanowires grown under the potentiostatic method are shown in Figure 2.7.

**ii) Galvanostatic Growth:** Galvanostatic growth is a method of electrochemical polymerization where the current flow in the working electrode is maintained to a constant value. A well-established low current polymerization technique involves a three step galvanostatic growth method [73]. In the first step, the current density is fixed to 0.08 $mA/cm^2$ for 0.5 h, which

generates particles to act as nucleation sites for growing extended polymer nanostructures. Next in the second step, the current density is reduced to 0.04 mA/cm$^2$ for 3 h and continued polymerization occurs at a slower growth rate. Finally in the third step, the current density is further reduced to 0.02 mA/cm$^2$ for 3 h, which continues to elongate the nanostructures into wires. Typical diameters of these nanowires are 50 to 70 nm with approximately 0.8 μm in length. For producing longer nanowires, higher current density that promotes a faster growth rate is required. Further, galvanostatically grown polyaniline promotes the formation of quinoid structures. This leads to the final production of *p*-benzoquinone, which prevents further growth of the polymer [74], [75].

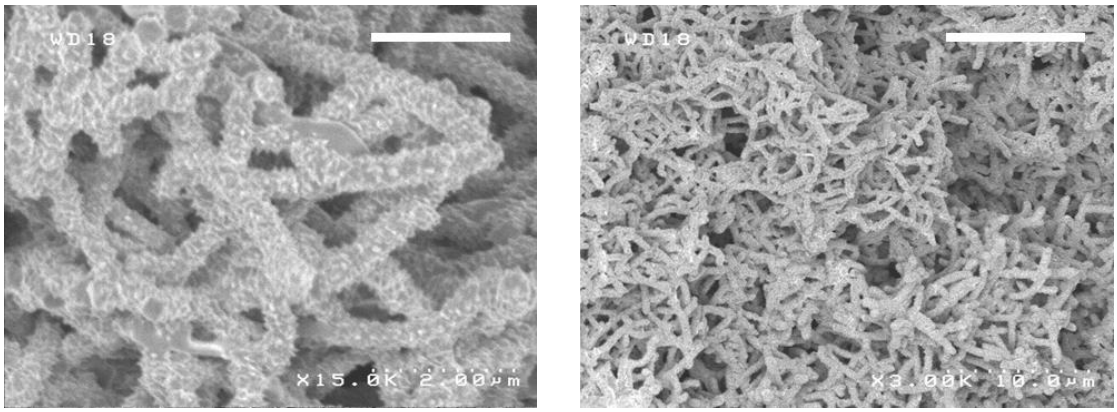


(a) (b)

Figure 2.7. SEM images of the electrochemically synthesized polyaniline nanowires at the magnification of: (a) 15,000× and (b) 3,000×. Scale bars are 2 μm in (a) and 10 μm in (b).

**iii) <u>Potentiodynamic Growth:</u>** Potentiodynamic growth involves scanning the potential of the anodic working electrode linearly from initial to final value in a forward and reverse direction with respect to the reference electrode repeatedly until the desired amount of polymer has been deposited [76], [77]. A sweeping voltage technique for the production of polyaniline is useful for elucidating basic aspects of the polymer growth and the redox mechanism [43]. It has been

reported that continuously cycling the potential of the working electrode produces a more uniformly deposited polyaniline film compared to that formed at constant potential and promotes better adhesion to the electrode surface [78].

Among the three aforementioned electrochemical methods, the potentiostatic growth promotes the fastest polymerization rate while the galvanostatic growth limits this rate to a fixed value. For the potentiodynamic growth, the rate of polymerization continuously changes. Since a fast growth rate is required to produce extended one dimensional nanowire structures, the potentiostatic growth is the preferred method for the nanowire synthesis.

### 2.2.4. Chemical Synthesis vs. Electrochemical Synthesis

Chemical synthesis method has the benefit of being able to produce large amounts of polyaniline nanowires with relatively simple setting. However, in terms of sensor fabrication, this method requires extra processing steps including the washing of the nanowires to remove strong oxidants such as APS, and drop-casting of nanowires on the electrode surface to implement a chemiresistor. Moreover, physically placing nanowires on the electrode does not guarantee a secure contact between the two materials, and may lead to large contact resistance. Therefore, the electrochemical synthesis is a preferred method for sensor applications two the following two reasons. First, electrochemical growth method allows for the direct synthesis of polyaniline nanowires on the surface of the electrode, which ensures a good electrical contact between the nanowires and the metal electrode. Second, since polyaniline grows on the surface of the electrode, the site-specific growth of the polymer nanowires can be obtained at the desired location.

## 2.3. Polyaniline Nanowire-Based Chemiresistive Sensors

Due to the unique electronic conduction properties as well as simple nanowire synthesis as described in section 2.2, polyaniline nanowires have attracted much interest in the research community as potential chemiresistive sensors. Therefore, this section focuses on the literature review of the reported polyaniline nanowire-based chemiresistors. Although polyaniline nanowires have been applied in different types of electrochemical sensors including potentiometric, amperometric, and voltammetric sensors, the conductometric sensing is the only transducing mechanism that truly takes advantage of the tunable conductivity property of polyaniline nanowires. A conductometric sensor measures the change in the resistance or the conductance of the sensing material as a detection mechanism. A chemiresistor is one such example of conductometric sensors that changes its resistance through the interaction with the target species.

### 2.3.1. Gas Sensors

Due to its tunable conductivity and large surface area, polyaniline nanowires have found applications in chemiresistive sensors, especially in gas sensing. The importance of a reliable and accurate gas monitoring system is well understood not only from safety but also from environmental standpoint. Most commercially available gas sensors are based on metal oxide semiconducting materials (such as tin oxide) operating at high temperature to increase sensitivity. The use of conducting polymers as an alternative to inorganic semiconducting materials for the gas sensitive layer offers many advantages such as, low cost, ease of synthesis, tunable conductivity, fast response due to porosity of the material [79], and high sensitivity at room temperature. Huang *et al.* have developed a gas sensor based on chemically synthesized polyaniline nanofibers and studied its response to 100 ppm of HCl and $NH_3$ vapor [67], [80].

Upon exposure to HCl vapor, the resistance of the polyaniline nanofibers reduced through the doping process, and an exposure to $NH_3$ had a dedoping effect that increased the resistance of the polymer. They also demonstrated that the nanofiber-based sensor responded much faster than the conventional film to both doping and dedoping due to the highly porous morphology of the nanofiber layer with small diameter of the fibers resulting in faster diffusion of gas molecules. Similar work was done in [12] where a polyaniline nanowire framework was formed to bridge the electrode junctions which acted as a resistive sensor, and its responses to HCl, $NH_3$, and ethanol vapors were demonstrated. Polyaniline chemiresistor has also been utilized for developing hydrogen gas sensors [10], [81] as well as humidity sensors [82], [83]. Combining polyaniline nanowires with other nanomaterials such as carbon nanotubes [84], gold nanoparticles [85] to form composite layer has shown to improve the sensitivity as well as the carrier mobility of the gas sensors.

### 2.3.2. Biosensors

The development of biosensors has emerged as a topic of great importance due to their applications in clinical diagnostics, environmental monitoring, food safety, and defense against biological warfare. An affinity-based molecule recognition method which uses the specific interactions of biomolecules such as antibodies to antigen binding, DNA hybridization, enzyme catalysis, is the most common method to ensure high specificity and selectivity of a biosensor. One of the earliest biosensors was developed by Clark and Lyons [86] who used glucose oxidase immobilized on a semi-permeable membrane, and glucose was monitored by measuring the oxygen consumed by the enzyme catalytic reaction. A glucose sensor is one of the most commercially successful electrochemical biosensors existing today. Most glucose sensors employ an amperometric measuring technique [87], however, this technology has major

limitations if the sensor is to be made smaller or if lower concentrations of analyte are to be measured. One of the strategies to overcome this limitation was the use of microelectrochemical transistors [88]. These devices make use of conductive polymers whose conductivity changes by several orders magnitude upon oxidation or reduction [89], [90]. This property of conducting polymers can be used to amplify signals transduced by electrochemical reactions. Therefore, polyaniline is an excellent candidate for biosensor applications in this regard [19], [20], [91]. This idea has been realized as a glucose sensor by attaching or embedding enzymes such as glucose oxidase to the polyaniline film [92]–[94]. Forzani *et al.* have developed a nanoscale glucose sensor by bridging a 20-60 nm electrode gap with polyaniline [95]. Pal *et al.* have used polyaniline nanowires as a direct charge transfer (DCT) electrical transducer for the detection of foodborne pathogen, *Bacillus cereus* [96]. In this method, polyaniline nanowires are attached to each antibodies and when these modified antibodies bind to antigen to form a sandwich complex via lateral flow immunoassay method, the nanowires form a bridge between two open electrodes to give resistive measurements [96]–[99]. Forzani *et al.* have developed a hybrid amperometric and conductometric chemFET-based sensor that can detect neurotransmitter dopamine even in the presence of ascorbic acid, an interference, whose concentration can be much higher than the analyte itself [100]. Polyaniline nanowires were also used for the detection of microRNAs [101]–[103], urea [104], [105], *E. coli* [106], and $H_2O_2$ [107]. The summary of polyaniline nanowire-based chemiresistive sensors and biosensors are shown in Table 2.1.

## 2.4. Current Limitations of Polyaniline-Based Sensors

As illustrated so far in this section, polyaniline nanowires offer many advantages both from the fabrication perspective and from the material characteristics standpoint, and therefore show great potential to be utilized as a nanoscale high density chemiresistive sensor array. However, a

Table 2.1. Summary of chemical and biological sensors based on polyaniline nanowires and their derivatives.

| Sensor Type | Sensing Material | Diameter (nm) | Analyte | Detection Limit (LOD) | Response Time | References |
|---|---|---|---|---|---|---|
| Surface acoustic wave | Polyaniline/$In_2O_3$ | 90 | $H_2$, $NO_2$, CO | ~ 2 ppm | ~ 30 s | [107] |
| Surface acoustic wave | Polyaniline | 30–50 | $H_2$ | 0.06% | ~ 100 s | [108,109] |
| Amperometric | Polyaniline | 60–80 | nitrite | $5 \times 10^{-8}$ M | ~ 5 s | [110] |
| Amperometric | Polyaniline/Au nanoparticles | 30–50 | glucose | $5 \times 10^{-7}$ M | ~ 5 s | [111] |
| Chemiresistive | Polyaniline/CSA | ~100 | $H_2$ | <1% | - | [15] |
| Chemiresistive | Polyaniline | 40–80 | $NH_3$, HCl, EtOH | ~0.5 ppm | ~100 s | [17] |
| Chemiresistive | Polyaniline/Au nanoparticles | 80 | $H_2S$, $CH_3SH$ | ~1 ppm | ~20 s | [101] |
| Chemiresistive | Polyaniline | 30–40 | CO | ~1 ppm | ~100 s | [100] |
| Chemiresistive | Polyaniline | 335 | $NH_3$ | 0.5 ppm | ~75 s | [99] |
| Chemiresistive | Polyaniline | 30–120 | HCl, $NH_3$, $N_2H_4$, $CHCl_3$, $CH_3OH$ | 100 ppm | 2~200 s | [3] |
| Chemiresistive | SWCNT/Polyaniline | 15 | $NO_2$, $H_2S$ | 500 ppb | ~10 min | [104] |
| Chemiresistive | Graphene/Polyaniline | 25–50 | $H_2$ | - | ~1 min | [105] |
| Chemiresistive | Polyaniline/Au nanoparticles | 250–320 | $H_2S$ | 0.1 ppb | <2 min | [106] |
| Chemiresistive | polyaniline | 100 | humidity | - | ~1 min | [102] |
| Chemiresistive | Polyaniline/PVB/PEO | 100 | humidity | - | ~50 s | [103] |
| Target-guided formation method | Polyaniline | - | microRNA | 5 fM | 30–60 min | [94] |
| Labeled direct charge transfer | polyaniline | ~200 | *Bacillus cereus* | ~10 CFU/ml | - | [112] |

few drawbacks and challenges that polyaniline nanowire-based chemiresistors are facing prevent them from becoming an effective chemical sensor. The three main challenges concerning polyaniline nanowires for application in chemiresistive sensor are: (1) the loss of conductivity in neutral pH; (2) polymer degradation and hysteresis, and (3) the lack of selectivity in chemical sensing.

Since polyaniline requires a large amount of protons attached to the polymer to be electrically conducting, it is a very poor conductor when the pH is greater than 5, which significantly limits its application. This is especially critical for biosensors where most enzymatic and cellular activities are pH sensitive, and those biomolecules function properly in neutral pH environment, typically between pH 6 and 8. Therefore, preventing the loss of protons bound to polyaniline structure in neutral pH solutions is the key to maintaining conductivity in such environment. There have been attempts to achieve this by attaching negatively charged anions to the polymer, which attracts positively charged protons to the polymer. MacDiarmid and Epstein have developed a 'self-doped' polyaniline which contains negatively charged sufonate groups covalently bound to the aromatic rings of polyaniline [108]–[110]. Such self-doped polyaniline can also be synthesized by electro-copolymerization of aniline with its ring-substituted derivatives such as aminobenzene sulfonate [111], [112]. Another method to achieve increased conductivity at neutral pH is the polymerization of aniline with large molecular weight organic acids. In this case, large molecular sized anions are trapped within the polyaniline matrix, thereby maintaining polymer's electronegativity in order to attract protons. Camphorsulfonic acid (CSA) [113]–[115] and dodecylbenzenesulfonic acid (DBSA) [116], [117] have been reported to be the most effective organic acids used for this purpose. Furthermore, the use of such organic acids enhances the solubility of the polymer and improves solution

processibility. Another approach is the use of polyelectrolytes as substitutes for organic acids, such as polyacrylic acid (PAA) [118], [119] and polystyrene sulfonate (PSS) [120], [121]. The aforementioned techniques have extended the polyaniline's electroactivity to the neutral pH environment, however its conductivity has only slightly improved. Further improvements on the conductivity in physiological pH are required in order to develop an effective biosensor.

Exposing polyaniline to elevated pH solutions such as pH 5 or higher causes an irreversible conductivity degradation to the polymer [122]. Some of the possible causes for this conductivity degradation are structural damage due to mechanical stretching or twisting of the polymer chain caused by electrostatic charge of the dopant, loss of anions to counterbalance the positive charge gained by proton adsorption [123], and the production of quinone-hydroquinone couples [53,81] that cleave the polymer chain structure. Therefore, minimizing the conductivity degradation is crucial in developing a repeatable and stable polyaniline-based sensor, which needs to be solved.

The conductivity of polyaniline is known to possess hysteresis, which is illustrated in the current versus potential sweep characteristics plots [90], [95], [126], [127] where the current response to the potential sweep in the positive direction is different from that to the reverse sweep of the potential. This existence of hysteresis is more closely related to the level of doping rather than the electrochemical potential or the pH of the polymer [128] and this apparent hysteresis or "memory effect" has been attributed to structural relaxations [129] caused by the change in the redox state of the polymer. Hence, a sensor calibration step is required to eliminate hysteresis in conductance measurements. A simple way to calibrate the sensor is to deprotonate the polymer in strong base solutions. However, this method is cumbersome and can also accelerate the conductivity degradation process. Therefore, a convenient and reliable self-calibration method is needed for the development of a hysteresis-free polyaniline-based sensor.

## 2.5. Conclusions

In this chapter, the basic principles and properties of polyaniline nanowires and its applications in chemiresistive sensing have been reviewed. The conductivity of polyaniline can change by a few orders of magnitude by varying its electrochemical potential and the solution pH. This unique property allows polyaniline nanowires to be utilized in nanoscale chemiresistive sensors. Moreover, the large surface area of the polyaniline nanowire network makes this a well-suited material for high sensitivity and fast responding gas sensors and biosensors. Electrochemically polymerized polyaniline nanowires have the advantages of being able to minimize the contact resistance and at the same time, site-specifically fabricate the nanowires. However, some of the major challenges regarding polyaniline nanowires include, but are not limited to, improving the conductivity in the physiological pH range, preventing or minimizing the conductivity degradation and hysteresis, and adding selectivity in chemical detection.

# 3. Synthesis and Characterization of a Polyaniline Nanowires

## 3.1. Introduction

As a first step toward achieving the final objective of developing a polyaniline nanowire-based chemiresistive sensor array, a single chemiresistor device is implemented which will serve as a prototype device for characterizing the polyaniline nanowire chemiresistor. The purpose of this chapter is to describe the design and fabrication of the electrodes, to illustrate the experimental setup and methods, and to present the results and the analysis of the synthesized polyaniline nanowires and the conduction current measurements obtained from the fabricated device. Since the conductance of the polyaniline-based chemiresistor depends on several factors such as the redox state, the solution pH, the amount of polymer synthesized, and the extent of polymer degradation, the device must be fully characterized in order to understand the device condition. In addition, a thorough conduction current measurement study is performed in order to elucidate the degradation and hysteresis problem inherent in the conductivity of the polyaniline nanowires.

## 3.2. Electrochemical Synthesis of Polyaniline Nanowires

In this section, the design and fabrication of the device, the experimental setup, and the procedure for the electrochemical synthesis of polyaniline nanowires are presented. The electrochemical polymerization technique rather than the chemical synthesis method is chosen for the nanowire synthesis since the electrochemical method has the advantages of site-specific growth, low contact resistance, and being able to directly use the device for sensing after the synthesis without any post-processing steps as described in 2.2.4.

### 3.2.1. Electrode Design

Figure 3.1 illustrates the schematic diagram of the polyaniline nanowire-based chemiresistive sensor.

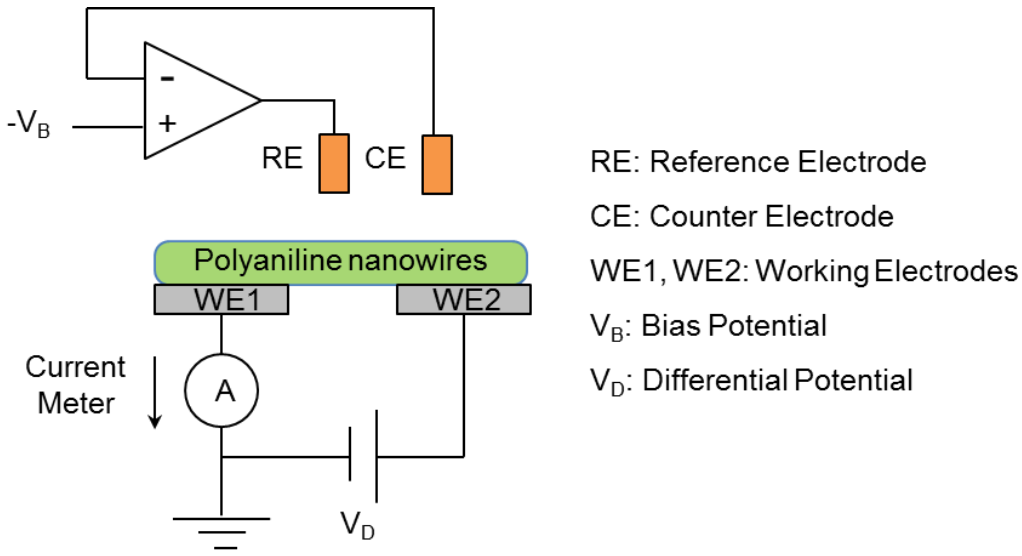


Figure 3.1. Schematic diagram of a chemiresistive sensor. The two working electrodes are connected via the growth of polyaniline nanowire network.

The device requires four individual electrodes: a reference electrode (RE), a counter electrode (CE), and two separate working electrodes (WE1 and WE2). A polyaniline nanowire network is formed at both working electrodes so that a 'conductive bridge' is established across the two working electrodes, which enables the measurement of the resistive current through the polymer bridge. The gap between WE1 and WE2 is made narrow to facilitate the bridging of the two electrodes through the polyaniline nanowire network. A reference electrode is required to control the electrochemical potential of the working electrodes, and controls the redox state of the polyaniline grown on the surface of both WE1 and WE2. A silver/silver chloride (Ag/AgCl) electrode is used as a reference since Ag/AgCl can easily be miniaturized and contains no liquid component unlike other reference electrodes such as a saturated calomel electrode. A large

current flow through the reference electrode can have a detrimental effect and can alter the reference potential. Therefore, in order to minimize the current flowing through the RE, an auxiliary electrode, also known as counter electrode is implemented where most of the current generated by the electrochemical reaction at the working electrodes will flow through the CE rather than the RE.

The electrode design patterned on a glass substrate is illustrated in Figure 3.2(a). The device shows a 5 µm-gap between the two working electrodes as shown in Figure 3.2(b).

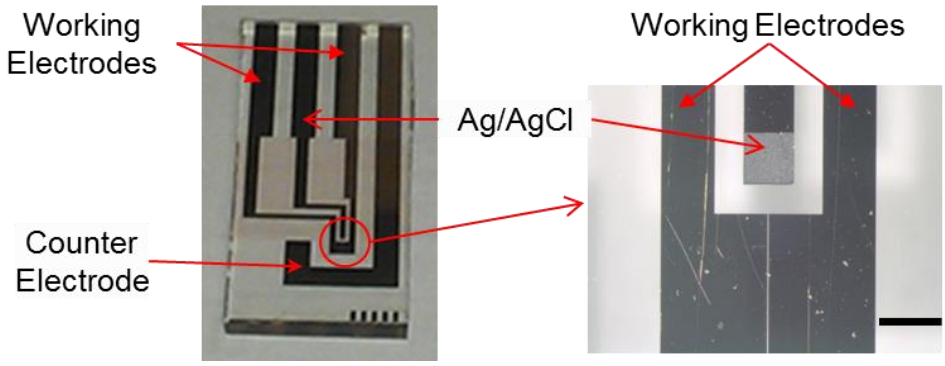


(a) (b)

Figure 3.2. The electrode design for the chemiresistive sensor showing the reference electrode, the counter electrode, and the two working electrodes: (a) electrode design showing Ti/Au (10 nm/50 nm) layer on a glass slide and (b) magnified image of the sensing area (the circled area from part (a)) with 5 µm gap between the working electrodes. Scale bar is 500 µm.

The electrodes were fabricated using a standard photolithography and a metal etching process. First, titanium (Ti) and gold (Au) layers with thicknesses of 10 nm and 50 nm, respectively, were deposited on a clean 1" x 3" glass slide (cleaned with tetrachloroethylene) using electron beam evaporation. The purpose of titanium is to promote adhesion between gold and the glass slide. Next, a positive photoresist (Shipley S1805, AZ Electronic Materials, Luxembourg) was coated by spin-casting at 2,000 rpm on the Ti/Au deposited glass then baked

at 115 °C for 1 minute. After baking, the photoresist layer was partially exposed to a ultraviolet (UV) light (365 nm wavelength) through a patterned bright field photomask (Telic Company, Valencia, CA, USA) with a dose of approximately 30 $mJ/cm^2$. The exposed part of the photoresist layer was removed by dissolving in a developing solution, Microposit 351 developer (Shipley, AZ Electronic Materials, Luxembourg) diluted in deionized water at 1:4 ratio. Afterward, gold and titanium layers were subsequently etched in a potassium iodide-based gold etchant diluted in deionized water at 1:10 ratio, and 1% hydrofluoric acid in deionized water, respectively. Finally, the masking photoresist layer was removed by an acetone, methanol, and deionized water treatment, in that order.

The working electrodes are partially covered with a thin layer of passivation coating to ensure that polymerization of nanowires only occurs on the designated area. Without this passivation layer, polyaniline nanowires will be polymerized on the entire surface of the working electrode as long as the electrode is in physical contact with the aniline monomer solution during the synthesis process. However, only the square area with the dimension 500 μm × 500 μm where the working electrode gap is located is the desired location for the polymer growth. The areas that are not covered by the resist layer are the square area at the electrode gap (chemiresistive sensing area), the reference electrode area and the counter electrode. Figure 3.3. shows the area on the electrode not coated with the protective layer. A photoresist (Shipley S1827) was used as a passivation layer to physically separate the unwanted areas of the electrodes from contacting the monomer solution. After patterning the passivation layer, the device was hard baked at 180 °C at least 30 minutes to stabilize the coating.

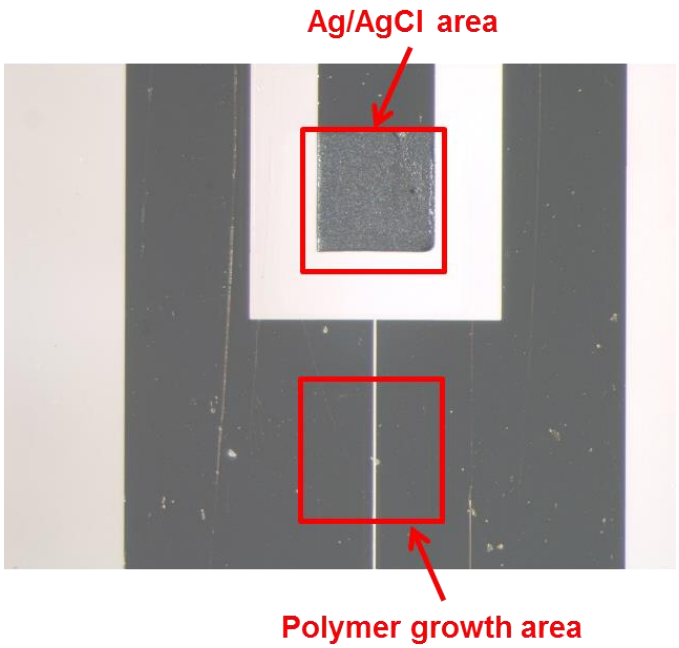


Figure 3.3. Passivation of the electrode surface. The areas not protected by the passivation coating are the Ag/AgCl reference electrode area and the polymer growth area indicated with red squares. The dimension of each square is 500 µm × 500 µm.

### 3.2.2. Electrochemical Setup

The fabricated device was partially immersed in a 10 ml solution containing the aniline monomers dissolved in acidic solution. If an on-chip reference electrode is desired, a silver and silver chloride layer can be deposited onto the gold electrode using an electrodeposition method. However a separate conventional Ag/AgCl reference electrode was also used during the material characterization for convenience. Figure 3.4 shows the electrochemical cell comprising the device, the precursor solution containing aniline, and a conventional reference electrode. The potentials of the working electrodes were controlled with a simple potentiostat circuit. The input voltage to the potentiostat was supplied by a LabView module.

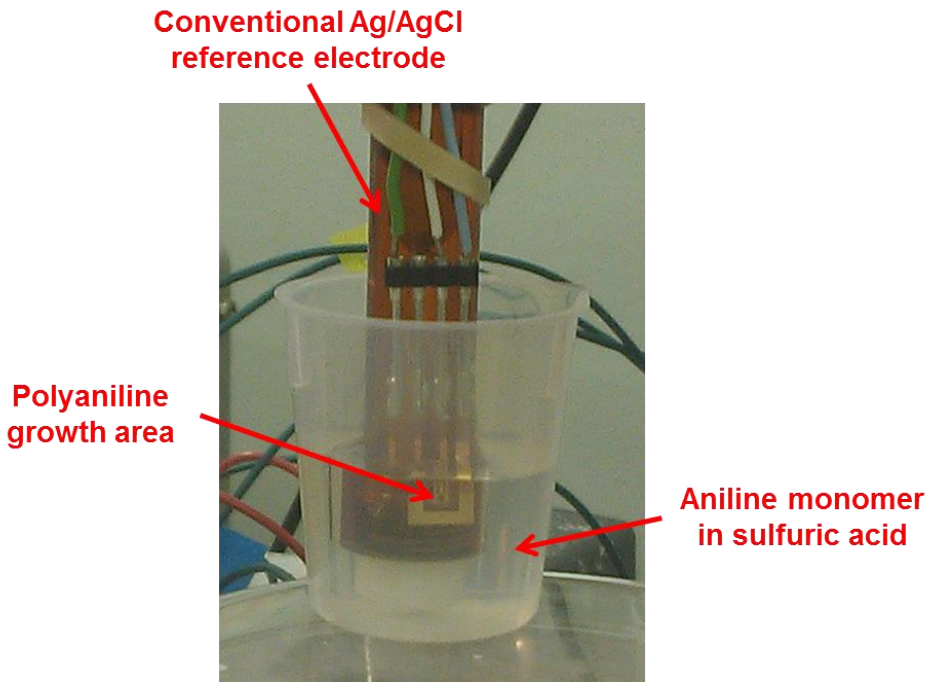


Figure 3.4. The electrochemical cell during the electropolymerization of polyaniline nanowires. The electrodes of the device are partially immersed in a precursor solution containing aniline monomers. A conventional Ag/AgCl reference electrode is often used for polyaniline synthesis and characterization.

### 3.2.3. Polymer Synthesis Process

The processing conditions for the polyaniline nanowire synthesis were adopted from [71] which uses a potentiostatic growth method. A 10 ml of precursor solution which contains 0.05 M of aniline completely dissolved in 1 M $H_2SO_4$ is typically used for the polymer synthesis. After setting up the electrochemical cell, the potential of the working electrodes were fixed at +0.8 V vs. Ag/AgCl. Since the electrochemical process is an oxidative polymerization, the anodic current is generated at the working electrode. As the polymerization step progresses, the anodic current continues to rise. The volume of the synthesized polyaniline nanowire network was estimated by monitoring a total charge that has passed through the working electrodes throughout the process. After the desired amount of the polyaniline material has grown, the

electrodes were removed from the solution and the potentiostat was disconnected. Then, the polyaniline-grown area was gently rinsed in deionized water to remove unbound aniline monomers and residues. A typical oxidative current generated from the potentiostatic polymerization of polyaniline is shown in Figure 3.5(a). For calculating the total charge accumulated from the electropolymerization, the oxidative current is integrated over time to obtain the plot in Figure 3.5(b).

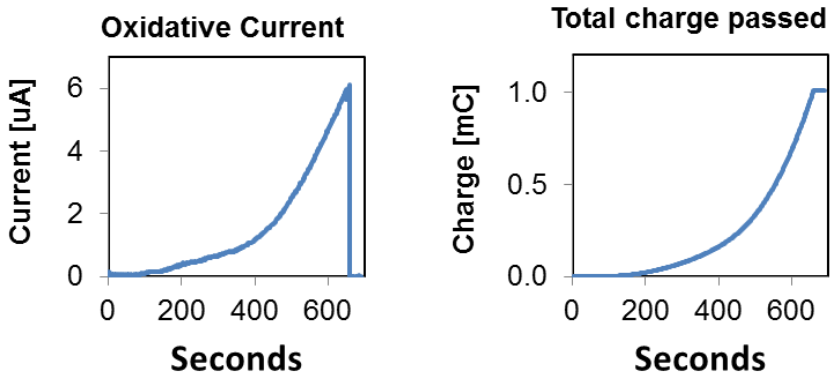


(a) (b)

Figure 3.5. A typical electrochemical current generated from the oxidative polymerization of polyaniline: (a) anodic current generated at the working electrodes and (b) the accumulated total charge.

The current vs. time relationship in Figure 3.5(a) indicates that the rate of polymerization is increasing over time. As the synthesis of polyaniline nanostructures continues on the electrode surface, the rate of polymerization increases due to the increased surface area of the polyaniline nanowires, which facilitates faster oxidation rate of the precursors in the solution. This increasing oxidative current eventually reaches a plateau as the rate of polymerization approaches the mass transfer limited electron transfer at the working electrodes. Figure 3.6 shows a microscope image of the synthesized polyaniline nanowire network that connects the two working electrodes.

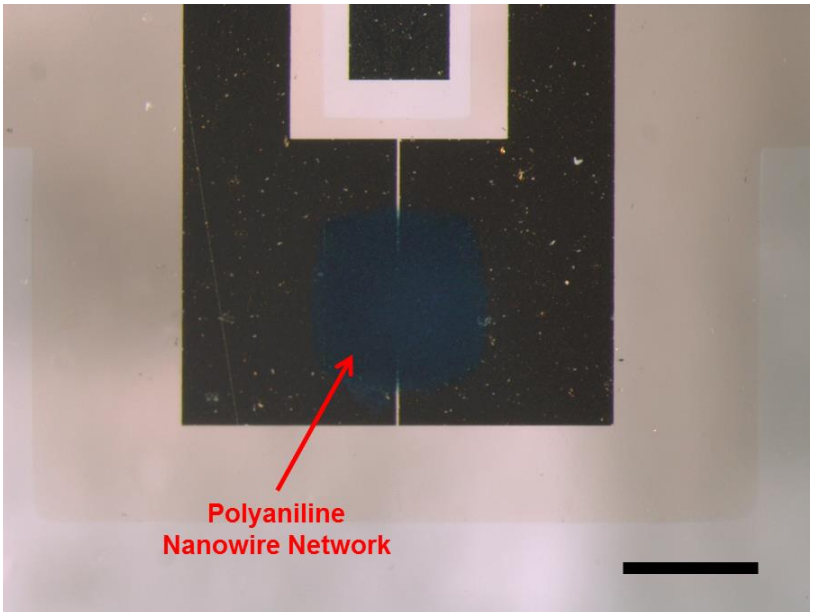


Figure 3.6. Image of the synthesized polyaniline layer for connecting the two working electrodes for the development of a chemiresistive sensing device. Scale bar is 500 µm.

### 3.3. Morphology Characterization of Polyaniline Nanowires

A typical scanning electron microscopy (SEM) images of the electrochemically synthesized polyaniline nanowires are shown in Figure 3.7. The average diameter of the nanowires is approximately 100 – 150 nm.

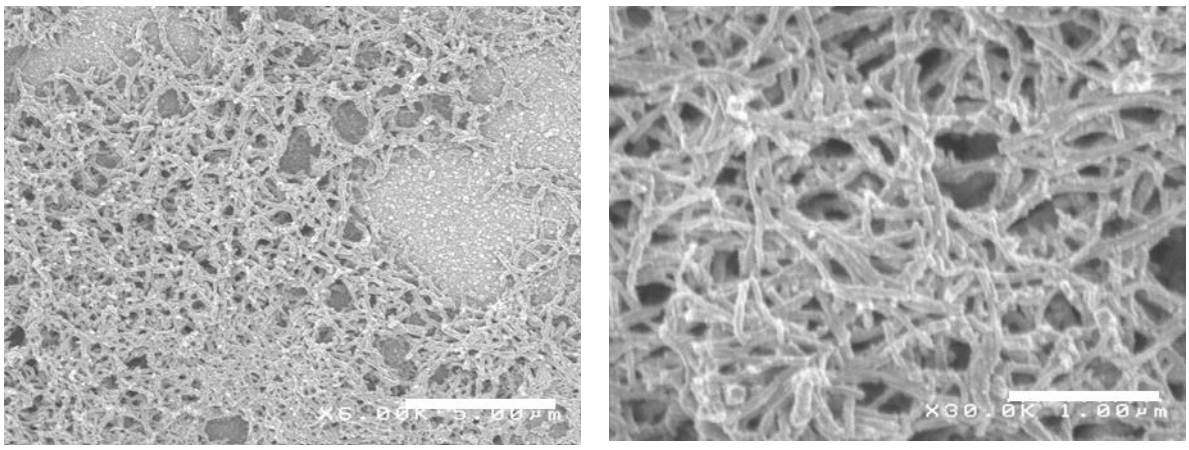

(a) (b)

Figure 3.7. SEM images of the electrochemically synthesized polyaniline nanowires. Scale bars are (a) 5 µm and (b) 1 µm.

The figure also shows areas not covered by the nanowire network, possibly due to the lack of aniline precursors available to initiate nanowire growth. However, small gains can be observed on such areas which are known to be the nucleation sites for the polyaniline [73], [130].

Figure 3.8 shows a set of SEM images of the polyaniline nanowires that were taken after 5 (0.07 mC), 10 (0.3 mC), 15 (0.8 mC), and 22 minutes (1 mC) of synthesis time with the total charge passed up to that point indicated in the parentheses.

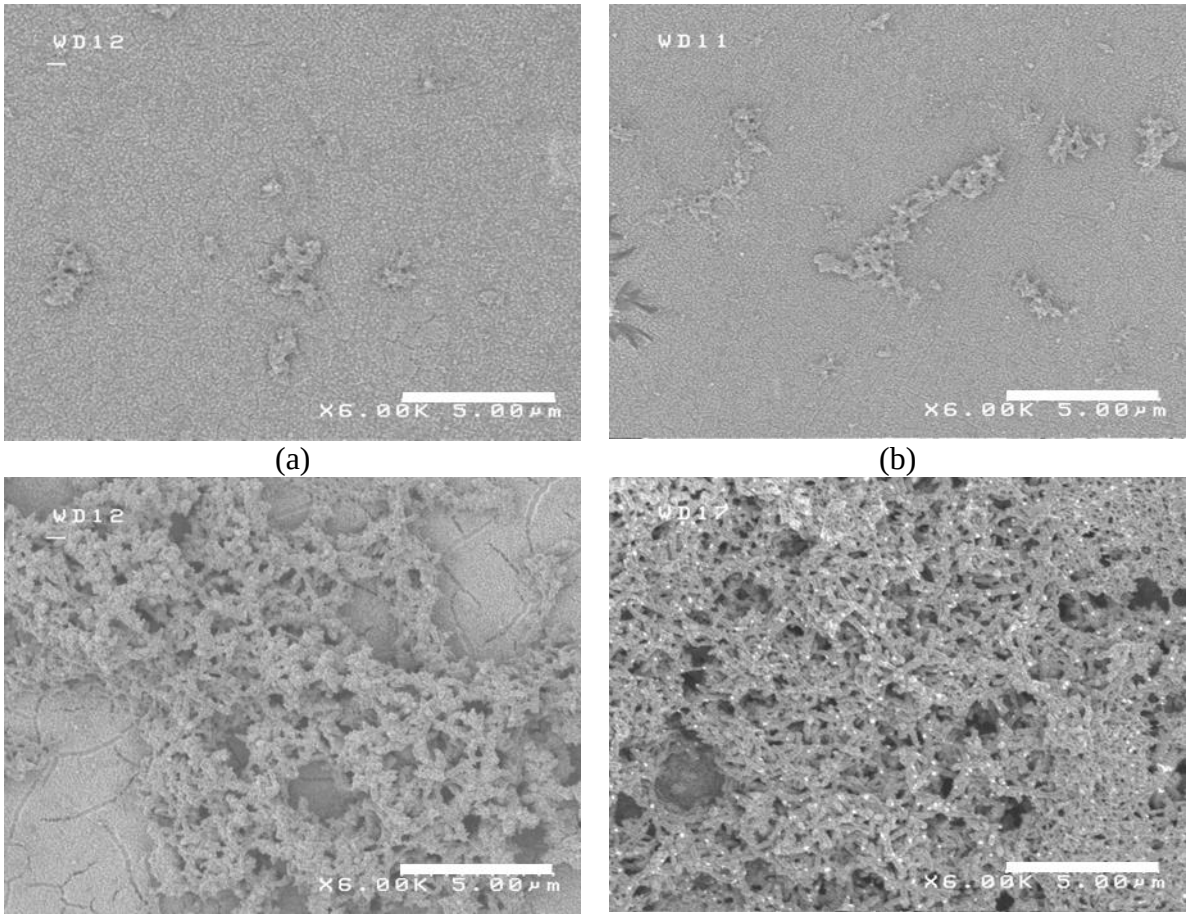


Figure 3.8. SEM images of polyaniline nanowires at various stages of the polymerization showing images taken after: (a) 5 mins (0.07 mC); (b) 10 mins (0.3 mC); (c) 15 mins (0.8 mC), and (d) 22 mins (1 mC) of reaction time. Scale bars are 5 µm.

As shown in Figure 3.8(a), nanowires have not been formed at the early stage of the polymerization, however small granular structures with approximate diameters of tens of nanometers are formed on the electrode surface. The granular structures are believed to be the nucleation sites for the growth of polyaniline nanowires. As the polymerization progresses the nucleation sites are further extended and aggregated together to form longer nanostructures. Figure 3.8(a) and 3.8(b) show the initial formations of such nanostructures. Further polymerization creates well-defined nanowires that are randomly grown to form an interconnected network as illustrated in Figure 3.8(c). Figure 3.8(d) shows a more densely filled but highly porous nanowire structures.

## 3.4. Chemiresistive pH Sensor

For measuring the conductance or the resistance of the polyaniline nanowire network grown between the two working electrodes, a small differential voltage $V_D$ is applied to induce a flow of conduction current through the polyaniline nanowires. For simplicity, the conduction current instead of conductance or resistance is used as a sensing signal. As illustrated in Figure 3.1, a current meter can be connected to one of the working electrodes to measure the conduction current in polyaniline nanowires. For actual measurement during the experiment, a simple operational amplifier based on a field effect transistor (LF 353, Fairchild Semiconductor, San Jose, CA, USA), with a feedback resistor connected between the output and the negative input of the amplifier was constructed for current measurement.

### 3.4.1. Conduction Current vs. Bias Potential Characteristics

Since the redox state of polyaniline is determined by the electrochemical bias potential $V_B$ as defined in Figure 3.1, the conductivity of polyaniline nanowires is strongly dependent on $V_B$. For characterizing the relationship between the conduction current ($I_C$) and bias potential, $V_B$

was linearly scanned from a negative to a positive potential so that the polyaniline can undergo a redox transformation from the fully reduced leucoemeraldine to the fully oxidized pernigraniline state. Figure 3.9 below shows the conduction current response of the chemiresistive device as the potential is scanned over a wide range of bias potentials.

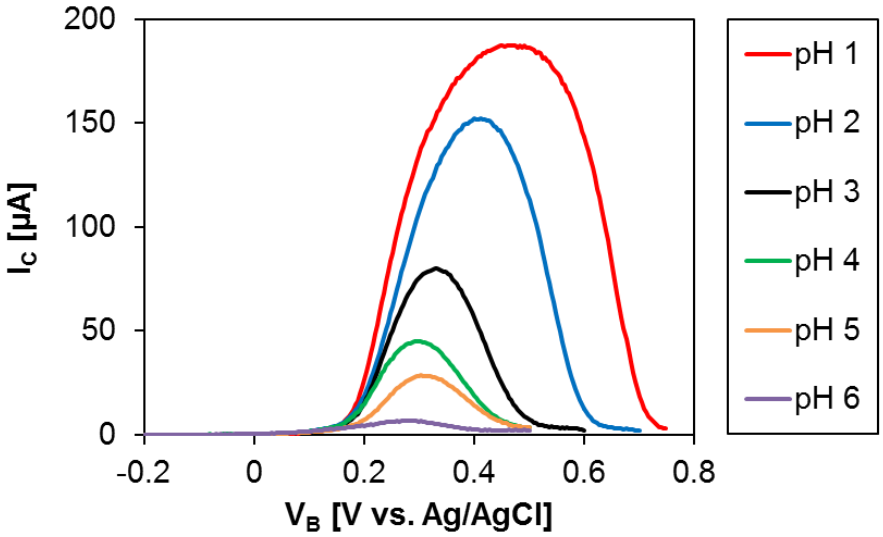


Figure 3.9. Conduction current vs. potential relationship of the polyaniline nanowire-based chemiresistor. The polyaniline nanowire network was synthesized until a total oxidative charge of 1 mC was passed. $V_D$ was set to 20 mV. $V_B$ was scanned at a rate of 20 mV/s from a negative to a positive potential.

The plot shows a bell-shaped conduction current response for a given pH, which is the result of the redox transformation of polyaniline from the fully reduced state ($V_B$ = -0.2 V) to the fully oxidized state. The potential at which the conduction current starts to rise (the left end of the bell-shaped curve) is similar for all pH values, at approximately +0.1 V. However, the potential at which the polymer becomes fully oxidized (the right end of the bell-shaped curve) varies with pH. This can be explained by observing the cyclic voltammetry curve of polyaniline which shows that the position of the second redox couple (peaks 2 and 2' in Figure 2.3) shifts to the left as the pH increases. Furthermore, the maximum current increases as the solution become

more acidic which further corroborates that increased proton doping enhances the electronic conduction in polyaniline.

### 3.4.2. Hysteresis Analysis

The conductivity of polyaniline is known to exhibit a hysteresis effect, which is evident from the conduction current vs. bias potential sweep characteristics [90], [95], [126], [127] showing that, for a fixed pH, the $I_C$ response to the $V_B$ sweep in the positive direction is different from that to the reverse sweep of the bias potential. To demonstrate the hysteresis phenomenon of the polyaniline-based chemiresistive sensor, the developed device was tested under the cycling of $V_B$ both in the forward and the reverse direction at a scan rate of 20 mV/s with a differential voltage of $V_D$ = 20 mV in a given pH solution. The conduction current response was plotted against $V_B$ in Figure 3.10. The graphs indicate that polyaniline has a 'memory effect' where its conductivity is influenced by the previous redox state. The existence of hysteresis is closely related to having a different level of doping at a given electrochemical potential of the polymer [128], which has been attributed to conformational changes caused by Coulombic repulsions [90], [129], [131]. As the polymer undergoes a change in redox state, the polymer experiences stretching and relaxation in the structure due to the charge of the dopant anions residing in the polymer. Therefore the direction of the potential scan plays an important role in applying a different mechanical stress to the polymer structure. Hence, it follows that, in order to obtain a hysteresis-free reading of the conduction current of polyaniline, one must initialize or reset the doping level of the polyaniline prior to each measurement such that the device would yield a reliable current reading.

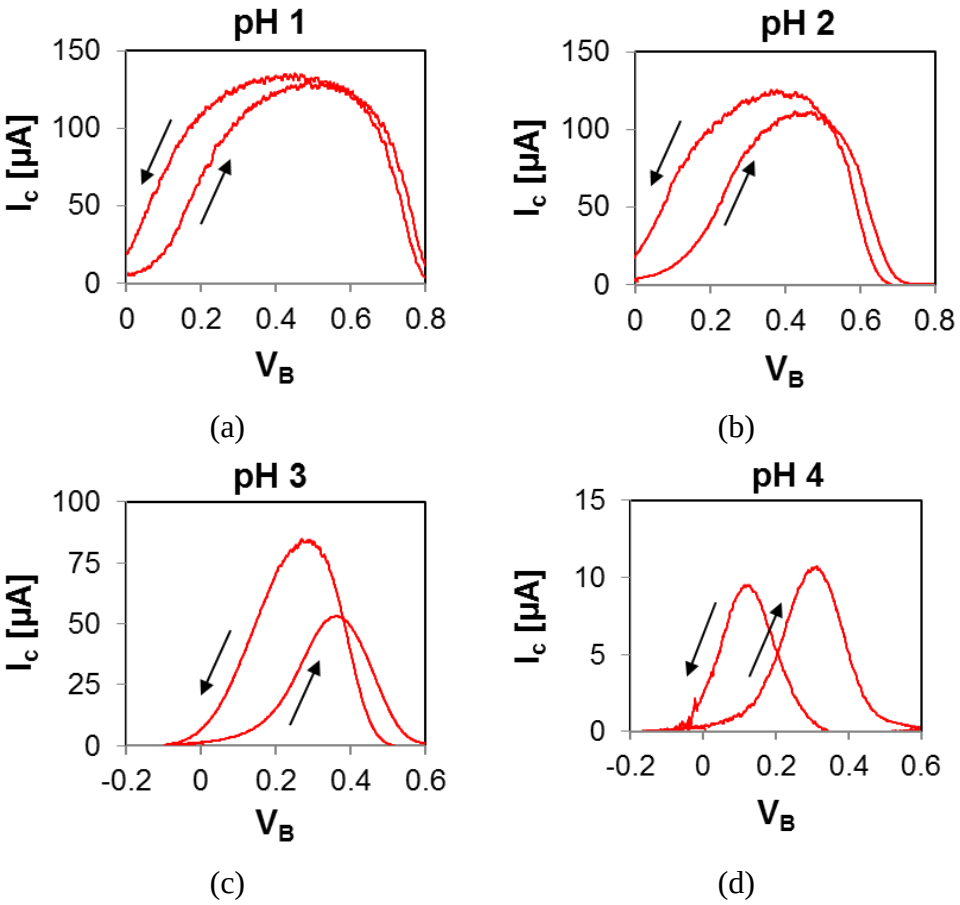


Figure 3.10. Hysteresis in the conduction current of polyaniline nanowire-based chemiresistor: the $I_C$ responses to the $V_B$ sweep in (a) pH 1, (b) pH 2, (c) pH 3, and (d) pH 4. The forward and reverse directions of $V_B$ sweep are indicated by the arrows.

One possible method to reset the device is to completely deprotonate the polymer by rinsing the device with a base solution to turn the polymer into emeraldine base form. However, this method is not only cumbersome and tedious, but also can accelerate the degradation of the polymer. Hence, a device resetting mechanism that will calibrate the doping level of polyaniline chemiresistor to yield hysteresis-free current measurement is needed in order to develop a reliable polyaniline-based chemiresistive sensor.

### 3.4.3. Repeatability Analysis

It is essential that the conduction current measurements give repeatable results in order to develop a reliable and reusable chemiresistor based on polyaniline nanowires. Therefore, the repeatability of $I_C$ measurements of the synthesized polyaniline material is characterized. The repeatability of the device was tested by repeatedly sweeping the bias potential of the polymer from $V_O$ to $V_R$ in the forward direction only, since the $I_C$ measurements of the forward potential sweep is different from the reverse sweep as have been pointed out in the previous section. Once the potential reaches the maximum positive value ($V_R$), it was immediately returned to the initial reducing potential ($V_O$) and the same potential sweep cycle is repeated. Figure 3.11 shows the current response to five cycles of the potential scanning for the polyaniline-based chemiresistor when it was immersed in various pH buffer solutions ranging from pH 1 to 6. For pH values from 1 to 3, the current response to the potential sweep is repeatable for a number of cycles. However when the pH is greater than 4, the peak current decay was observed. The lack of reproducible $I_C$ plots in high pH solutions in terms of the peak current reduction over a number of potential scan cycles may be attributed to the low concentration of protons in the solution. When $V_B$ is held at a sufficiently negative potential, for example at -0.2 V vs. Ag/AgCl, polyaniline is fully reduced to leucoemeraldine form where almost all nitrogen atoms in the polymer chain becomes an amine nitrogen by forming covalent bonds with hydrogen atoms. It can be expected that these hydrogen atoms are being supplied by the bulk solution in the form of protons. Such protonation of the nitrogen sites in the polyaniline backbone is fast in strong acids, especially when the pH is 3 or less, due to the shear abundance of protons available in the solution for binding. However, in weak acids, the conversion of the polymer to leucoemeraldine

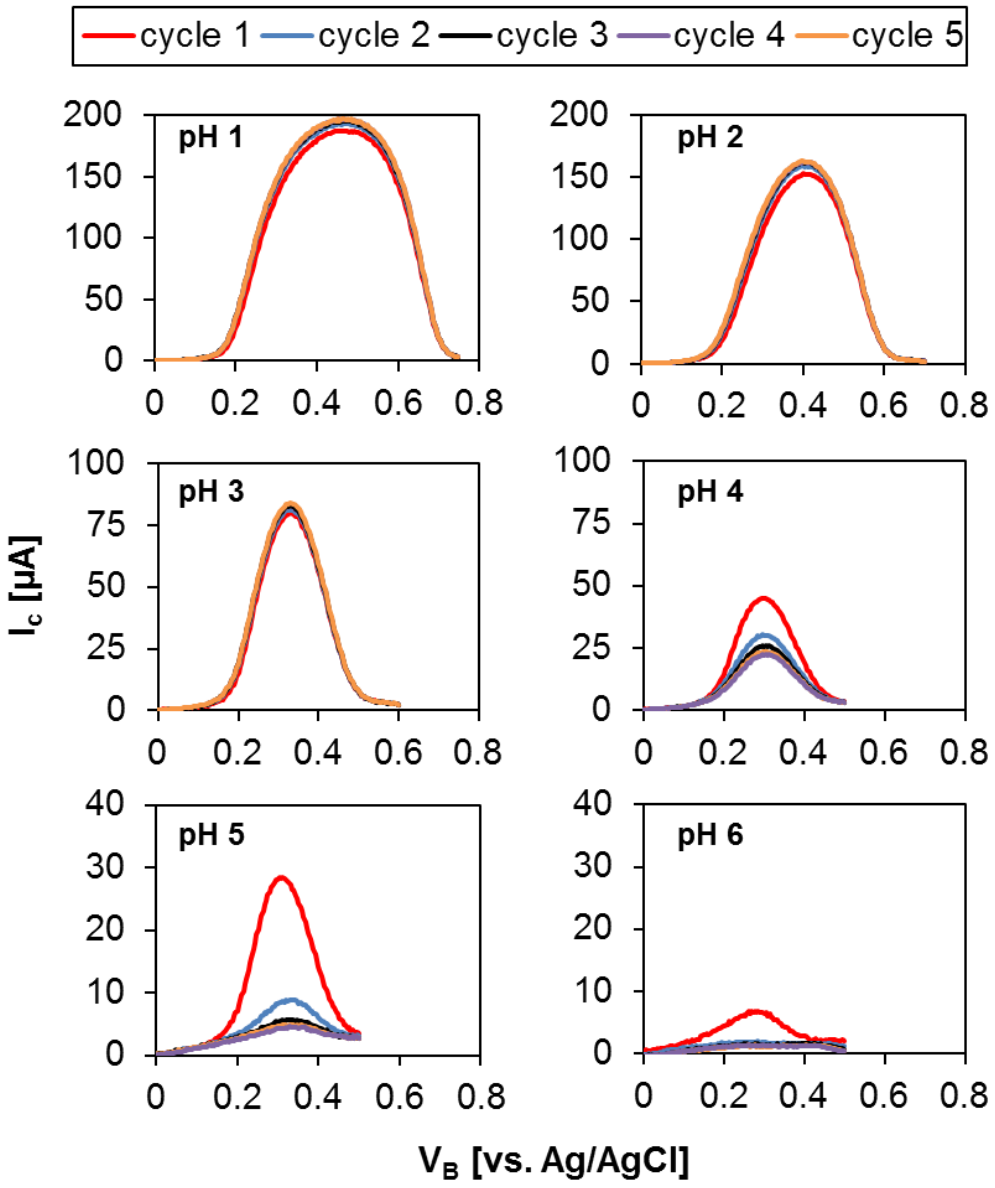


Figure 3.11. Repeatability test for conduction current response vs. potential sweep over a number of cycles in a buffer solution ranging from pH 1 to 6.

will be more difficult due to the scarcity of protons. Hence, longer time will be required to fully reduce the polyaniline at $V_R$. Furthermore, longer diffusion length of protons from the bulk solution into the polyaniline will be involved contributing to the slower reduction time. When the potential increases to a more positive value, the hydrogen atoms that are covalently bound to the nitrogen atoms lose electrons (one electron for every two nitrogen sites [28], [44]) to generate

radical cations responsible for the electrical conduction of the polyaniline. As the polyaniline is further oxidized at higher potentials i.e. at $V_O$, by losing another electron for every two nitrogen atoms, the protons are separated from the polymer backbone and liberated into the surroundings. If $V_B$ is immediately returned to $V_R$ to begin the second cycle of the potential sweep, some of the protons that are released from the polymer during the oxidation process of the first cycle will be recaptured during the reduction process in the second cycle. The rate of proton recovery between the two consecutive sweep cycles is close to unity at strong acids. However, in weak acids, not all protons that were initially bound to the polymer can be recovered in the subsequent cycles due to limitations associated with proton loss into the bulk solution. Hence, the rate of proton recovery in high pH solution is relatively low. This explains the decrease in the peak current for repeated cycling of potentials in solutions with pH values greater or equal to 4.

### 3.4.4. Degradation

As one of the major drawbacks of polyaniline, the conductivity of polyaniline nanowires is prone to degradation due to the aging effect of the polymer [132]. The degradation is related to the shortening of the conjugated polymer chain as a result of various irreversible damages to the polymer. For degradation analysis, the same potential sweep test performed in section 3.4.3 was carried out a multiple number of times. Figure 3.12 shows the normalized maximum peak values ($I_{MAX}/I_O$) of the conduction current obtained for a given pH over the number of test runs. The number of test runs corresponds to the number of times that the potential sweep test was repeated. As indicated in the plot, the conduction current of polyaniline decreases irreversibly over time and over repeated number of use.

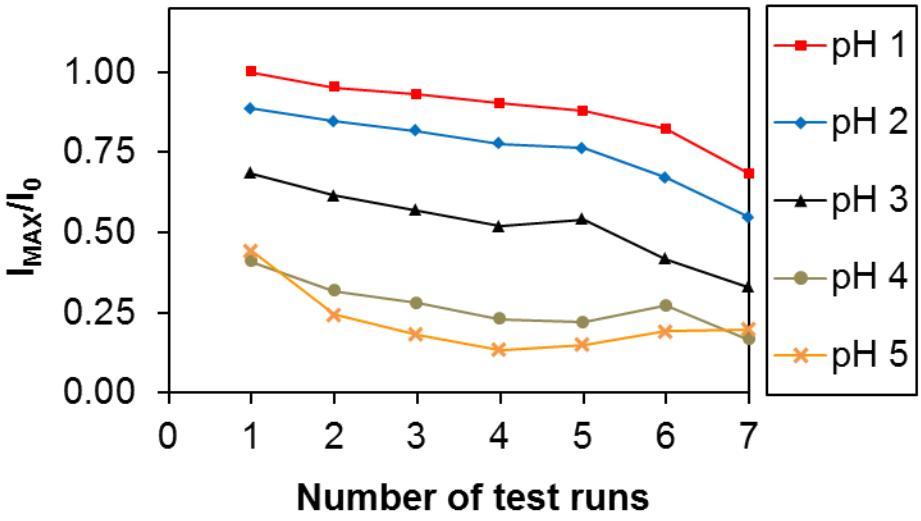


Figure 3.12. A graph illustrating a decrease in conductivity over repeated number of use. $I_0$ is the maximum $I_C$ value obtained in pH 1.

It has been reported that the decrease in conductivity is especially prominent when it is exposed to high pH solutions (e.g., pH 4 or higher) due to inevitable degradation of the polymer [122]. This degradation cannot be restored even if the polymer is re-exposed to a strong acid. Possible causes for this irreversible conductivity degradation are structural damage due to mechanical stretching or twisting of the polymer chain caused by electrostatic charge of the dopant, and damage to the polymer backbone structure caused by the generation of quinone-hydroquinone couples as a result of hydrolysis [22], [125]. Therefore, if the polyaniline nanowire-based chemiresistive sensor is to be used repeatedly, conductivity degradation must be minimized. One strategy is to introduce alkyl chains or other chemical compounds attached to the polymer to prevent hydrolysis or other types of oxidative degradation [132]. Another possible solution is to develop a self-calibration mechanism that will reset or compensate for the degradation in polyaniline nanowire material which will be investigated in the following chapter.

### 3.4.5. Polystyrene Sulfonate-Doped Polyaniline

Polyaniline is a poorly conducting polymer when the pH of the environment is 5 or greater. This severely limits the use of polyaniline in applications that require neutral pH environment, especially in biosensors. As mentioned in section 2.4, polyaniline synthesized with large molecular chain anions such as polystyrene sulfonate (PSS) can improve the conductivity of polyaniline at near neutral pH range. To experimentally verify the concept, polyaniline was electrochemically polymerized in a solution of 0.2 M aniline and 0.5 M PSS (MW ~ 70,000, Sigma-Aldrich, St. Louis, MO, USA) in 1 M $H_2SO_4$ with the same growth method described previously. The use of PSS-doped polyaniline nanowires ensured that polyaniline nanowires maintain good conductivity with the baseline conductance current ($I_C$) in the neighborhood of 50 μA with a bias potential of $V_B$ = 0.05 V and a differential voltage of $V_D$ = 20 mV at pH 6.

## 3.5. Conclusions

In conclusion, a polyaniline nanowire-based chemiresistor device was designed, fabricated, and characterized in an electrochemical cell setup. The device characterization was mainly focused on the nanowire morphology, $I_C$ vs. $V_B$ characteristics, hysteresis effect, repeatability study, and degradation analysis. The developed chemiresistor showed bias potential and pH-dependent conductivity, with increased maximum conductance as the pH is reduced. The result demonstrated the potential for the device as a polyaniline-based chemiresistive pH sensor. However, the main disadvantages of a polyaniline-based chemiresistor are the lack of reproducibility in the conduction current due to the irreversible degradation in conductivity, the presence of hysteresis in conduction current, and the loss of conductivity at near neutral pH. While much work has been recently reported to improve the conductivity of polyaniline at or near the neutral pH region [108], [113], [121], [133], [134], less attention has been paid to

address the problem of repeatability and hysteresis. Therefore, an improvement in obtaining repeatable measurements is highly required. A reliable device resetting and calibration function could improve the performance and practicality of the polyaniline-based chemiresistive sensor which yields minimum hysteresis and reproducible measurements in the conduction current.

# 4. Self-Calibration of a Polyaniline Nanowire-Based Chemiresistive pH Sensor

## 4.1. Introduction

From the previous chapter, it has been demonstrated that the polyaniline nanowire-based chemiresistor suffers from the lack of repeatability. The unrepeatable conduction current is associated with two separate phenomena: degradation and hysteresis of the polymer. In this chapter, the goal is to address these issues so that the chemiresistive sensor can produce repeatable measurements. In section 3.4.3, it was observed that, when the bias potential of the polyaniline nanowires was forward scanned repeatedly, the peak response of $I_C$ decreased as the number of the scan cycle increased in high pH solutions. It was concluded that the peak current reduction was due to the proton release from the polymer into the bulk solution and the rate of peak reduction was believed to be related to the level of pH. Such rate of peak current decrease may provide useful information in terms of measuring the pH of the unknown solution. Based on the prior observations, the objective of this chapter is to investigate the possibility of utilizing the rate of peak decrease resulting from the repeated potential scan as a measure to predict the pH level. Here, we propose a novel device calibration mechanism that produces repeatable and low hysteresis measurements in pH sensing application. The contents of this chapter is taken from the previously published journal article titled "Self-calibration of a polyaniline nanowire-based chemiresistive pH sensor," published in 2014 in *Microelectronic Engineering* [135].

## 4.2. Working Principle

The same polyaniline nanowire-based chemiresistive device described in Chapter 3 is used. All electrochemical potentials are given with respect to the silver/silver chloride (Ag/AgCl)

reference electrode unless otherwise noted. Figure 4.1(a) shows the proposed method of a device calibration and resetting mechanism.

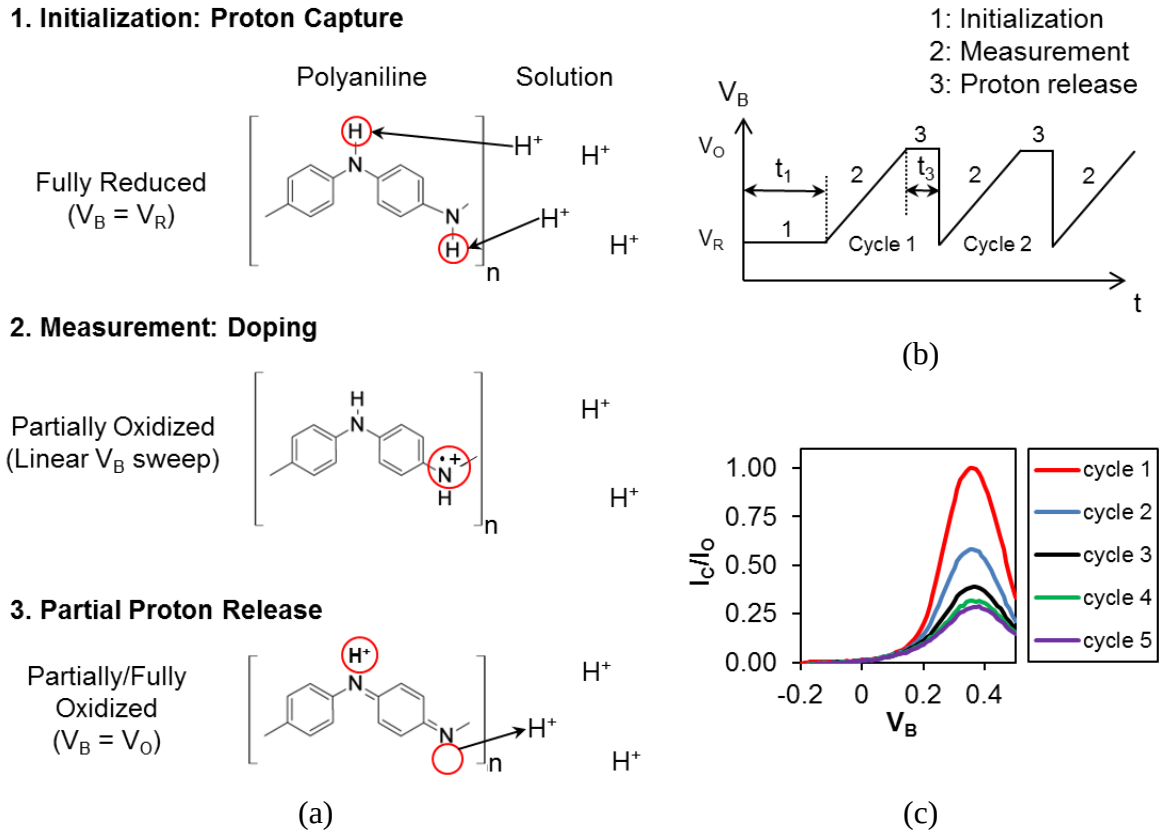


Figure 4.1. The proposed self-calibration technique: (a) a three step calibration involving initialization (resetting), measurement (doping), and partial proton release; (b) the corresponding bias potential ($V_B$) input signal, and (c) an example of the normalized $I_C$ response of the first 5 cycles of the potential scan in pH 4. $I_O$ is defined as the maximum $I_C$ in the first cycle.

The proposed method consists of the three-step calibration procedure. In the first step, $V_B$ is held at a potential sufficiently negative ($V_R$) for the duration of $t_1$ in order to convert the redox state of the polymer into the fully reduced state. This initialization step allows the protons in the solution to be covalently attached to the nitrogen binding sites of the polyaniline and hence serves as a proton capturing mechanism. In the second step, $V_B$ is linearly scanned from $V_R$ to $V_O$ and, during this process, polyaniline nanowires undergo a change in the redox state from

leucoemeraldine to partially oxidized emeraldine. As a result, polyaniline becomes conductive due to the generation of the radical cations. The conduction current continues to rise until the maximum value is reached. As $V_B$ approaches near $V_O$, the polyaniline is further oxidized past the half-oxidation point, and some amine nitrogen atoms are converted to imine nitrogens by losing protons. Consequently, the conductivity of polyaniline decreases. Once $V_B$ reaches $V_O$, the third step in the calibration procedure begins which involves holding $V_B$ at $V_O$ for a brief period of $t_3$ to allow the protons to be released into the bulk solution. This three-step calibration cycle is repeated without the initialization step. The reason for omitting the initialization step in the subsequent cycles is to create a peak current reduction between the cycles. The implemented input signal waveform for $V_B$ is shown in Figure 4.1(b) and a typical conduction current response over a repeated number of cycles is given in Figure 4.1(c). The term 'self-calibration' is used to describe the proposed mechanism since the device resetting is done electrochemically and does not require any external rinsing or calibrating solution. It should also be noted that, since only positive potential sweep is considered, the potential dependent hysteresis can be eliminated. This is further evidenced by the alignment of the peak current positions with respect to the potential as shown in the plot of Figure 4.1(c). It has been reported that exceeding the potential beyond +0.6 V vs. Ag/AgCl can be detrimental to the conduction of polymer due to over oxidation [122], [136]. Therefore $V_O$ must not exceed +0.6 V but, at the same time, should be large enough that the peak currents for pH 1 ~ 6 can be observed. This leads to the range of $+0.45\ V < V_O < +0.6\ V$ for a suitable choice for $V_O$. $V_O = +0.5$ V is typically used for the experiments. The differential voltage of $V_D = 20$ mV is used throughout the experiment.

### 4.3. Peak Current vs. Potential Sweep Characterization

The proposed method of pH sensing was tested on the fabricated chemiresistive sensor in various pH environments. The device was allowed to be initialized for $t_1$ = 1 min, and for the proton release time $t_3$ = 1 s was used. A reducing potential of $V_R$ = -0.2 V and an oxidizing potential of $V_O$ = +0.5 V were selected as the window of the potential sweep. The response of $I_C$ for the first three sweep cycles of $V_B$ is shown in Figure 4.2.

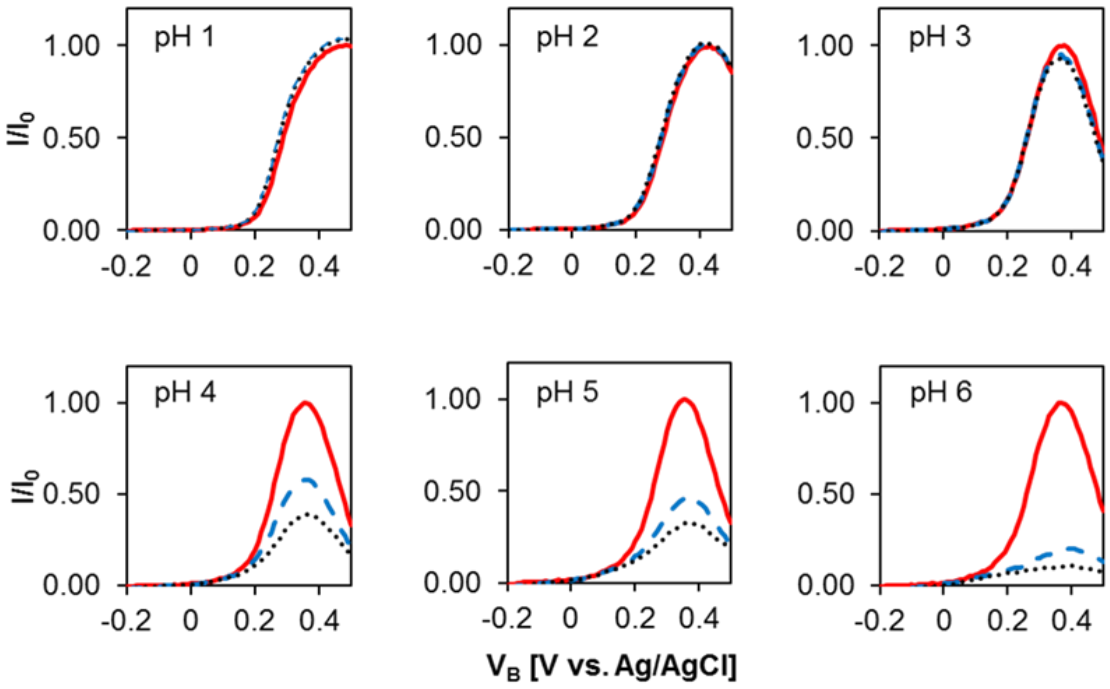


Figure 4.2. The conduction current responses of the polyaniline-nanowire based chemiresistor in pH 1 ~ 6 solutions under 3 cycles of the bias potential sweep at a scan rate of 50 mV/s. The solid, dashed, and dotted lines represents the first, the second, and the third cycle of the potential scan, respectively. The currents are normalized with respect to $I_O$ the maximum $I_C$ value in pH 1.

It is observed from the plots that the waveforms are generally reproducible over a repeated number of cycles when the pH of the solution is within the range 1 to 3. However, for the solutions with pH values of 4 or greater, the peak of the waveform decreases with the repeated potential scan. It can be further noted that, in the pH range of 4 to 6, the rate at which this peak

drops is related to the pH of the solution. For example, in the pH 4 solution, the peak current of the second scan cycle (blue dashed line) was about 55% of that of the first cycle (red solid line). In pH 6, however, the magnitude of the peak current in the second cycle is less than 20% of the first. Using this difference in the rate of peak current decay, a method could be formulated that uses the peak values of $I_C$ in the first and the second scan cycle to predict the pH of the solution.

### 4.4. pH Detection Utilizing the Ratio of Peak Current Reduction

In order to further establish the relationship between the peak $I_C$ values and the number of $V_B$ sweep cycles, the normalized maximum $I_C$ at each cycle is plotted in Figure 4.3(a). For further clarification, the plots for pH 1 – 3 are separately shown in Figure 4.3(b).

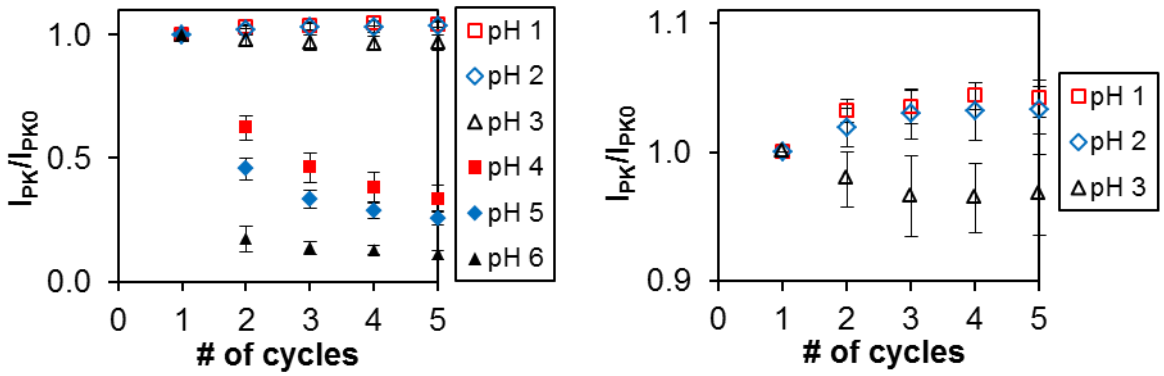


(a) (b)

Figure 4.3. The peak IC values ($I_{PK}$) of the first five cycles normalized to the $I_{PK}$ value of the first cycle ($I_{PKO}$): (a) in the range pH 1 to 6 and (b) in the range pH 1 to 3 only for a clearer distinction.

Although the $I_{PK}$ values do not show a clear distinction in the range pH 1 – 3, for higher pH values, the faster rate of decay for $I_{PK}$ can be observed as the pH of the solution increases. Here, a new variable, $P_1$, describing the peak conduction current ratio of the first and the second cycles is introduced which is defined as

$$P_1 = \frac{I_{PK}(2)}{I_{PK}(1)}, \tag{4.1}$$

where $I_{PK}(n)$ denotes the $I_{PK}$ value of the *n*-th potential sweep cycle. In other words, $P_1$ is the ratio of the peak conduction current of the second sweep scan with respect to the first. The peak ratio between subsequent cycles, for example $I_{PK}(3)/I_{PK}(2)$ would be significantly different from $P_1$ since a substantial amount of protons would have been lost during the first cycle, especially in high pH solutions. Therefore, in order to obtain $P_1$, only two cycles of the $V_B$ is required. Figure 4.4 gives a pictorial description of the two components $I_{PK}$ (1) and $I_{PK}$ (2) for obtaining $P_1$.

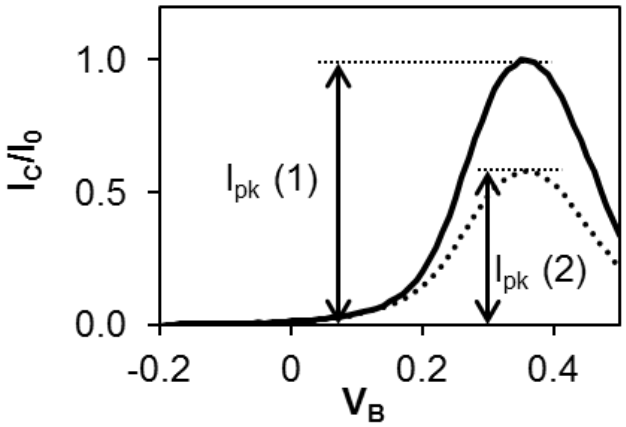


Figure 4.4. An illustration of the two components $I_{PK}$ (1) and $I_{PK}$ (2) for obtaining $P_1$. The solid and the dashed lines correspond to the $I_C$ responses to the first and the second $V_B$ scan cycles, respectively.

Using the $P_1$ value as a measure for pH sensing, the proposed method was applied to the polyaniline-based chemiresistive pH sensor and the obtained $P_1$ values for each pH solution are plotted as shown in Figure 4.5.

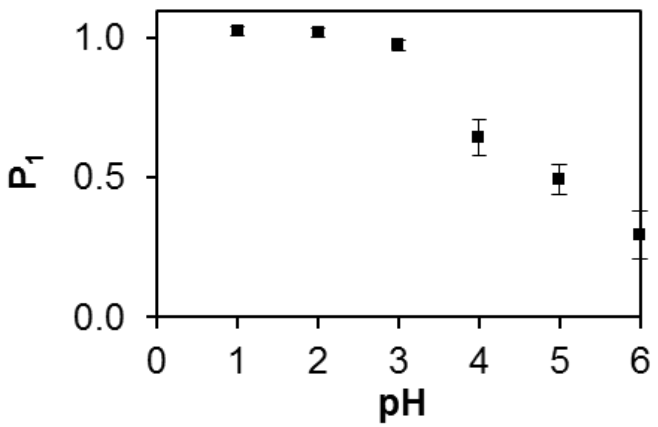


Figure 4.5. The measured $P_1$ values from the polyaniline-based chemiresistor for the given buffer solutions with pH 1 to 6.

The solutions in the pH range from 4 to 6 give distinct $P_1$ values, and thus, the pH of the solution could be determined in this pH range. However, in stronger acids in the pH range between 1 and 3, the $P_1$ values are all close to unity. Therefore, low pH detection with high resolution is difficult with this variable alone. This is expected as the peak values do not change drastically over a number of scan cycles in low pH solutions (e.g., pH 1 – 3) as indicated in Figure 4.3(b). Therefore, a different pH sensing mechanism needs to be implemented for a low pH range detection.

### 4.5. pH Detection with $I_C$ at $V_B$ = +0.5 V

As shown in Figure 4.2, although the $I_C$ curves in pH 1 – 3 solutions exhibit a negligible peak current drop over repeated cycles, the values of $I_C$ at $V_B$ = +0.5 V are significantly different between pH levels of 1 – 3. This difference in $I_C$ at $V_B = V_O$ is illustrated in Figure 4.6. For example, at pH 1, the value of $I_C/I_O$ at $V_B$ = +0.5 V is similar to the peak value while at pH 3, the value of $I_C/I_O$ at $V_B$ = +0.5 V is approximately 42% of the peak value.

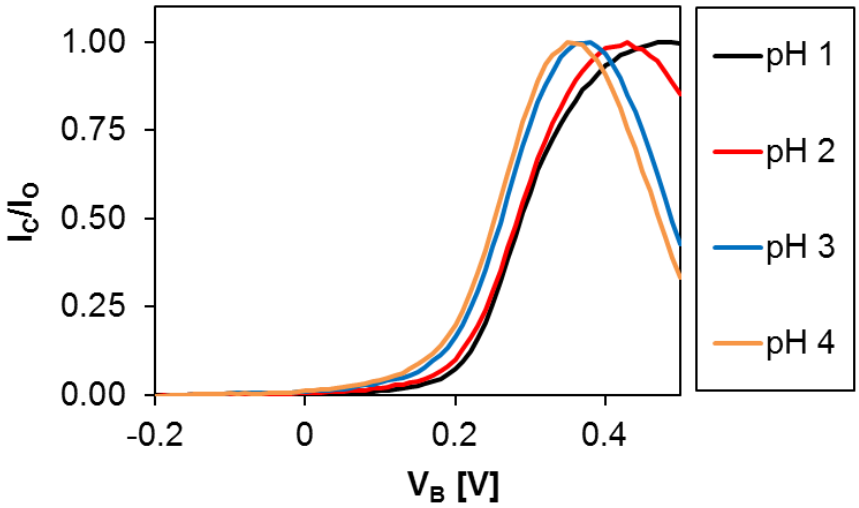


Figure 4.6. $I_C$ curves for pH 1 – 4 normalized to their corresponding $I_O$ value: the plot shows different $I_C/I_O$ values when $V_B$ = +0.5 V.

Based on this observation, another variable $P_2$ can be defined as

$$P_2 = \frac{I_C(V_O)}{I_{PK}(1)}, \tag{4.2}$$

where $I_C(V_O)$ is the value of $I_C$ at $V_B = V_O$, and in this experiment, $V_O$ was chosen to be +0.5 V. Therefore, $P_2$ represents the ratio of the conduction current response at $V_B$ = +0.5 V with respect to the peak value of the $I_C$ response in the first scan cycle. For measuring $P_2$, a multiple $V_B$ scan cycle is not required since both components, $I_C$ and $I_{PK}$, can be obtained from the first cycle of the potential scan alone. Figure 4.7 illustrates the two components $I_C(V_O)$ and $I_{PK}(1)$ for determining the values of $P_2$ from a low pH solution (pH 1 – 4), and using this formula, the obtained $P_2$ values of various pH buffer solutions can be plotted as a function of pH as shown in Figure 4.8.

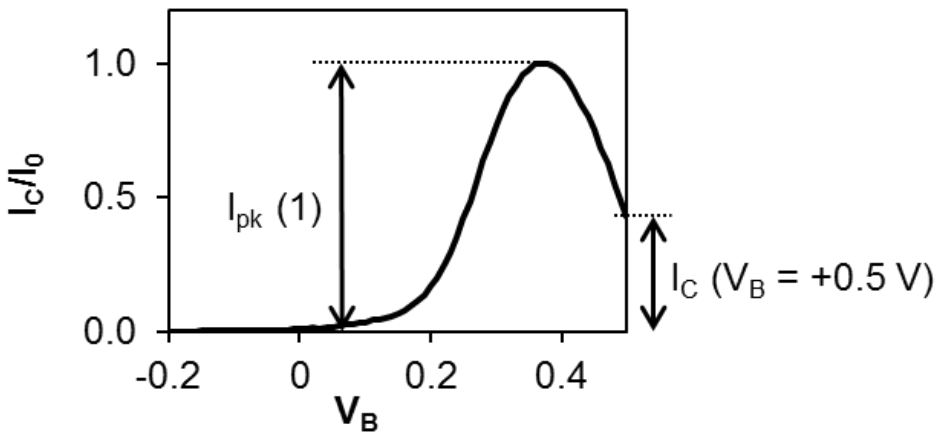


Figure 4.7. The description of the two $I_C$ components measured for calculating $P_2$: the peak value, $I_{PK}(1)$, and the value at $V_B$ = +0.5 V, $I_C$ ($V_B$ = +0.5 V).

The plot of $P_2$ in Figure 4.8 shows that, for a low pH range (pH 1 – 3), distinguishable $P_2$ values are obtained, which allows the pH sensing capability in this pH range. However, as the pH of a solution increases, $P_2$ converges to the same value which no longer can distinguish the different pH levels. Therefore, unlike $P_1$ that is better suited for high pH detection, $P_2$ is optimized for low pH sensing.

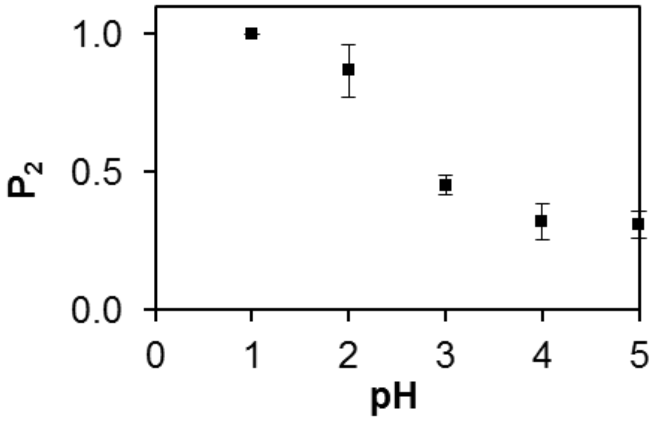


Figure 4.8. The measured $P_2$ values from the polyaniline-based chemiresistor for the given buffer solutions with pH 1 to 6.

### 4.6. Repeatability Test

To demonstrate that the values $P_1$ and $P_2$ are reproducible over a repeated number of uses even as the conductivity degradation of polyaniline continues, the repeatability test was performed on the developed polyaniline nanowire-based chemiresistor. For each test run, the values $P_1$ and $P_2$ were measured by exposing the sensor to each buffer solution ranging from pH 1 to 5. The test was repeated five times. For each pH solution, the device was initialized at $V_R$ = -0.2 V followed by two cycles of $V_B$ scan from -0.2 V to +0.5 V. Afterward, the values of P1 and P2 were plotted as a function of the number of test runs as shown in Figure 4.9.

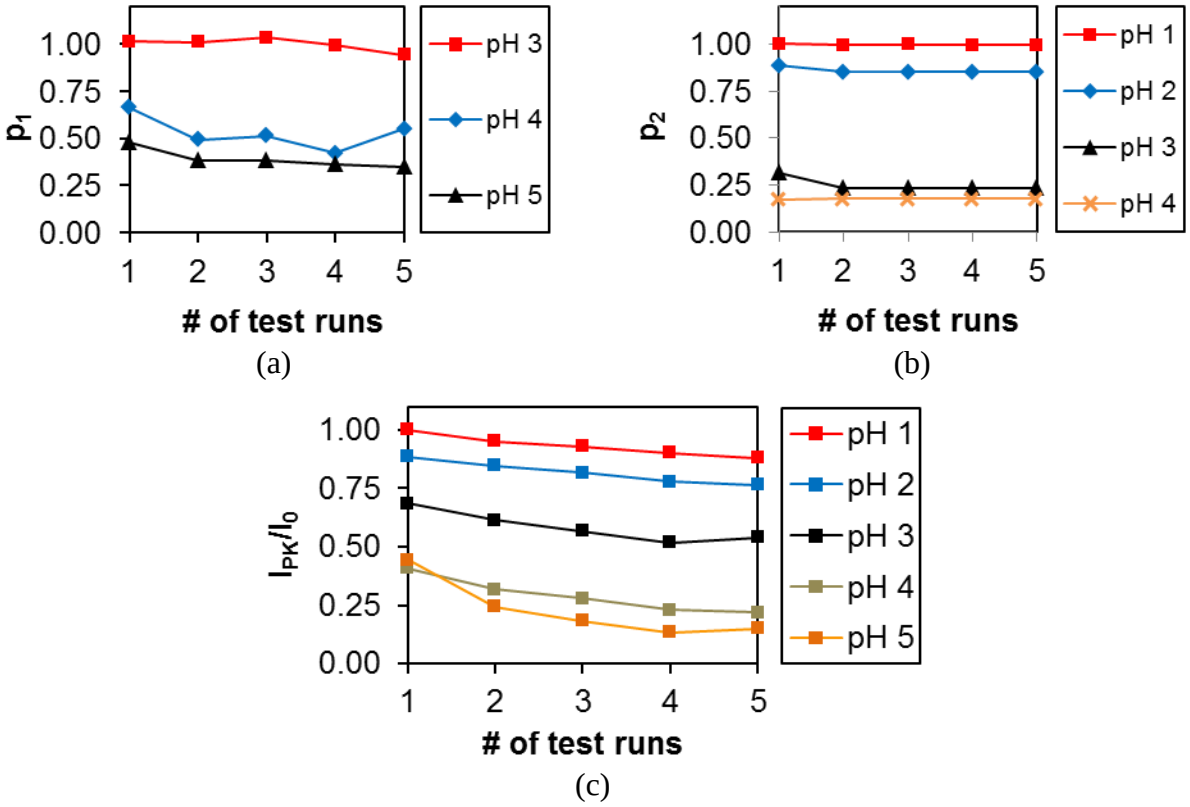


Figure 4.9. Repeatability test showing the values of: (a) $P_1$ in the pH range of 3 ~ 5; (b) $P_2$ in the pH range 1 ~ 4, and (c) the normalized peak conduction current over five repeated tests.

Figure 4.9(a) and Figure 4.9(b) show that the $P_1$ and $P_2$ values were reproducible, and the influence of the conductivity degradation of polyaniline on $P_1$ and $P_2$ was less significant. In comparison, Figure 4.9(c) shows that, during the same test runs, the peak conduction current has decreased, which confirms that the conductivity degradation has occurred. Therefore, this result demonstrates that the proposed self-calibration technique improves the repeatability in pH sensing by utilizing $P_1$ and $P_2$ measurements from the bias potential scan cycles.

It is well-accepted that the electrochemical potential at which the second redox reaction in the cyclic voltammetry curve occurs, which is related to the conversion from emeraldine to pernigraniline, depends on the pH of the solution. In fact, the peaks associated with the second redox process in the CV curve shift to the more positive potential as the pH decreases [28]. As a result, the 'potential window' where polyaniline becomes conducting is broader for low pH solutions than that for the less acidic environment [44]. This allows us to use $P_2$ values to differentiate the pH of the solutions especially in the low pH range. For example, polyaniline exhibits maximum conductivity at $V_B$ = +0.5 V in pH 1 while it is nearly insulating at this potential if the pH of the solution is 4 or higher.

## 4.7. Conclusions

In this chapter, a new approach to obtain a reproducible conduction current measurement covering a wide range of pH has been developed and demonstrated for a polyaniline nanowire-based chemiresistor. The presented self-calibrating mechanism avoids the need to reset the device via a rinsing or a dedoping step. Two parameters have been suggested for measuring the pH of an unknown solution: $P_1$, the ratio of the peak current values of the two consecutive potential sweep cycles, and $P_2$, the ratio of the current at $V_B = V_O$ with respect to the peak current. The variable $P_1$ is more optimized for measuring high pH range (pH 3 to 6) while $P_2$ is

optimized for measuring low pH range (pH 1 to 3). By sweeping the potential in one direction from the fully reduced state to the oxidized state, the hysteresis effect which is dependent on the direction of the potential scan has been eliminated. The results indicate that the two parameters $P_1$ and $P_2$ are minimally influenced by the declining of the polyaniline conductivity caused by the polymer degradation. The demonstrated technique enables a calibration-free and reusable polyaniline nanowire-based pH sensor in acidic environment. This technology has potential applications in continuous monitoring of chemical and gas species, or reusable bio-analytical devices.

# 5. A Selective Sensor Based on Polyaniline Nanowires with Catalysts

## 5.1. Introduction

The two most critical issues with regards to chemiresistive sensors are the lack of reproducibility and selectivity. In the previous chapter, improvements in repeatable and low hysteresis measurements were made by implementing a device calibration mechanism which utilizes the electrochemical conversion of the polymer's redox state. However, the lack of selectivity in polyaniline nanowire-based chemiresistors is another limitation that requires much attention. Aside from being pH-sensitive, the conductivity of polyaniline does not respond well to most chemicals. In other words, a polyaniline-based chemiresistor is most sensitive to protons ($H^+$) and hydroxyl ions ($OH^-$). In an effort to enhance the selectivity in polyaniline-based chemiresistors, a novel technique utilizing catalysis is proposed. In order for the polyaniline-based chemiresistors to respond selectively to target chemical species, nanoparticle-based catalysts are incorporated into the polymer nanowires whose catalytic activities would selectively influence the conductivity of the chemiresistors. This chapter discusses the basic principles and the method for modifying the polyaniline nanowires with metal and oxide based nanoparticles that behave as catalysts for achieving selective chemiresistive detection. As a demonstration of this concept, a selective detection of hydrogen peroxide using polyaniline nanowires modified with silver nanoparticles is presented in the later part of this chapter.

## 5.2. Basic Principle of a Catalyst-Assisted Chemiresistive Sensor

Since the conductivity of polyaniline is sensitive to pH, the basic principle for enhancing the selectivity in a polyaniline-based chemiresistor is to influence a pH change near the polyaniline nanowires caused by a selective chemical reaction initiated of the target analyte.

Since catalysis is specific to the chemicals involved, a catalytic reaction can provide selectivity to polyaniline-based chemiresistors as long as the pH can be altered as a result of such catalysis. Certain nanoparticles are known to enhance catalytic activities due to their large surface area and their ability to lower the activation energy, resulting in an increased reaction rate. Figure 5.1 illustrates the basic concept of a catalyst-based selective chemical detection with a pH sensitive polyaniline-based chemiresistor.

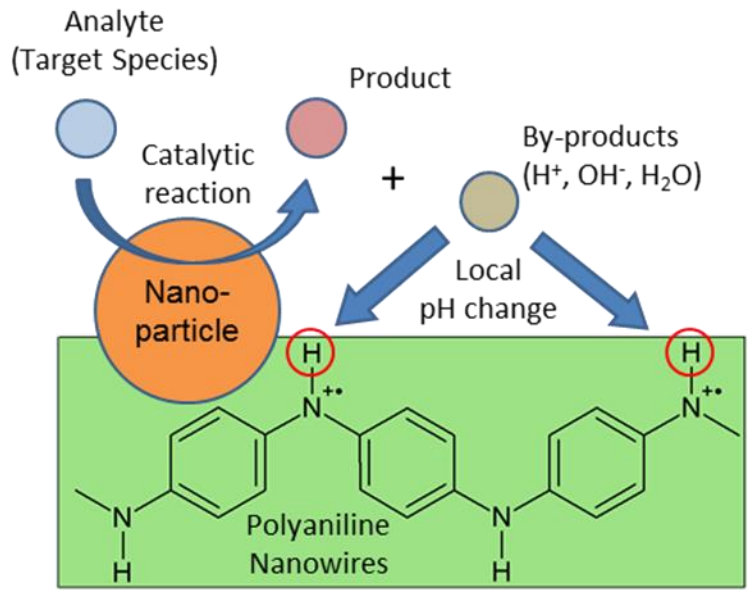


Figure 5.1. Schematic diagram illustrating the concept of catalyst-assisted selective detection of target analyte using nanoparticles acting as catalysts.

When the target molecular species (analyte) make contact with the nanoparticle, the analyte is consumed to generate a product. If protons, hydroxyl ions, or other molecules are also generated as by-products, a local pH change caused by such by-products can be detected by measuring the resistance of the chemiresistor based on polyaniline nanowires. Since the catalysis increases the rate of reaction, the change in the resistance of the catalyst-modified polyaniline nanowires will be much greater than the pristine polyaniline nanowires without nanoparticles.

Hence, a larger conductance change would be observed compared to the unmodified chemiresistor. As an example, Figure 5.2 further describes the case when the resistivity of the polyaniline-based chemiresistor is increased due to the formation of hydroxyl ions as a by-product of the catalysis.

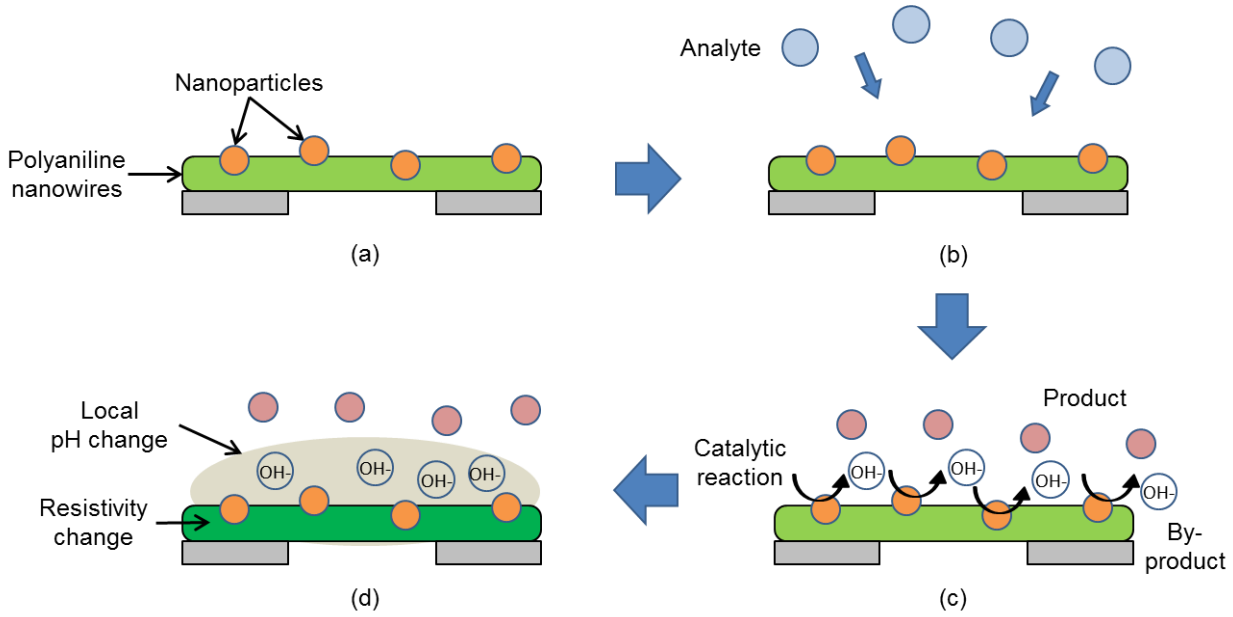


Figure 5.2. Illustration of the selective analyte detection based on a catalytic effect: (a) a polyaniline nanowire-based chemiresistor with catalytic nanoparticles; (b) approaching of the analytes to the surface of the chemiresistor; (c) catalytic reaction and the generation of by-products (e.g., hydroxide ions), and (d) the resistivity change of polyaniline chemiresistor due to the local pH change.

As the catalytic reaction is initiated by the approaching of the analyte (Figure 5.2(b)), hydroxide ion by-products are formed in the vicinity of the polymer nanowires (Figure 5.2(c)). As a result of an increase in the hydroxide ion concentration near polyaniline, the pH is locally increased which influences the polyaniline nanowires by raising its resistivity (Figure 5.2(d)).

There are several advantages of the catalyst-assisted chemiresistive sensors. First, each nanoparticle possesses unique catalytic activities that are different from other types of nanoparticles. Hence, the use of catalysts adds selectivity to the sensors. Second, as long as the

reacting chemical species is present, the catalytic reaction continues to occur and consequently amplifies the signal that can be picked up by the chemiresistor. Third, since the nanoparticles are not consumed, the rate of reaction will only be determined by the concentration of the analyte. Other advantages of using nanoparticle-based catalysts are minimum degradation, and long shelf life, among others. However, some disadvantages also exist such as the dependence of the catalytic activity on various factors, including the pH and the temperature of the environment, and the requirement of the catalytic reaction to produce either protons or hydroxyl ions in order to cause pH change in the local proximity of the polyaniline-based chemiresistor. In this work, an appropriate baseline pH is chosen to circumvent one of the disadvantages as a starting point.

## 5.3. Experimental Methods

In order to prove the concept of catalyst-enabled selective detection with polyaniline-based chemiresistors, several nanoparticles and selected chemicals were experimentally tested. It was desired to use a neutral pH solution as the background environment since a small amount of protons or hydroxyl ions can significantly shift the pH of the environment. Moreover, most catalytic reactions are pH-dependent and favor neutral pH. Similar environment is also favored by the biological catalysts such as enzymes which may be utilized in biosensors.

### 5.3.1. Preparation of Catalyst Nanoparticles

Four types of nanoparticles well-known for their catalytic activities are chosen as catalysts: silver (Ag), iron (III) oxide ($Fe_2O_3$), nickel (Ni), and titanium dioxide ($TiO_2$). The nanoparticles are incorporated into the polyaniline nanowires by placing a droplet of the nanoparticles dispersed in aqueous solution. Each nanoparticle-suspended solution was prepared by adding 1 mg/ml of nanoparticles and 1 mg/ml of sodium dodecyl sulfate (SDS) into 10 ml of deionized water and sonicating for 1 hour. While some nanoparticles, such as silver, iron oxide, and

titanium dioxide were quite stable after ultra-sonication, suspension of other nanoparticles, such as nickel, were not stable and the nanoparticles eventually settled to the bottom after a short period of time. After the nanoparticle dispersion, a droplet containing the suspended nanoparticles was placed on the polyaniline nanowires to physically attach the nanoparticles to the polymer surface. Figure 5.3 shows the image of the various nanoparticles suspended in deionized water.

After polyaniline nanowires have been synthesized, a pipette was used to drop approximately 5 µl of the nanoparticle-dispersed liquid onto the surface of the polyaniline nanowires. The device was placed on the hotplate to allow the liquid to dry at 50 °C. A total of three drops were placed on the sensing area of the polyaniline-based chemiresistor to ensure sufficient amount of nanoparticle deposition.

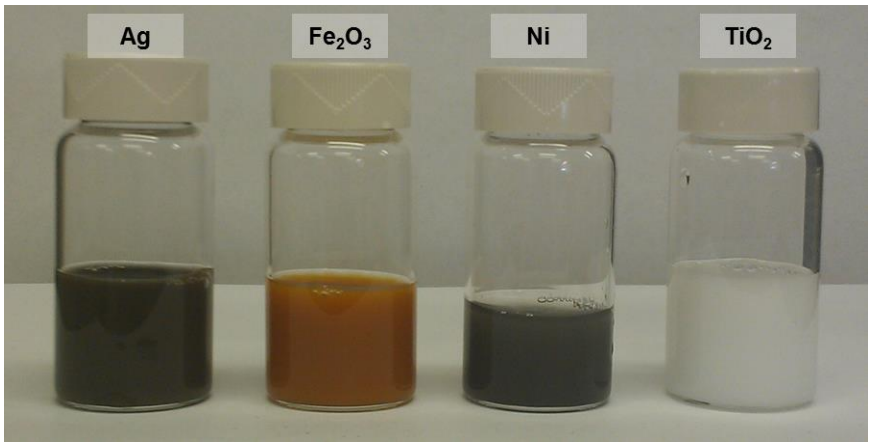


Figure 5.3. Four different nanoparticles, silver, iron oxide, nickel, titanium dioxide, with concentration of 1 mg/ml with 1 mg/ml of SDS suspended in aqueous solution.

### 5.3.2. Background pH Environment

Most catalytic reactions are pH-dependent and are more effective in a higher pH environment rather than in a low pH solution. Therefore, a high pH environment is a preferred background pH for the catalyst-modified chemiresistive sensor. However, the conventional

polyaniline chemiresistor synthesized in sulfuric acid is non-conducting for pH > 6 and cannot detect a pH change in a high pH environment (pH > 6) even if catalytic reaction occurs. This limits the use of high pH solutions as the background reference solution. Therefore, modifying polyaniline nanowires to have enhanced conductivity at elevated pH is needed. Since it is known that the poly(sodium 4-styrenesulfonate) (PSS)-doped polyaniline shows an improved conductivity at near neutral pH as described in section 3.4.5, this material was adopted for the catalyst-assisted sensing of chemical species. The polyaniline nanowires doped with PSS anions resulted in an improved conductivity showing a conductance current of approximately 50 μA at pH 6. Therefore, pH 6 was chosen as the background environment under which the polyaniline-based chemiresistive sensors were operated.

## 5.4. Selecting Target Chemical Species

To demonstrate that nanoparticles can indeed produce catalytic reaction and promote selectivity of a polyaniline-based chemiresistive sensor, common laboratory chemicals were chosen as test target species to verify whether each catalytic nanoparticle group responds differently to a given species of interest. Four different chemicals, hydrogen peroxide ($H_2O_2$), ethanol ($C_2H_6O$), methanol ($CH_3OH$), and acetone ($(CH_3)_2CO$) were tested as analyte.

In a typical experiment, the polyaniline chemiresistive sensor was immersed in 10 ml of a pH 6 buffer solution with $V_B$ = 0.05 V and $V_D$ = 20 mV. The bias potential was chosen so that the maximum DC conduction current was observed. After the current was stabilized to a constant value, an incremental volume of test analyte was injected with a pipette and the container was gently stirred for about 5 seconds.

Figure 5.4 shows the conduction current response of the polyaniline-based chemiresistive sensors modified with different types of nanoparticles when each sensor was exposed to 100 µl of 30% $H_2O_2$ (~100 mM).

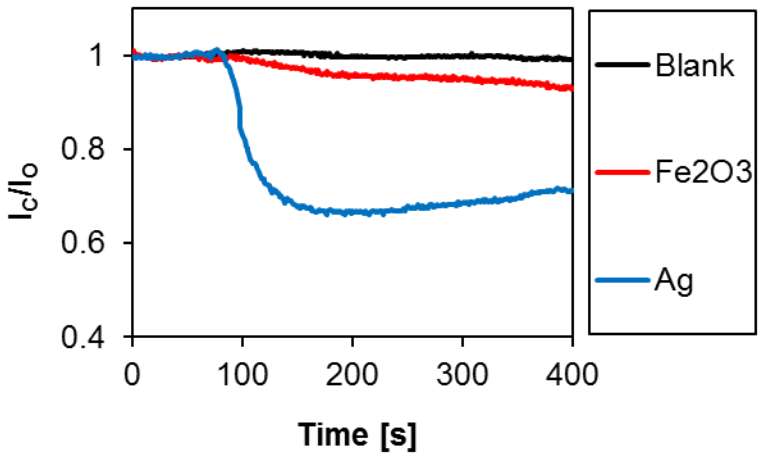


Figure 5.4. Conduction current response ($I_C$) of the polyaniline-based chemiresistive sensors to an exposure to 100 mM of $H_2O_2$. Three types of chemiresistors were tested: polyaniline nanowires without any modification (blank), with iron oxide nanoparticles ($Fe_2O_3$), and with silver (Ag) nanoparticles.

The graph indicates that the chemiresistive sensor modified with Ag nanoparticles resulted in the largest current response. $Fe_2O_3$-modified chemiresistors also produced a weak form of catalytic activity which was not as effective as silver. Furthermore, the $I_C$ response of Ag-modified sensor resulted in a large initial current drop followed by a gradual rise. This can be explained by mass transport-limited reaction where the abundance of hydrogen peroxide present near the sensing area was quickly consumed creating a large initial current drop followed by the gradual restoring of the current due to the reduced reaction rate limited by the rate of mass transport of the reactant. On the other hand, the $I_C$ response of the $Fe_2O_3$-modified sensor continues to drop which may be explained by the electron transfer rate being slower than the mass transfer rate. The graph also confirms that, without the aid of catalysts, the conduction

current does not experience significant current drop. This result gives evidence that catalytic nanoparticles such as Ag and $Fe_2O_3$ can generate selective catalytic activities for the detection of $H_2O_2$ species. To further demonstrate the selectivity of the nanoparticles, the device modified with nanoparticles was exposed to various chemicals as shown in Figure 5.5.

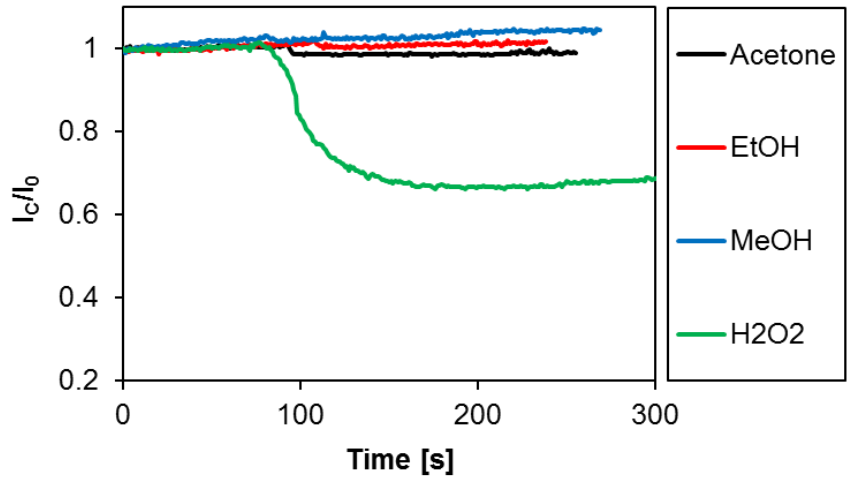


(a)

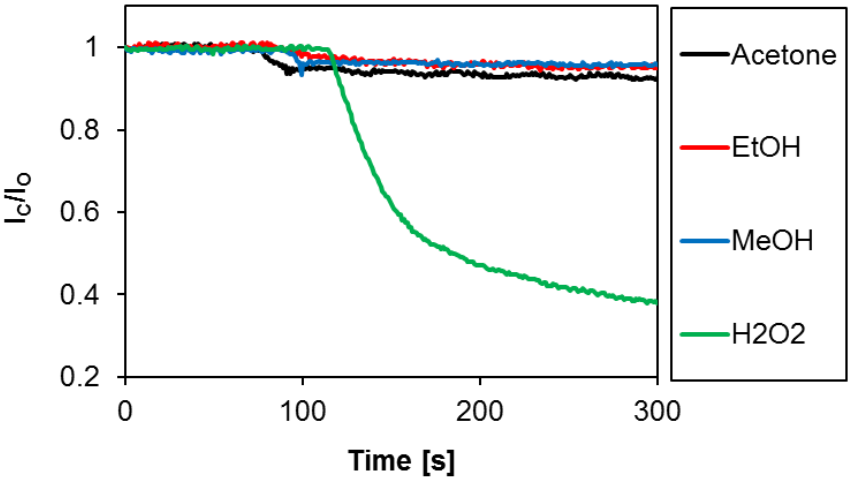


(b)

Figure 5.5. Comparison in response to acetone, ethanol (EtOH), methanol (MeOH), and hydrogen peroxide (30% $H_2O_2$): (a) 100 µl of each analyte exposed to a silver nanoparticle-modified polyaniline-based chemiresistor and (b) 400 µl of each analyte exposed to a $Fe_2O_3$-modified polyaniline-based chemiresistor.

Figure 5.6 shows the current response of the $Fe_2O_3$/polyaniline-based chemiresistive sensor when the device was exposed to varying amounts of $H_2O_2$. As shown in the graph, higher concentration of target sample results in steeper current drop probably due to the higher rate of catalytic reaction determined by the amount of target species present near the nanoparticles. When 1 mL of deionized water was injected to the sample, little change in $I_C$ is observed confirming the selectivity of the sensor in the detection of $H_2O_2$ given by the catalytic nanoparticles.

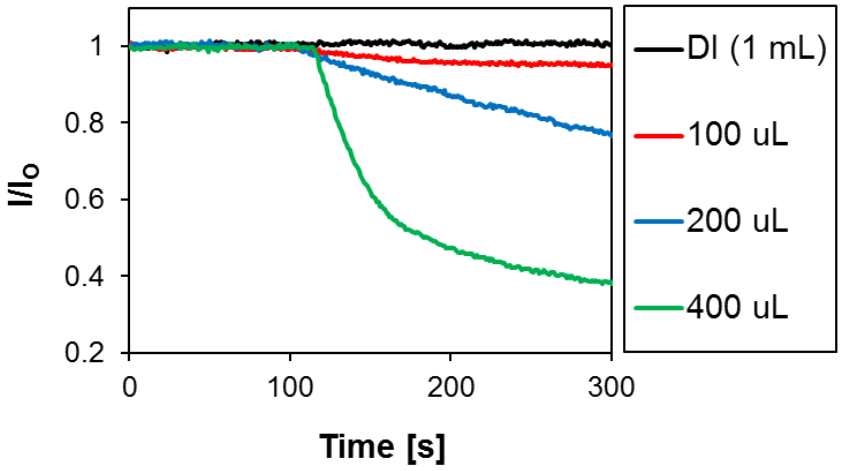


Figure 5.6. Conduction current ($I_C$) response of the $Fe_2O_3$/polyaniline-based chemiresistive sensor to an exposure to 100, 200, and 400 µl of 30% $H_2O_2$. The response of the sensor to 1 ml of deionized water is also shown to confirm selective detection $H_2O_2$ as a result of catalytic reaction.

## 5.5. Selective Detection of Hydrogen Peroxide using Silver Nanoparticles as Catalysts

This section presents the implementation and characterization of a hydrogen peroxide sensor using catalytically modified polyaniline nanowires. The contents of this section was taken and modified, from the original article published in the *Journal of the Micromechanics and Microengineering* [137].

### 5.5.1. Motivation

As mentioned in the previous section, a catalyst-based approach has been suggested in this chapter in order to improve the selectivity of a polyaniline nanowire-based chemiresistors. To demonstrate the proposed concept, silver nanoparticles have been chosen as catalysts for the selective detection of hydrogen peroxide. Accurate sensing of $H_2O_2$ is of great importance in many areas including pharmaceutical, clinical, and environmental applications [138]. $H_2O_2$ also plays a crucial role in living organisms in terms of regulating various biological functions and signaling. There are several commonly used methods for detecting $H_2O_2$ in a solution phase including fluorimetry, chemiluminescence, fluorescence, and spectrophotometry. However, the equipment used in these methods is bulky, complex, expensive, and can be time consuming. On the other hand, an electrochemical detection method can offer a simple, inexpensive, rapid, sensitive, and miniaturizable alternative in accurate $H_2O_2$ measurements. Recently, it has been reported that silver nanoparticles (AgNPs) exhibit catalytic reaction with hydrogen peroxide causing the production of hydroxyl ions and water [139], [140]. The proposed method utilizes this catalytic activity of the AgNPs to influence the conductivity of polyaniline nanowires by attaching the catalysts onto the surfaces of polyaniline-based sensing area.

### 5.5.2. Working Concept

A pictorial description of the proposed concept has been given previously (see Figure 5.1 and Figure 5.2). When the target analyte, i.e., $H_2O_2$ molecules make contact with the silver nanoparticles, the following catalytic reduction of $H_2O_2$ has been suggested to occur [139], [140]:

$$H_2O_2 + e^- \leftrightarrow OH_{(ads)} + OH^- \quad (5.1)$$

$$OH_{(ads)} + e^- \leftrightarrow OH^- \quad (5.2)$$

$$2OH^- + 2H^+ \leftrightarrow 2H_2O \quad (5.3)$$

The generation of the byproducts such as OH- and $H_2O$ on the surfaces of the AgNPs lowers the proton concentration, and therefore increases the pH near the close proximity of the polyaniline nanowires. Since the conductivity of polyaniline is highly dependent on the pH level of the environment, with its conductivity increasing as the pH decreases, polyaniline responds to this pH change by reducing the conduction current flowing through the polymer nanowires.

Figure 5.7 illustrates the schematic configuration of a polyaniline-based chemiresistive sensor for measuring the conduction current through the nanowires. A reference electrode maintains the electrochemical potential of the polyaniline at a fixed voltage $V_B$ in order to stabilize the conduction current. A small differential voltage of $V_D$ generates a DC current flow between the two working electrodes (from WE2 to WE1) via the polyaniline nanowire network.

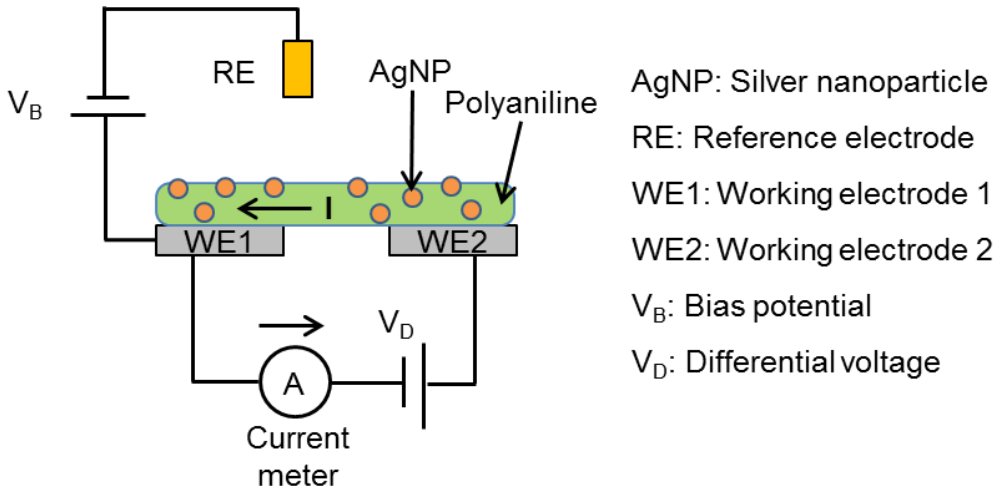


Figure 5.7. A schematic diagram of a polyaniline-based chemiresistor: the electrochemical potential of polyaniline is controlled with $V_B$ while a conduction current through the polyaniline is induced by applying a differential voltage $V_D$.

### 5.5.3. Experimental Methods

Device Design and Fabrication - The fabricated sensor design is depicted in Figure 5.8. The device fabrication technique was similar to as described in Chapter 3.2. The sensing device consists of two gold working electrodes separated by a 5 µm gap and an on-chip silver/silver chloride (Ag/AgCl) reference electrode. The Ag/AgCl reference electrode was fabricated by electroplating the 400 µm × 400 µm area of gold electrode with Cyless II RTU silver solution (Technic Inc.). A silver layer was formed by applying a cathodic current of 0.5 mA/cm$^2$ to the electrode for 30 minutes. Afterward, AgCl layer was deposited over the electroplated silver by supplying an anodic current of 0.5 mA/cm$^2$ in 1 M KCl solution for 30 minutes. A passivation layer, which was lithographically patterned using a positive photoresist (Shipley S1827) followed by hard baking at 180 °C to stabilize the resist layer, defines an opening at the two working electrodes (200 µm × 500 µm) where polyaniline is to be grown in order to bridge the two electrodes.

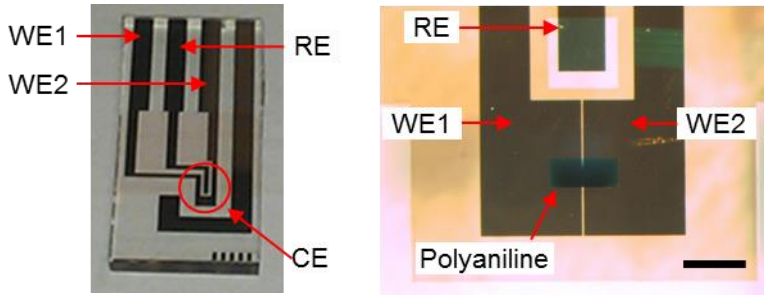


(a) (b)

Figure 5.8. Images of the fabricated device: (a) the electrode design showing Ti/Au (10 nm/50 nm) layer on glass substrate and (b) a magnified image of the sensing area (the circled area from part (a)) with 5 µm gap between the working electrodes. The polyaniline area is 200 µm x 500 µm. Scale bar is 500 µm.

Nanowire Synthesis - The polyaniline nanowires were electrochemically synthesized in a solution containing 0.2 M aniline, 0.05 g/ml of poly(sodium 4-styrenesulfonate) (PSS, MW ~

70,000, Sigma-Aldrich), and 1 M sulfuric acid. PSS is a large molecular weight polymeric anion which has been reported to extend the conductivity of polyaniline nanowires to the neutral pH range when incorporated during the synthesis process [121], [141]. An anodic current density of 1 $mA/cm^2$ was allowed to flow through the two working electrodes for 10 minutes, which caused the oxidation of aniline monomers and subsequently resulted in the formation of polyaniline nanowires.

AgNP Dispersion and Deposition - A liquid suspended silver nanoparticle (AgNP) dispersion was prepared by adding 1 mg/ml of silver nanoparticles (particle size < 100 nm, Sigma-Aldrich) and 1 mg/ml of sodium n-dodecyl sulfate (SDS, Alfa Aesar) into deionized water, and the mixture was sonicated for at least 3 hours. For the deposition of the silver catalysts onto the polyaniline nanowires, several drops of the silver nanoparticle suspended liquid was placed drop-wise on the polyaniline area with each droplet being 1 µl in volume. For the deposition of multiple droplets, each drop was completely dried before the next droplet was placed on the surface of the device.

$H_2O_2$ Detection Experiments - For measuring the $H_2O_2$ concentration, the electrochemical potential of the polyaniline chemiresistor was maintained at $V_B$ = +0.1 V vs. Ag/AgCl to optimize the polymer's conductivity. The potential difference between the two working electrodes was fixed at $V_D$ = 20 mV. The background solution used was a pH 5 buffer made with appropriate portions of 0.1 M $KH_2PO_4$ and 0.1 M $NaH_2PO_4$ in deionized water. After stabilizing the conduction current through the polyaniline in the background solution, the device was quickly immersed into the pH 5 buffer containing $H_2O_2$ of a given concentration. The change in the conduction current was measured with a current meter based on a feedback operational amplifier circuit.

### 5.5.4. Results and Discussion

Comparison between Polyaniline Nanowires with and without AgNP Catalysts - Figure 5.9 compares the current responses of the polyaniline-based chemiresistors with various amounts of AgNP deposition when the sensors were exposed to 20 mM of $H_2O_2$. Given the average particle size and the density of the silver nanoparticles, a rough estimate of the number of nanoparticles suspended in 1 µl of liquid dispersion can be calculated. It is also assumed that the number of AgNPs deposited on the surfaces of the polyaniline is linearly proportional to the number of drops placed on the device. The total number of the estimated AgNPs deposited on the polyaniline area (200 µm × 500 µm) is shown in the legend which corresponds to 0, 2, 3, and 4 drops of the liquid dispersion, as listed in the legend from top to bottom.

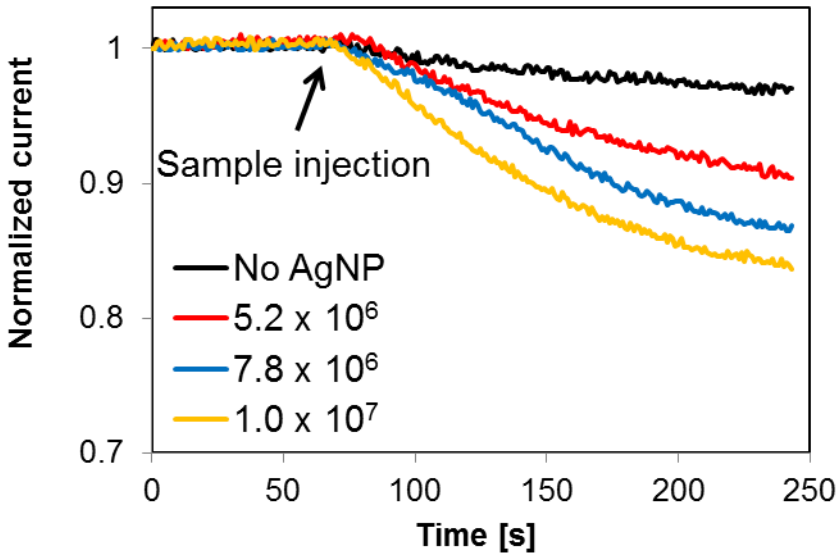


Figure 5.9. The conduction current response of a polyaniline-based chemiresistive $H_2O_2$ sensor with various amounts of AgNPs deposited on the polyaniline area. The legend indicates an estimated number of AgNPs on the sensing area. For each curve, the sensor was exposed to 20 mM of $H_2O_2$.

When silver catalysts are absent in the vicinity of polyaniline nanowires, a direct interaction between $H_2O_2$ species and polyaniline causes a small decrease of about 3% of the total conduction current through the polymer as indicated in the plot with no AgNP. Since $H_2O_2$ is an oxidizing agent, polyaniline is expected have a slight reaction to $H_2O_2$ by converting its redox state to a more oxidized form which may have an impact on its conductivity. However, when the surfaces of the polyaniline nanowires were treated with a rich dispersion of silver nanoparticles, a much greater current change was observed which confirms that the nanoparticles serve as catalysts for causing the current change for the polyaniline. A decrease in the conduction current indicates that the pH near the polyaniline area has increased which is believed to have been caused by the generation of hydroxide ions and water as a result of the catalytic reaction between $H_2O_2$ and AgNP as shown in the reactions (5.1) – (5.3). It was also observed that the rate of the current drop increased as the amount of the AgNP loading increased. This further confirms that the catalytic reactions between AgNPs and $H_2O_2$ are indeed occurring and that the amount of the generated $OH^-$ and $H_2O$ byproducts is proportional to the amount of AgNPs deposited on the sensing area, given that the amount of $H_2O_2$ in the sample is constant.

Calibration Plot, Sensitivity, and Detection Limit - For a fixed amount of AgNP loading ($1.0 \times 10^7$ particles) on the polyaniline-based chemiresistor, the rate of conduction current drop was solely dependent on the concentration of $H_2O_2$. Figure 5.10 shows the changes in the conduction current through the polyaniline under various concentrations of $H_2O_2$. As illustrated in the graph, a higher concentration of $H_2O_2$ causes faster current drop which indicates that rate of the byproduct formation is not limited by the number of AgNPs. However, it can be expected that, in the case where the amount of AgNP loading is insufficient, the rate of the byproduct

generation can be limited by the low quantity of AgNps. By observing the graph in Figure 5.10, the limit of detection for the developed sensor is approximated to be 5 mM.

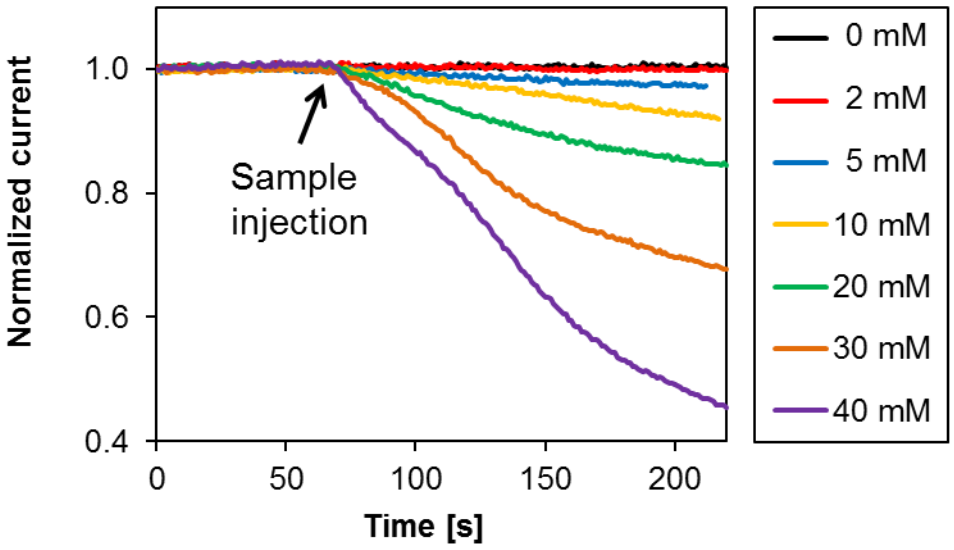


Figure 5.10. The conduction current response of the polyaniline/AgNP-based chemiresistor to various concentrations of $H_2O_2$.

Although a direct reading of the current drop for the determination of the $H_2O_2$ concentration is possible, some inherent limitations are associated with this technique. First, due to the continuous generation of the catalytic byproducts, it may take a long time for the conduction current to stabilize before any measurement can be made. Secondly, since the current cannot drop below zero, there is an upper limit on the measureable concentration. However, observing the results in Figure 5.10, one can envision a chemiresistive $H_2O_2$ sensor that utilizes the rate of the conduction current change, i.e., the slope of the current, as a measure to quantify the $H_2O_2$ concentration in a solution. Figure 5.11 shows a calibration plot showing the initial slope of the current versus the concentration of the analyte which can be used to estimate the concentration of $H_2O_2$. The calibration plot was obtained by measuring the tangential slope at

every 5 seconds after sample injection (for the first 25 seconds) and by calculating the average slope for each concentration. By fitting a straight line through the calibration plot, the average sensitivity of the sensor was obtained to be 0.0126 μA/mM-s. Although Figure 5.11 indicates that the detection limit is slightly higher than 5 mM due to the relatively large error bars, the slope measurement technique offers the advantage of rapid measurement rather than having to wait for the current to stabilize. On the other hand, direct current reading method as shown in Figure 5.10 gives the detection limit of as low as 5 mM, however the response time is longer compared to the slope measurement method. The large error bars in Figure 5.11 are probably due to the non-linear current decrease upon exposure to $H_2O_2$ caused by convective flow and disturbances in the sample solution. A microfluidic platform with low Reynolds number could be applied to minimize the uncertainties present in the slope measurements.

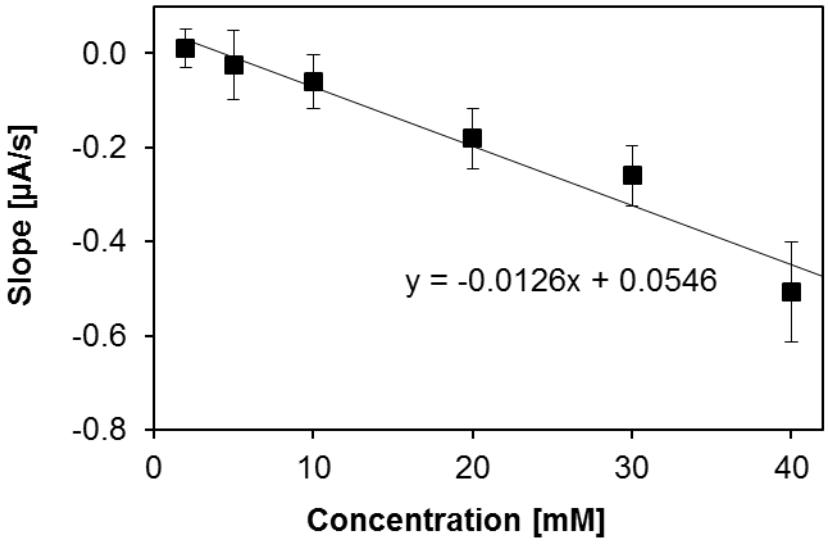


Figure 5.11. The plot showing the initial slope vs. $H_2O_2$ concentration for the conduction current response of the polyaniline/AgNP-based chemiresistive sensor. The error bars indicate 1 standard deviation with sample number of n = 5.

Selectivity of the Sensor - To demonstrate the selective nature of the AgNP catalysts, the polyaniline/AgNP-based device was also tested under other chemical species other than hydrogen peroxide. Figure 8 shows the conduction current response of the sensor when it was exposed to 200 mM of ethanol, methanol and acetone. For comparison, the graph also shows the current response for 40 mM of $H_2O_2$. As indicated by the negligible changes in the conduction current, it can be concluded that the AgNPs only exhibit catalytic reaction with hydrogen peroxide but not with the other three solutions tested in this experiment.

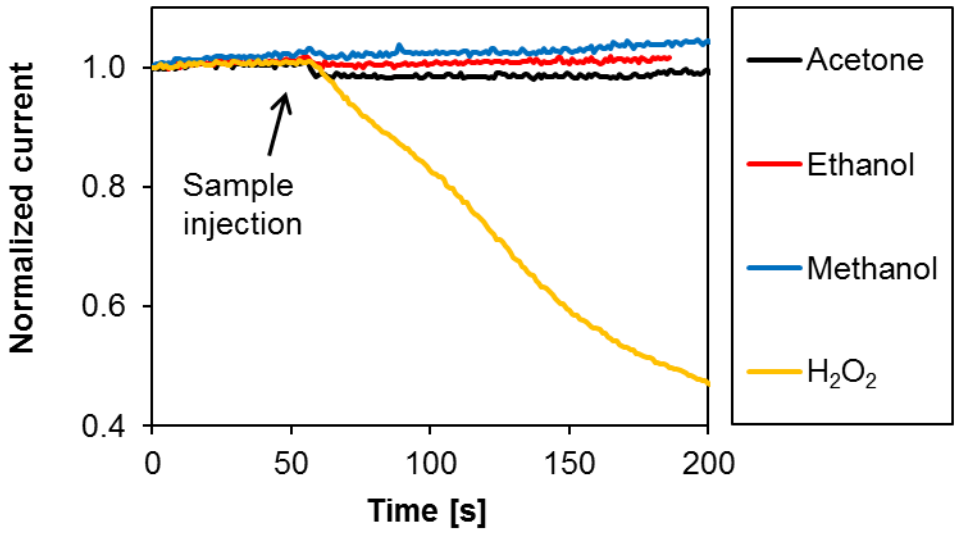


Figure 5.12. The conduction current response of the polyaniline/AgNP-based chemiresistive sensor when the device was exposed to 200 mM of each analyte solution except for $H_2O_2$, which was 40 mM.

## 5.6. Conclusions

In this chapter, a novel technique to allow selective detection of chemical species using polyaniline-based chemiresistive sensor is proposed and described. Catalysts that produce either protons or hydroxyl ions were used as signal amplifiers that drastically change the local pH of the environment causing the polyaniline to respond by changing its resistivity. Since catalytic

behavior is selective to certain chemical species, by selecting an appropriate catalyst, selectivity could be achieved in a polyaniline-based chemiresistive sensor.

To demonstrate this concept, a selective chemiresistive hydrogen peroxide sensor was developed by incorporating catalytic silver nanoparticles into the polyaniline nanowire network. The experimental results confirm the presence of a selective catalytic reaction between hydrogen peroxide and silver nanoparticles, and the $H_2O_2$ concentrations can be predicted by observing the slope of the conduction current of the polyaniline nanowire network. The sensor's selectivity in chemical sensing was also confirmed when the device only responded to $H_2O_2$ while other chemical species yielded negligible current change. Although the limit of detection for the proposed sensor was higher than other previously reported $H_2O_2$ sensors, the main contribution of this work is to suggest and demonstrate a new detection strategy that is both simple to fabricate and selective to the target analyte. Moreover, most electrochemical $H_2O_2$ sensors incorporate biological materials such as enzymes which may lead to instability and limited shelf-life. Since non-enzymatic catalysts are used, the proposed sensor offers improved reliability and longer shelf-life.

There are a few areas regarding this technology that need further improvements. First of all, the polyaniline area could be made thinner with high surface area in order to lower the detection limit of the sensor. Secondly, a more repeatable and reliable method to uniformly deposit the nanoparticles onto the polyaniline nanowires must be developed. Uniform dispersion of nanoparticles on a flat substrate is difficult due the 'coffee ring' effect [142] resulting in migration of nanoparticles toward the edge of the liquid droplet. Another difficulty is the loss of nanoparticles due to the weak adhesion between the polymer/substrate and the nanoparticles. To ensure that a fixed number of nanoparticles be uniformly attached to the polyaniline, one option

is to encapsulate or embed the nanoparticles into the bulk of the polyaniline nanowires. This involves trapping the nanoparticles inside the polymer during the polymerization process.

The work presented here serves as a step toward achieving the ultimate goal of developing a generic polyaniline-based sensor array in which various catalysts may be employed in each sensing element for achieving multi-analyte detection capability. Aside from hydrogen peroxide detection with silver nanoparticles, selective sensing of other chemical species using different catalytic nanoparticles should also be demonstrated. Further investigation to find other nanoparticles that catalytically respond to different analyte is needed in order to develop an integrated multi-analyte sensing array.

# Multi-Analyte Detection with Polyaniline-Based Sensor Array

## 6.1. Introduction

In chapter 5, it was demonstrated that polyaniline nanowires can be modified by attaching catalysts, such as silver nanoparticles, to the nanowires in order to produce a selective chemiresistive sensor that responds to a specific chemical species. In this chapter, this concept is expanded further for the construction of a sensor with simultaneous multi-analyte detection capability. The final objective here is to develop an array of sensors that is able to identify (classification of analyte) and to quantify (estimating the concentration) each individual species in a mixture of analyte samples. This chapter is organized as follows: first, a brief overview on multi-analyte sensors is first given in section 6.2. In section 6.3, the process for selecting the appropriate catalysts and target analytes is described, and Section 6.5 discusses the calibration curve for the three analyte of interest obtained from each sensing component. In section 6.6, a multivariate algorithm for classification of analyte is described. Quantitative detection of the individual species is given in section 6.7. Concluding remarks are given in section 6.7.

## 6.2. Cross-Reactive Sensor Array: A Brief Overview and Our Approach

In the past, the traditional approach to multi-analyte sensor array has been the use of the so called “lock-and-key” type receptors where each sensing element is highly selective to one specific analyte with minimum cross-reactivity between the sensors in the array [143], [144]. However, this approach has several drawbacks. First of all, these types of sensors require each sensing element to be fabricated individually in a unique way. For example, each sensing element may have a different geometry or architecture. This is costly from a manufacturing point of view since the fabrication process can be quite complex. Secondly, the sensing elements may

have different transduction mechanism such as optical, electrical, and chemical sensing methods. This makes the measurement of the signals from each sensing element difficult and expensive. Thirdly, developing each individual sensing element to respond only to one specific analyte is a non-trivial task. In other words, it is difficult to produce a sensor array with a 1-to-1 mapping between each sensing element and the corresponding analyte resulting in a near 100% selectivity [145].

As such, in recent years, the trends and directions in this research field has shifted from the aforementioned approach to the cross-reactive sensing strategy, also known as differential sensing [144], [146]. In cross-reactive sensors, each sensing element is less selective and may respond to multiple analytes. However when the measured signals from the individual sensing elements are combined and analyzed, each analyte can be discriminated from others by observing a unique signature response or a " fingerprint" signal. This concept of multi-analyte sensing approach is inspired by the biological olfactory system for odor detection where the responses from many different types of olfactory receptors, although each receptor not being highly selective, are processed together to detect and identify the odor from an unknown sample. Hence, the term electronic nose, or e-nose, was coined to describe a multi-analyte sensor array for gas detection. For solution-based sensor array, electronic tongue, or e-tongue is commonly used.

The concept of e-nose and e-tongue has been suggested by many, and some work has been done to show the feasibility to develop such sensors. A colorimetric e-tongue has been reported [147], [148] and conducting polymer-based multiple vapor detection has also been reported [149]. However, none has been able to demonstrate a 'generic sensor array' consisting of a single sensing material. A truly generic sensor array, with each sensing element having an identical

sensing platform, has the benefit of being able to tailor each sensing element according to the user's needs by modifying with the appropriate catalyst.

The benefit of using the cross-reactive sensors is that the selectivity requirement for each sensing element is lenient, and this allows for the sensing elements to be designed and fabricated in a cost effective way. Furthermore, the development of a generic sensor platform can be achieved where each sensor in the array contains the basic chemiresistor that is common and identical throughout the array. In addition to this basic platform, each sensing component can be slightly modified or "tweaked" to give a distinct response. If this generic sensor configuration can be realized, the sensor array can be custom designed according to the user's need. Moreover, if this approach is to have significant merit, the method to modify the generic sensing element must be simple and effective.

Our approach is to use pristine polyaniline nanowire network as a generic sensing material, and the sensing elements in the array are functionalized with different types of catalysts so that each sensing element contains a single type of catalyst. By modifying each sensor in a unique way, the response signal from each sensor element will be diverse. In other words, differently modified sensors will produce different signals for a given target species. Since the selectivity is somewhat relaxed, certain analytes will lead to similar signals from more than one sensing element. However, combining the information provided by the signal responses from the individual sensors, it may be possible to identify the composition of the unknown sample of interest.

We will also attempt to quantify the concentration of each analyte in the sample solution. Some of the immediate challenges regarding this approach is (a) choosing the right catalysts and finding the detectable analyte; (b) dealing with cross-reactivity present in the sensor array, and

(c) developing an algorithm for classification and quantification of the individual species. To simplify the problem, the number of target analyte will be limited to 2, but will later be extended to large numbers.

### 6.3. Device Design and Fabrication for the Chemiresistive Sensor Array

The electrodes for the sensing device were redesigned and modified from the devices used in the previous chapters. In an extremely low concentration range, making the polyaniline bridge narrower could improve the sensing performances including the limit of detection and sensitivity. However for detecting a relatively larger concentrated analyte, for example, in the millimolar (mM) range, the dimensions of the chemiresistor area plays a less important role since the change of resistivity per unit area will remain roughly the same. In such cases, having a chemiresistive bridge with minimum thickness and large surface area is desirable for enhancing the sensing performances. Since the detection limit of the developed sensors are on the millimolar range, the sensor dimension need not be further reduced. However, in the new design, the sensing area was made smaller to better control the amount of nanowires grown to ensure that thin and high porosity polyaniline nanowire network is formed across the electrodes.

The image for the new device is shown in Figure 0.1(a) where each device contains two sensing components (Sensor 1 and Sensor 2). Figure 0.1(b) shows the magnified image of the electrode area (circled part in Figure 0.1(a)) where polyaniline is to be grown. The electrode gap is 10 μm and the width of the electrode is 50 μm. A passivation layer was coated on top of the electrode leaving a window of opening with a dimension of 200 μm × 100 μm at the electrode gap so that polyaniline can be grown in that area.

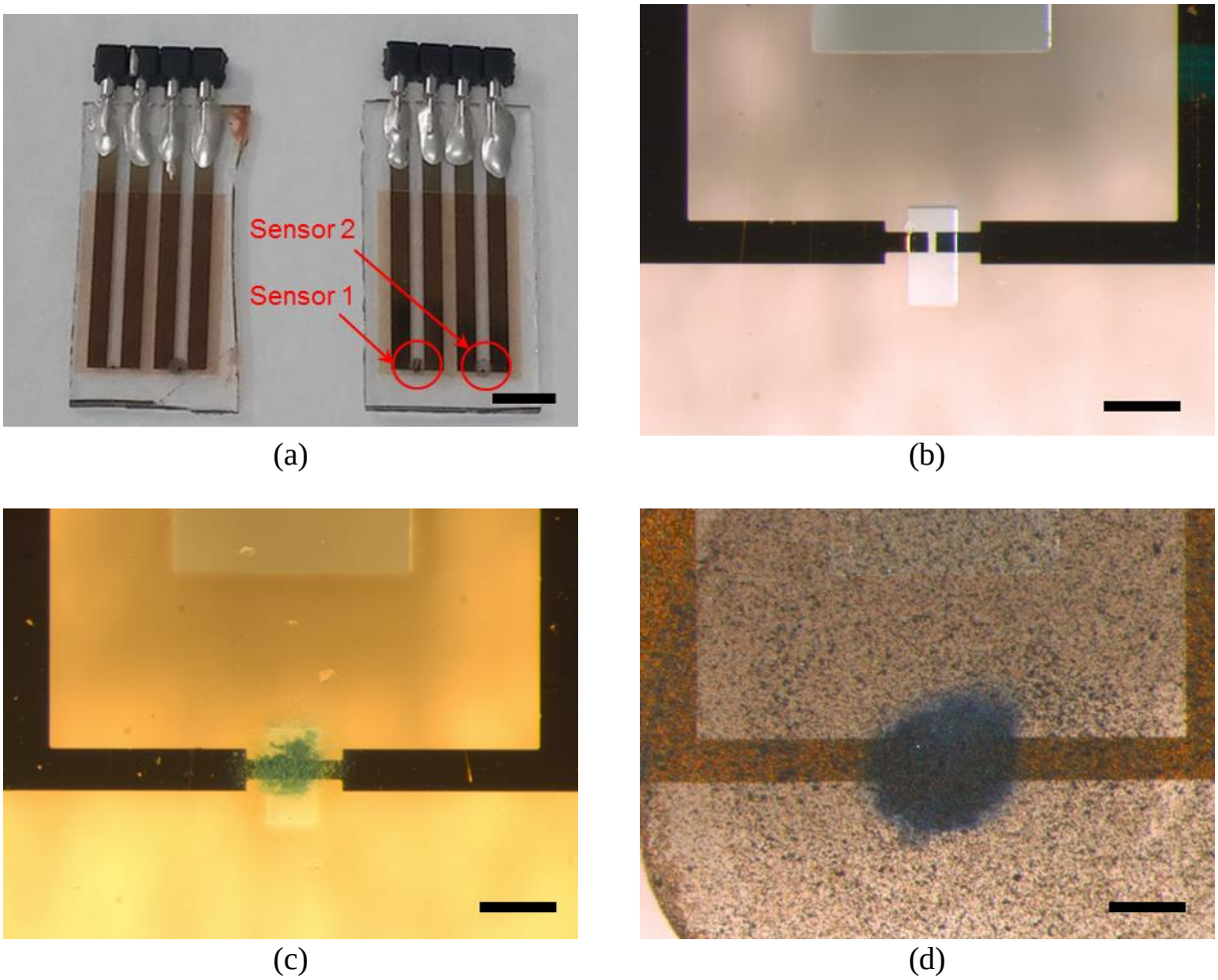


Figure 0.1. New device design showing (a) the image of the device containing two sensing elements (scale bar: 5 mm); (b) the electrode gap with passivation layer (scale bar: 200 µm); (c) the synthesis of polyaniline nanowire network to bridge the electrode gap (scale bar: 5 mm), and (d) the deposition of the catalysts (scale bar: 5 mm). In this image, copper oxide (CuO) is deposited on polyaniline.

After the device fabrication, polyaniline was potentiostatically grown at the unpassivated electrode area from a solution containing 0.1 M aniline in 1 M $H_2SO_4$ at a constant potential of 0.8 V vs. Ag/AgCl until a total charge of 0.25 mC has passed through the working electrodes. Figure 0.1(c) shows that polyaniline was grown at the electrode gap to bridge the two electrodes. After polyaniline synthesis, several drops of nanoparticle dispersion were deposited on top of the polyaniline as shown in Figure 0.1(d). The nanoparticle dispersions were prepared by adding 1

mg/ml of select nanoparticles in deionized water and treating with ultrasonication for 3 hours. Since dispersion of silver nanoparticles in water was difficult, 0.1 mg/ml of sodium dodecyl sulfate (SDS) was added to facilitate the dispersion.

### 6.4. Selecting the Proper Catalysts and Analyte for Multiple Species Detection

In this section, the goal is to search for several types of nanoparticles that can potentially be used as catalysts on polyaniline nanowires for selective detection of certain analytes. In connection with applications in biosensing, there have been many publications in recent years that report the use of catalytic nanoparticles for selective electrochemical detection of biologically relevant chemical species such as glucose, ascorbic acid, dopamine, and uric acid. Zhang and co-workers have used nickel oxide (NiO)-modified multi-walled carbon nanotubes (MWCNT) as a nano-composite electrode for amperometric detection of glucose [150]. A similar approaches have been taken by two other groups in glucose sensing except they have used copper oxide (CuO) instead of NiO to modify the MWCNT electrode [151], [152]. Kalakodimi and Nookala have implemented a polyaniline-coated nickel for the electro-oxidative detection of ascorbic acid (AA) [153]. Luo and co-workers have modified the gate surface of the ion-sensitive field-effect transistor (ISFET) with manganese dioxide ($MnO_2$) nanoparticles which generated a local pH change upon exposure to AA [154]. Tashkhourian and co-workers have used silver nanoparticles modified MWCNT paste electrode for simultaneous detection of AA and dopamine (DA) [155].

In this work, several nanoparticles were chosen as candidates to be used as catalysts for the polyaniline-based sensor array. Each nanoparticles were tested with various analytes to observe catalytic responses. Table 0.1 summarizes the nanoparticles and the analytes that were tested in this study.

Table 0.1. The potential nanoparticles and analyte under study.

| Nanoparticles | Analyte |
|---|---|
| Ag, CuO, $Mn_2O_3$ | AA, DA, $H_2O_2$ |

To observe the diversity and variations in the sensor responses, the polyaniline nanowire-based chemiresistor was modified with each catalysts listed in Table 0.1 and was exposed to 10 mM of each analyte in the table. For all experiments, the bias potential $V_B$ and the differential voltage $V_D$ were set to 0.1 V vs. Ag/AgCl and 50 mV, respectively. Figure 0.2 shows the summary of the conduction current responses from each sensors. Figure 0.2(a) shows that all sensing elements, with the exception of the Ag-modified sensor, responds to AA by increasing their conduction current. This is in part due to the lowing of the pH of the sample solution caused by the addition of AA (adding 10 mM of AA in pH 5 lowers the pH to 3.92). The difference in the current amplitude among the sensors, for example, between the CuO-modified and the blank sensors, is expected to be caused by the catalytic activity that is unique to the each sensing element. The Ag-modified sensor did not experience much current rise probably due to the improved conductivity by the attachment of highly conductive silver nanoparticles. Therefore, the effect of the pH change will have less influence on its overall conductivity. Figure 6(b) shows that the sensor response to DA is distinct only for the sensor functionalized with $Mn_2O_3$ nanoparticles where the measured current is reduced upon exposure to DA. The response for all other sensors increase in a positive direction and it is likely due to the minor pH change of the sample solution. In figure 6(c), the three sensing components modified with the nanoparticles give negative responses with varying degrees when exposed to $H_2O_2$, whereas the pure polyaniline-based (blank) sensor shows a minimal response. This is indicative of the presence of cross-reactivity between the sensors that show similar responses. Based on the results shown in Figure 0.2, it can

be concluded that the three nanoparticles under study (i.e. $Mn_2O_3$, CuO, and Ag) all possess catalytic activity of various strength with one or more target analyte, and that they demonstrate reasonable selectivity and sensitivity toward the target species.

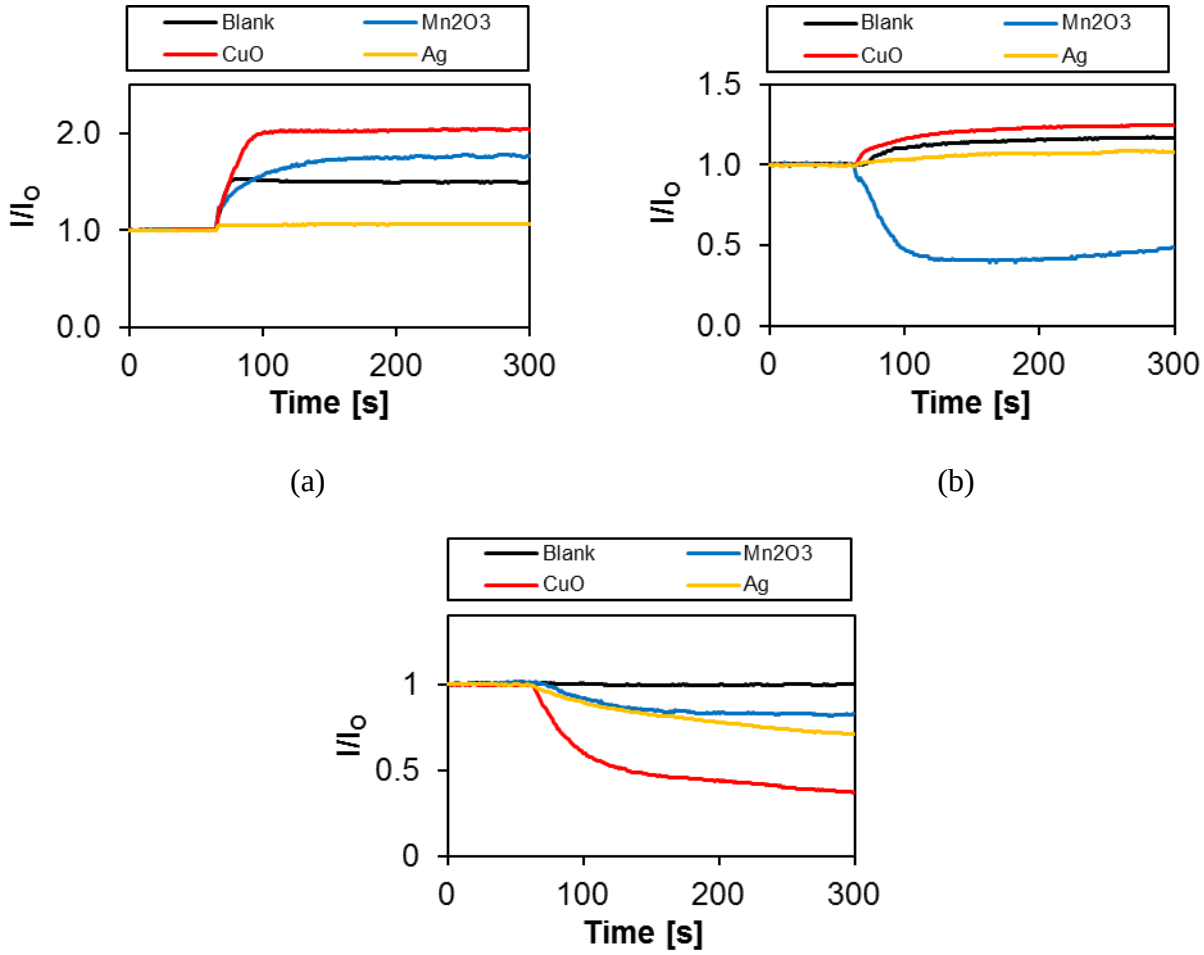


Figure 0.2. Current responses from each sensor modified with no catalyst (blank), manganese oxide ($Mn_2O_3$), copper oxide (CuO), and silver (Ag) nanoparticles after exposing the sensor to 10 mM of (a) ascorbic acid; (b) dopamine, and (c) hydrogen peroxide.

Due to the cross-reactive nature of the sensors, each analyte triggers current responses from not only one sensing component but from multiple sensing elements in the array. Figure 0.3 summarizes the changes in the conduction current of each sensing element, normalized to the

initial reference current, for a given analyte in a set of bar graphs. It is interesting to note that, while in Figure 0.3(a) and (c), the responses from the four sensing elements, although different in magnitude, are in the same direction such as positive change for Figure 0.3(a) and negative change for Figure 0.3(c). However in Figure 0.3(b), three sensors (i.e. Blank, CuO, Ag) respond in the positive direction while one ($Mn_2O_3$) undergoes a negative current change. This variation in the polarity of the responses can be beneficial in further enhancing the selectivity of the sensor array.

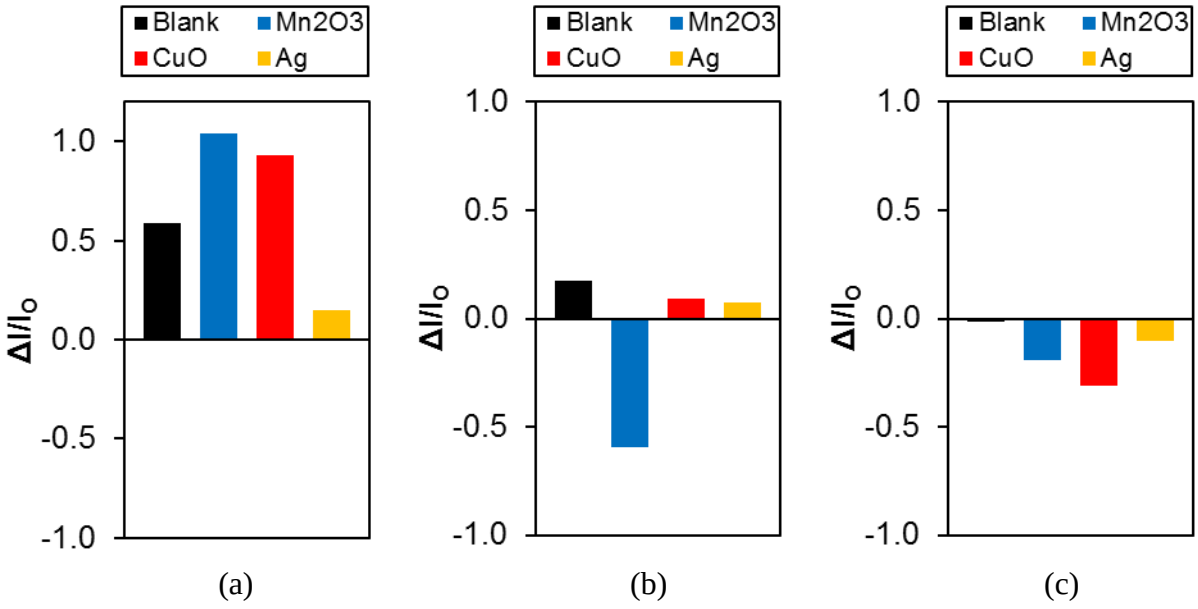


Figure 0.3. Bar graph showing the conduction current changes of each sensing element caused by exposure to 10 mM of (a) ascorbic acid; (b) dopamine, and (c) hydrogen peroxide.

### 6.5. Calibration Curves

The plots shown in Section 6.3 confirms that the addition of specific nanoparticles causes each polyaniline-based sensing elements to respond differently to a given analyte. Now that the type of catalysts (i.e. None, $Mn_2O_3$, CuO, and Ag) and the target analyte (i.e. AA, DA, and $H_2O_2$) have been selected, it is desirable to define a measureable concentration range of each

analyte. A calibration curve plotting the current response versus concentration will provide the range of concentration that can be measured as well as other information such as the limit of detection (LOD) and sensitivity. The calibration curve for each analyte was obtained by measuring the sensor response with varying concentrations of the analyte. The sensor signals were first stabilized for 30 minutes before the samples were injected. The measurements were taken 2 minutes after sample injection. The voltage parameters remained the same as before (i.e. $V_B$ = 0.1 V vs. Ag/AgCl, $V_D$ = 50 mV).

### 6.5.1. Ascorbic Acid

Ascorbic Acid (AA) is commonly detected biochemical species that is critical in human physiology, particularly in immune system, and plays a crucial role in metabolic process and redox reactions [156]. It is also widely used as an antioxidant in food industry [157]. Therefore the detection of AA in a suitable manner is an important task. AA is generally detected by electrochemical methods however, accurate measurement of AA can be challenging if there are interfering species with similar oxidation potentials such as dopamine, uric acid or glucose. Hence, accurate sensing of AA in the presence of other common interfering species is the topic of great interest.

Among the catalysts that were tested in Section 6.3, CuO were shown to be the most responsive to AA. A possible chemical reaction that may be occurring at the surfaces of the nanoparticles are [158]:

$$\underset{\text{(AA)}}{C_6H_8O_6} \rightarrow \underset{\text{(DAA)}}{C_6H_6O_6} + 2H^+ + 2e^- \quad (1)$$

where DAA stands for dehydroascorbic acid. Since more protons are produced as a result of the catalytic oxidation of AA, the conductivity of polyaniline nanowire network is expected to increase as the catalysis occurs at vicinity of the nanoparticles.

Figure 0.4 shows the current response of each sensing element under a given concentration of AA. The steady state current values for the blank and the CuO-modified sensors increase proportionally as the concentration is increased, and the response saturates beyond 5 mM of AA. However, $Mn_2O_3$-functionalized sensor responds differently from the other sensing elements. For

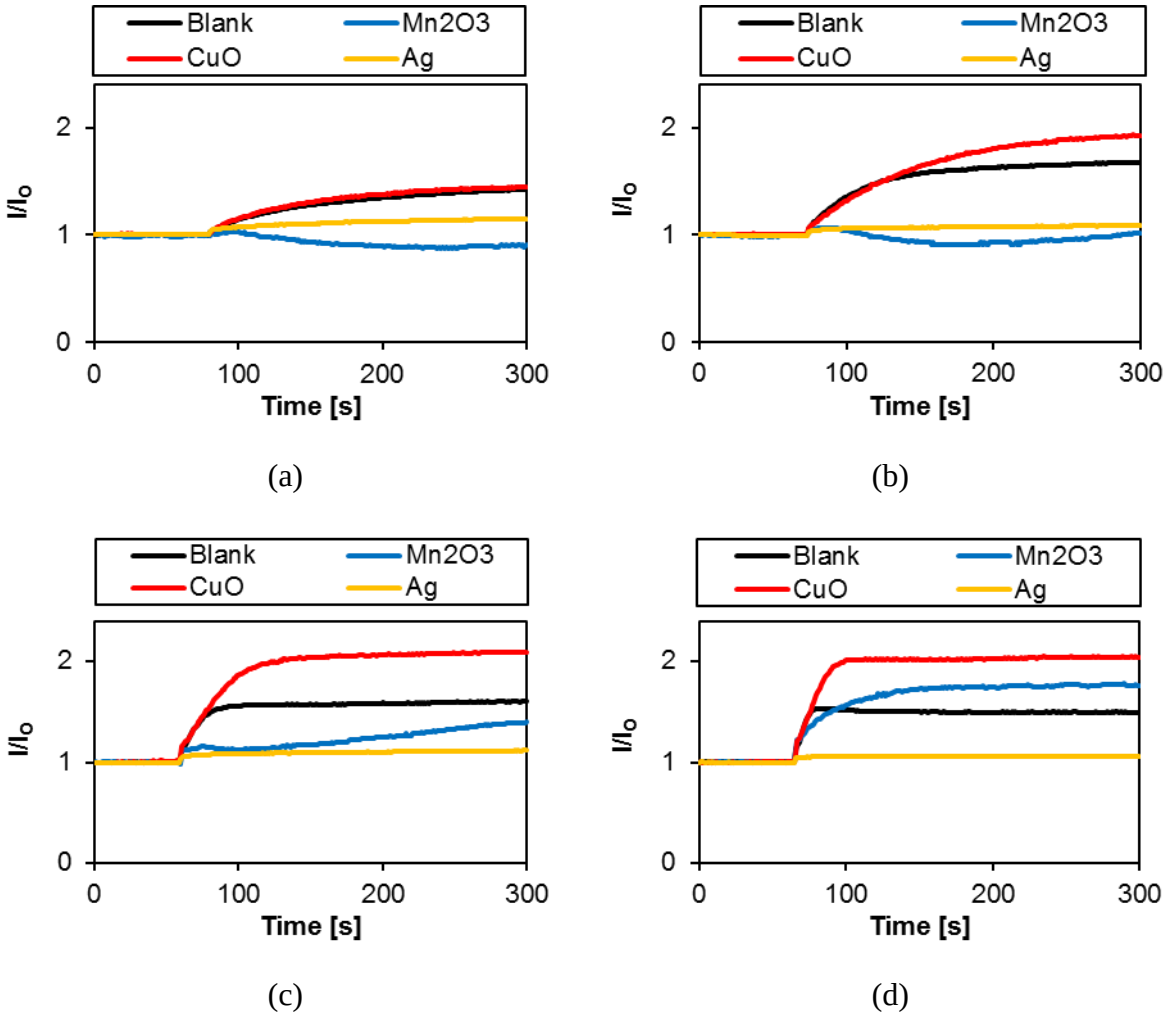


Figure 0.4. The current response of the four sensing components when exposed to (a) 1 mM; (b) 2 mM; (c) 5 mM, and (d) 10 mM of ascorbic acid. Sample injection time was t = 60 s.

the case of 1 mM of AA in Figure 0.4(a), the current drops to about 90% of the initial current ($I_O$). As the concentration increases in Figure 0.4(b) and (c), the initial current drop is followed by a gradual current increase to above $I_O$. There seem to be two competing reactions involved in the $Mn_2O_3$-modified sensor: on the one hand, the catalytic reaction between $Mn_2O_3$ and AA may be generating byproducts that decrease the conductivity of polyaniline. On the other hand, due to the lowering of pH by the acidity of AA, the conductivity of polyaniline is increased upon exposure to a larger quantity of AA (above 5 mM). Based on the plots in Figure 0.4, a calibration curve can be obtained for AA with concentrations ranging from 1 mM to 10 mM as shown in Figure 0.5. The measurements from the sensors were taken 2 minutes after the sample injection. Since the blank polyaniline, the CuO-functionalized, and the Ag-functionalized sensors all seem to have a negligible differences in the response for AA concentrations greater than 5 mM, the measureable range for AA is defined to be between 0 and 5 mM.

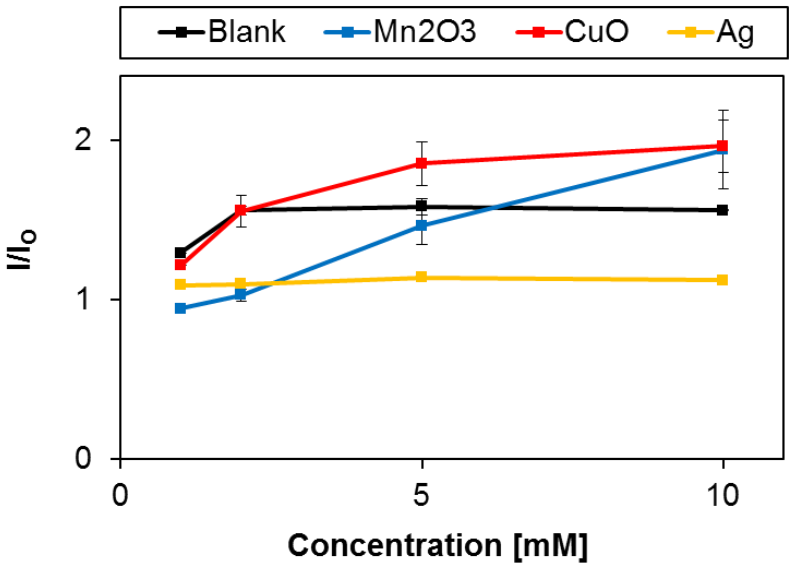


Figure 0.5. Calibration curve for ascorbic acid detection using polyaniline nanowires functionalized with various types of catalytic nanoparticles. The data points were measured at 2 mins after sample injection.

### 6.5.2. Dopamine

Dopamine (DA) is a neurotransmitter in both the central and the peripheral nervous system, and is known to be linked to many neurological disorders such as schizophrenia, epilepsy, and Parkinson's disease [159]. The ability to measure accurate concentrations of DA can therefore be potentially beneficial for diagnosis, therapeutics and evaluation of various mental disorders [160]. DA is commonly detected using electrochemical methods however, the main difficulty with DA sensing is that other interfering species, such as ascorbic acid and uric acid, are generally much higher in concentration by up to several orders of magnitude than that of DA. Therefore, there is a need to develop a sensor that gives accurate readings of DA concentration in the biological samples without the interference of other chemical species.

Figure 0.6 shows a typical current response from each sensing element under a given concentration of DA. It is evident from the graph that $Mn_2O_3$-functionalized sensor is dominant in terms of the magnitude of the response. As mentioned in the previous section, while the other three sensors respond in a positive direction (for example in Figure 0.6(d)), the current reading for the $Mn_2O_3$-modified sensor drops in a negative direction. This suggests that a unique catalytic reaction is occurring only on the surfaces of $Mn_2O_3$ nanoparticles and not on others.

Based on the plots in Figure 0.6, a calibration curve can be obtained for DA with concentrations ranging from 1 mM to 10 mM as shown in Figure 0.7. The data points for the measurements from the sensor components were taken 2 minutes after the sample injection in order to ensure that steady state current was achieved. The calibration curve shows that for blank, CuO, and Ag modified sensors, the current response is negligible or slightly increasing, but shows a dramatic decrease in current for the $Mn_2O_3$ modified sensor.

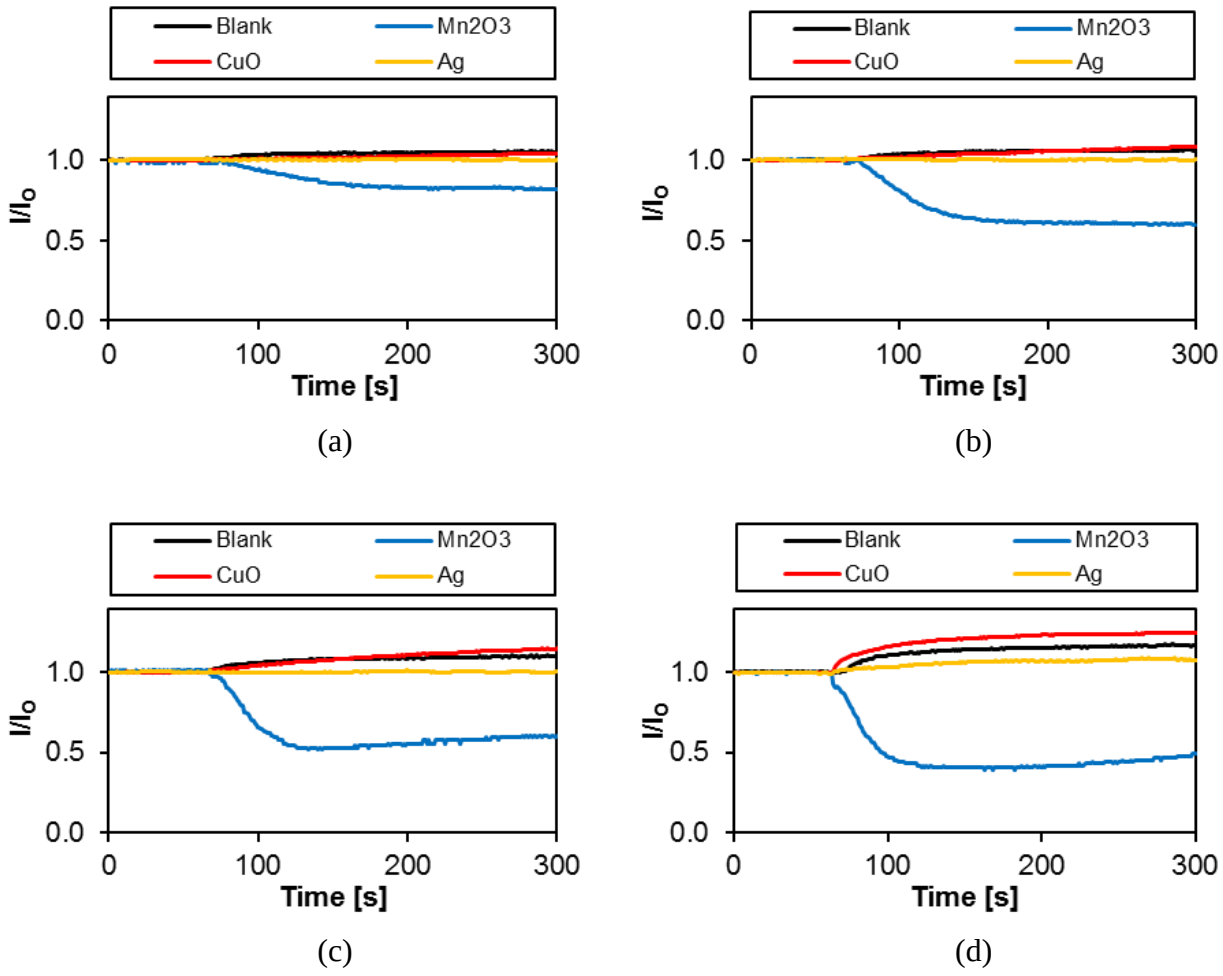


Figure 0.6. The current response for the sensing elements when exposed to (a) 1 mM; (b) 2 mM; (c) 5 mM, and (d) 10 mM of dopamine. Sample injection time was t = 60 s.

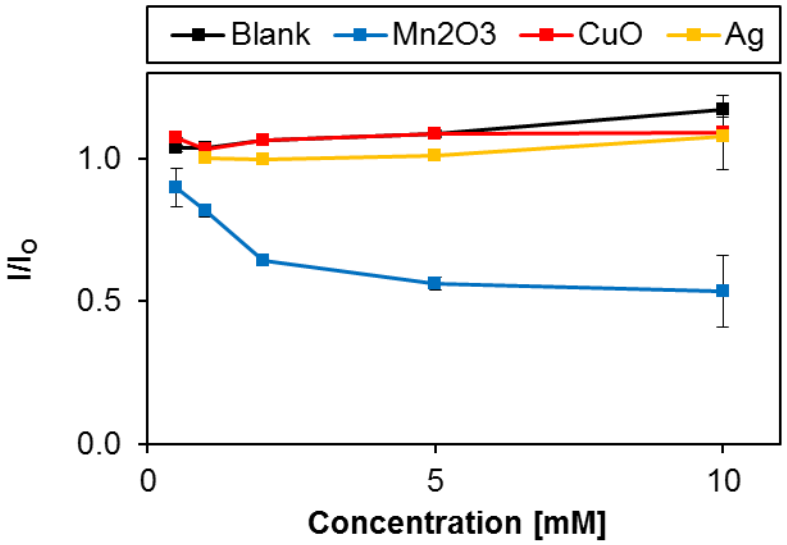


Figure 0.7. Calibration curve for dopamine detection using polyaniline nanowires with various functionalization of catalytic nanoparticles. The measurements were read at 2 mins after sample injection.

### 6.5.3. Hydrogen Peroxide

The importance of hydrogen peroxide ($H_2O_2$) detection in biology and physiological applications has been described previously in section 5.5 and, as a demonstration, silver nanoparticles (AgNPs) were used as catalysts to amplify the signal response from polyaniline nanowires. Although AgNPs were successful in enhancing the selectivity of the $H_2O_2$ sensor, other nanoparticles that were chosen in this chapter (i.e. $Mn_2O_3$, CuO) were also tested with $H_2O_2$ to examine whether the selectivity toward $H_2O_2$ can be further improved. Figure 0.8 shows the response from the four sensing elements when exposed to the given concentration of $H_2O_2$. The most notable signal change is from the CuO-modified sensor where the change in current value is somewhat proportional to the concentration of $H_2O_2$. The $Mn_2O_3$ and Ag-based sensors seem to have a weaker response, with $Mn_2O_3$-based sensor having a slightly larger change, but nevertheless do differentiate themselves from the unmodified blank sensor.

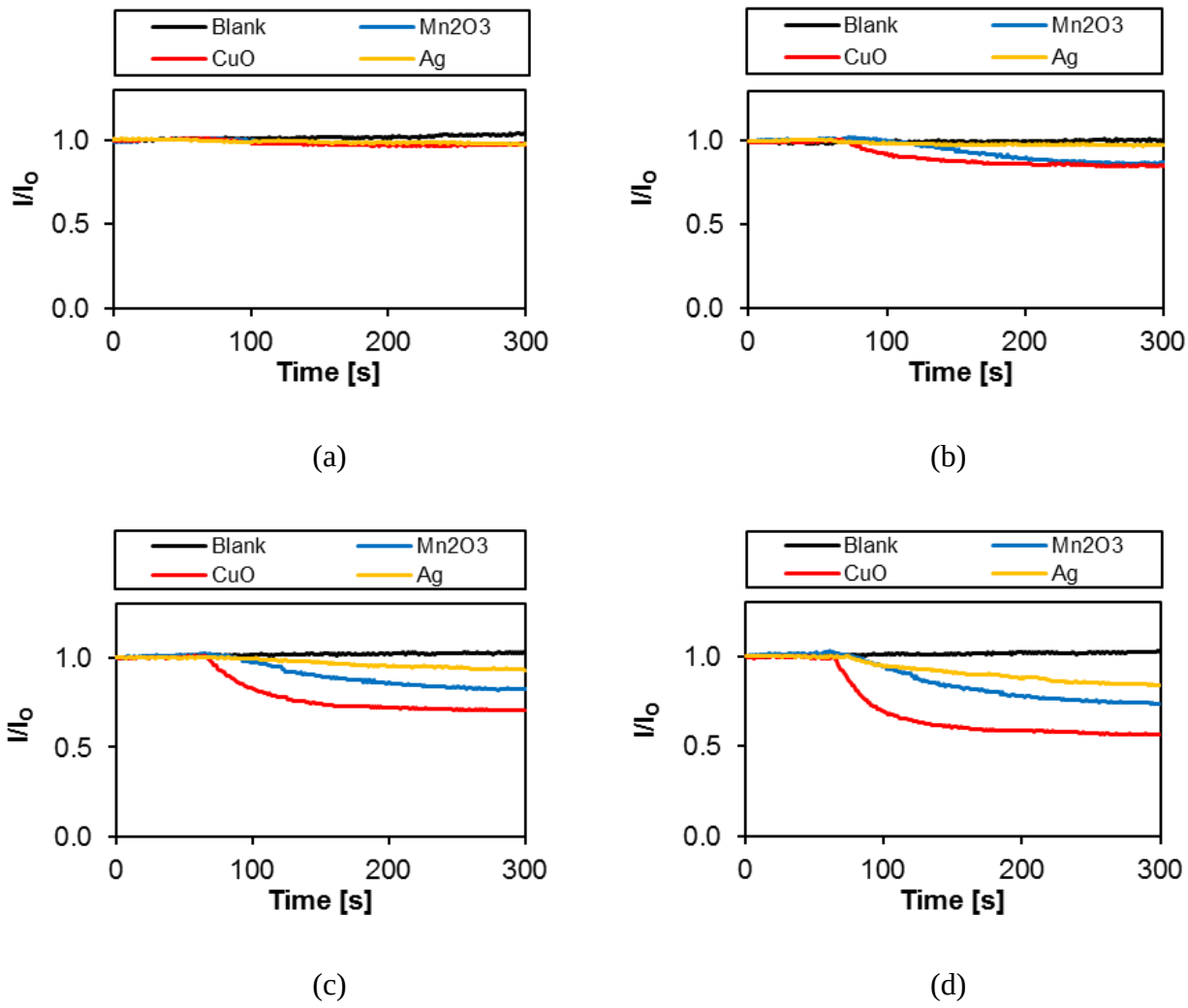


Figure 0.8. The current response from each sensing element when the sensor array is exposed to (a) 1 mM; (b) 2 mM; (c) 5 mM, and (d) 10 mM of $H_2O_2$. Sample injection time was t = 60 s.

Based on the graphs in Figure 0.8, a calibration curve of $H_2O_2$ sensing from the four sensing elements can be obtained, as shown in Figure 0.9. As previously noted, the data points in the calibration curve were obtained by stabilizing current for 2 minutes after the sample injection to ensure that steady state value was achieved.

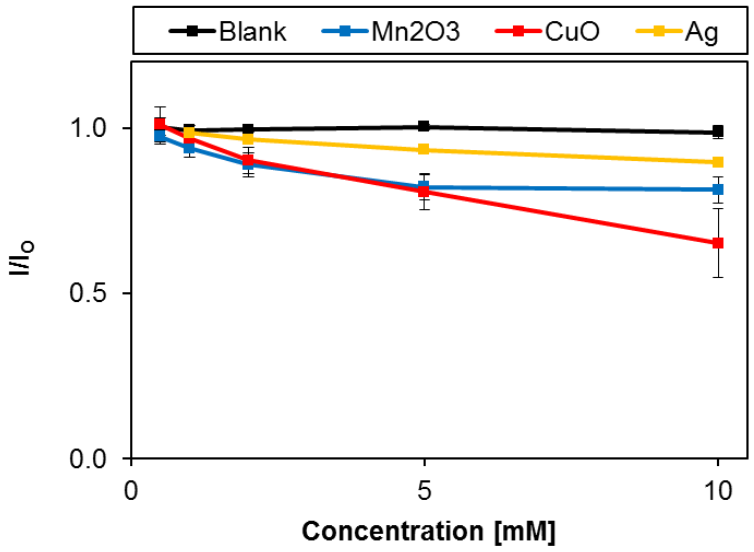


Figure 0.9. Calibration curve for $H_2O_2$ sensing with polyaniline nanowires modified with various catalytic nanoparticles. The sensor measurements were taken after 2 mins from sample injection.

A possible catalytic reaction mechanism for $H_2O_2$ that results in the decreasing of the conductance of polyaniline has been suggested in section 5.5.2. For $H_2O_2$ detection, all three catalyst-modified sensors respond to the analyte in a similar trend with the only difference being the magnitude of the current change. Therefore the CuO-modified sensor alone seems to be sufficient in determining the analyte concentration. In this case, all other signals from the remaining sensing elements can be considered as giving redundant information. However, it will be shown in the later section that in the case where the sample contains a mixture of $H_2O_2$ and another analyte, for instance, ascorbic acid or dopamine, the signals obtained from the four sensing elements will show different trends, providing the information needed to differentiate one analyte from the other.

The following sections discuss a statistical technique to analyze the signals in order to identify the sample composition. Multi-analyte detection can be divided into two categories: classification and quantification. Classification is only concerned with identifying the type of

analyte present in the sample, whereas quantification also requires estimating the quantitative information about a given analyte such as concentration.

## 6.6. Classification of Target Analyte

Based on the preliminary data from the previous sections, an algorithm is to be designed such that an unknown sample containing one of the three possible species, i.e. AA, DA and $H_2O_2$, can be identified. For simplicity, a sample solution is assumed to contain 10 mM of only one of the three target analyte. For this study, a Principal Component Analysis (PCA) method, which is one of the most widely used method in sensor arrays for analyte classification, is investigated to test its feasibility for this application.

### 6.6.1. Principal Component Analysis

Many recently developed sensor arrays, especially for volatile organic compound (VOC) detection [161], [162] or qualitative analysis of beverages [163], [164], the array comprises a large number of sensing elements resulting in a large data set for processing and analysis. Therefore, a systematic method to handle and interpret a large volume of data in order to extract meaningful information and to make proper prediction from the data is necessary. Multivariate analysis methods (MVA) is the field of studies that use various mathematical tools such as statistical analysis and linear algebra to analyze multi-dimensional data set [165]. Hence, MVA techniques can be useful in identifying and quantifying the analyte in the mixture of unknown substances. Some of the most commonly used MVA methods in chemical sensor arrays include Linear Discriminant Analysis (LDA) [147], Principal Component Analysis (PCA) [149], Partial Least Squares (PLS), Cluster Analysis (CA), and Artificial Neural Networks (ANN) [166].

In a typical multi-dimensional sensor arrays with many sensing elements, it is often difficult to extract only the useful information from a large data set since a significant portion of that raw data contains redundant or unnecessary information embedded in it. Therefore, reducing the dimensionality of the sensor array in a way that filters out the redundancy can greatly simplify the problem at hand. Moreover, visualization of the data using graphical methods such as 'mapping' of the data points on a 2-dimensional or 3-dimensional space is not possible if the number of sensing elements exceeds three.

Principal Component Analysis (PCA) is the most fundamental and commonly used method in reducing the dimensionality of the multivariate data into a simplified, lower dimensional representation. PCA is based on the linear transformation of the response variables (i.e. the signals measured from the individual sensing elements) into a set of new vectors called principal components (PC). The PCs are defined in a way that they are mutually orthogonal meaning that they are mutually uncorrelated, or independent. Furthermore, the PCs are arranged in the order of significance so that the first PC accounts for the largest variation in the data set. The second PC, which is orthogonal to (and therefore independent from) the first PC, is defined in the direction that picks up the second largest variation in the data. The remaining PCs can be defined accordingly until the number of PCs matches the number of the sensors. Generally however, the first few PCs are sufficient to adequately represent the raw data set (with a minimum loss of information), therefore only the first two or three PCs are selected for analysis and the remaining PCs, which are less important or contain redundant information, can be discarded. In summary, PCA procedure can reduce the dimensionality of the data collected by the sensor array and condense it into lower dimensional orthogonal vectors with minimal loss of meaningful information.

### 6.6.2. Classification of Ascorbic Acid, Dopamine, and Hydrogen Peroxide using PCA

The first step in applying the PCA method is to derive the principal components (PCs) from a set of data points which were experimentally obtained, also referred to as the training data set. The PCA procedure will define the PCs in such a way that they will maximize the variance within the training data samples. Once the PCs are defined, any new measurements that are obtained from the sensor array will be mapped onto the new principal component domain in order to identify which class of analyte the sample belongs to. The following table shows a set of data that is used to derive or to train the principal component vectors.

Table 0.2. The training data sets for deriving the principal component vectors. Each value indicates $\Delta I/I_O$.

| Analyte | Concentration (mM) | Blank | $Mn_2O_3$ | CuO | Ag |
|---|---|---|---|---|---|
| AA | 1 | 0.322 | -0.095 | 0.351 | 0.118 |
| AA | 2 | 0.605 | -0.091 | 0.747 | 0.072 |
| AA | 5 | 0.577 | 0.218 | 1.049 | 0.100 |
| AA | 10 | 0.495 | 0.735 | 1.019 | 0.060 |
| DA | 1 | 0.039 | -0.182 | 0.022 | 0.004 |
| DA | 2 | 0.067 | -0.337 | 0.049 | 0.000 |
| DA | 5 | 0.077 | -0.414 | 0.099 | 0.010 |
| DA | 10 | 0.155 | -0.592 | 0.223 | 0.072 |
| $H_2O_2$ | 1 | -0.007 | -0.062 | -0.057 | -0.015 |
| $H_2O_2$ | 2 | -0.006 | -0.112 | -0.133 | -0.035 |
| $H_2O_2$ | 5 | 0.003 | -0.179 | -0.274 | -0.051 |
| $H_2O_2$ | 10 | 0.017 | -0.188 | -0.408 | -0.105 |

The training data set is generally represented in a matrix format, where the number of rows indicate the number of samples (observations) and the columns indicate the number of variables (or the number of sensing elements). Using the data presented in Table 0.2, the following data matrix $X$ with the dimensions $12 \times 4$ can be constructed.

$$X = \begin{bmatrix} 0.322 & -0.095 & 0.351 & 0.118 \\ 0.605 & -0.091 & 0.747 & 0.072 \\ 0.577 & 0.218 & 1.049 & 0.100 \\ 0.495 & 0.735 & 1.019 & 0.060 \\ 0.039 & -0.182 & 0.022 & 0.004 \\ 0.067 & -0.337 & 0.049 & 0.002 \\ 0.077 & -0.414 & 0.099 & 0.010 \\ 0.155 & -0.592 & 0.223 & 0.072 \\ -0.007 & -0.062 & -0.057 & -0.015 \\ -0.006 & -0.112 & -0.133 & -0.035 \\ 0.003 & -0.179 & -0.274 & -0.051 \\ 0.017 & -0.188 & -0.408 & -0.105 \end{bmatrix}$$

The PCA algorithm on matrix *X* was executed using MATLAB® software, which generates a score matrix *T* and a loading matrix *P* such that

$$X = TP',$$

where the *P'* indicates a transpose of the matrix *P*. In essence, the matrix *P'* is a coordinate transformation matrix that relates the matrix *X* to the new coordinate matrix *T*. Therefore the rows of the matrix *T* are the coordinates of each sample of *X* in the transformed coordinate space where the principal components are the basis vectors. In other words, *T* is the representation of *X* in the principal component space, and the columns of the matrix *P* are the principal component vectors. The columns of *P* are arranged in a way such that

$$\text{Var}(PC_1) > \text{Var}(PC_2) > \text{Var}(PC_3) > \text{Var}(PC_4).$$

Since the first column of T is the coordinate corresponding to $PC_1$, it contains the most information about the variance of the data set. The values of matrices *T* and *P* are shown below.

$$T = \begin{bmatrix} 0.165 & -0.076 & 0.046 & 0.082 \\ 0.592 & -0.272 & 0.137 & -0.017 \\ 0.964 & -0.104 & -0.011 & -0.017 \\ 1.130 & 0.393 & -0.051 & -0.006 \\ -0.257 & 0.044 & -0.054 & 0.006 \\ -0.293 & -0.109 & -0.045 & -0.017 \\ -0.281 & -0.200 & -0.061 & -0.022 \\ -0.223 & -0.431 & -0.058 & 0.003 \\ -0.288 & 0.193 & -0.055 & 0.010 \\ -0.372 & 0.178 & -0.021 & -0.001 \\ -0.514 & 0.170 & 0.047 & 0.004 \\ -0.625 & 0.215 & 0.124 & -0.025 \end{bmatrix},$$

$$P = [PC_1 \quad PC_2 \quad PC_3 \quad PC_4] = \begin{bmatrix} 0.384 & -0.224 & 0.894 & 0.060 \\ 0.437 & 0.894 & 0.030 & 0.096 \\ 0.809 & -0.362 & -0.426 & -0.181 \\ 0.084 & -0.141 & -0.137 & 0.977 \end{bmatrix}$$

As mentioned earlier, the PCs are arranged in the order of descending component variance. For example, $PC_1$ is aligned in the direction with the maximum variance, $PC_2$ in a second largest variance, and so on. The *pca(X)* function in MATLAB® also provides the variance information for each component which is summarized in Table 0.3.

Table 0.3. The proportional variance and the cumulative variance for each principal component.

| | $PC_1$ | $PC_2$ | $PC_3$ | $PC_4$ |
|---|---|---|---|---|
| Proportion of variance | 0.84339 | 0.14180 | 0.01280 | 0.00201 |
| Cumulative variance | 0.84339 | 0.98519 | 0.99800 | 1.00000 |

The table shows that over 98.5% of the data variation in the set $X$ is accounted for by the first two principal components (i.e. $PC_1$ and $PC_2$) and therefore, these two vectors can be adequately

describe the data in *X* without significant loss of information. It is also evident from the table that the combined contributions from $PC_3$ and $PC_4$ account for less than 0.5 % of the data variation in *X*.

Using the first two PCs as basis vectors, the data points in *X* can be plotted on a 2-dimensional space by taking the first and the second columns of the matrix T as the first and the second coordinates in the reduced dimensional space, respectively. Figure 0.10 shows the 2-D mapping of the 12 data points in the matrix *X* used for deriving the principal components. The dotted line divides the 2-dimensional space into 3 regions onto which each analyte is mapped.

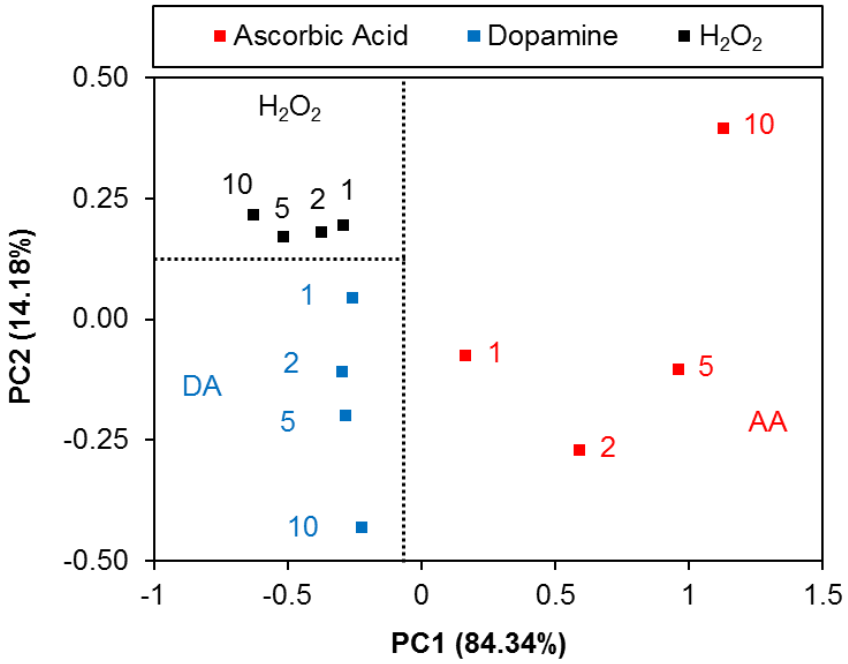


Figure 0.10. Two-dimensional mapping of the data matrix X using $PC_1$ (variance = 84.34 %) and $PC_2$ (variance = 14.18 %). The numbers next to the data points indicate the concentrations of the analyte in mM. The data points for AA, DA, and $H_2O_2$ are indicated in red, blue, and black, respectively.

The mapping of DA and $H_2O_2$ shows some directional trend with respect to the concentration. For DA case, $PC_2$ decreases as concentration increases while $PC_1$ remains more

or less the same. $H_2O_2$ shows greater variation in the $PC_1$ direction, with decreasing $PC_1$ component as concentration increases. Therefore mapping of data points to the principal component domain seems to depend on the concentration of the analyte. The quantification of analyte will be further discussed in section 6.7. For classification of the mixed species where two or more target analyte are present in the sample solution, the similar approach can be taken to map the mixed species onto the 2-dimensional space. The following measurements shown in Table 0.4 were obtained for the mixture of analytes.

Table 0.4. Responses from the sensor array upon exposure to a mixture of analytes.

| Concentration (mM) | | | Blank | $Mn_2O_3$ | CuO | Ag |
|---|---|---|---|---|---|---|
| AA | DA | $H_2O_2$ | | | | |
| 1 | 10 | | 0.417 | -0.152 | 0.671 | 0.267 |
| 2 | 10 | | 0.702 | 0.094 | 0.911 | 0.386 |
| 5 | 10 | | 0.884 | 0.494 | 1.985 | 0.215 |
| 1 | | 10 | 0.189 | 0.016 | -0.657 | -0.081 |
| 2 | | 10 | 0.331 | -0.091 | -0.411 | 0.018 |
| 5 | | 10 | 0.543 | 0.008 | 0.019 | 0.150 |
| | 10 | 5 | 0.161 | -0.591 | -0.276 | 0.077 |
| | 5 | 10 | 0.102 | -0.352 | -0.456 | 0.002 |
| | 10 | 10 | 0.150 | -0.537 | -0.405 | 0.024 |

The data in Table 0.4 was combined with that in Table 0.2 as the new training data set (matrix *X*) to re-evaluate the principal components, and each data point in *X* was plotted on the new 2-dimensional space defined by the first two principal components as illustrated in Figure 0.11. Similarly to the previous case in Figure 0.10, the first two principal components in Figure 0.11 give the cumulative variance of over 67%, meaning that minimal information is lost due to the discarding of the third and the fourth PCs. Although some mixtures such as DA + $H_2O_2$ give unique mapping which does not overlap with regions occupied with other types of analyte, certain mixtures of analyte can create overlapping, one example being the overlap between AA

and AA + DA as shown in Figure 0.11. It is also conceivable that increasing the concentrations of certain analyte beyond the measurable range may further impair the classification ability of this technique.

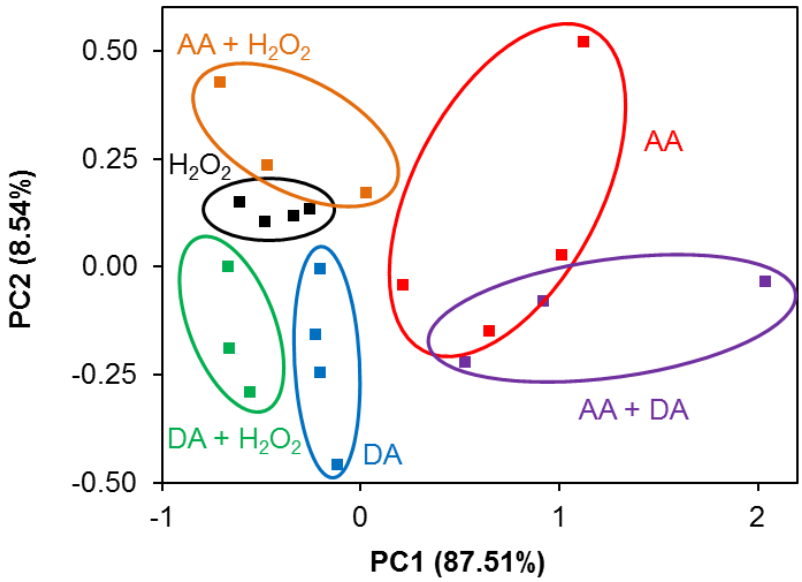


Figure 0.11. Two-dimensional mapping of the data in Table 0.2 and Table 0.4 using $PC_1$ (variance = 87.51 %) and $PC_2$ (variance = 8.54 %). The data points are grouped together and color-coded according to the types of analyte, i.e. AA, DA, $H_2O_2$, and the mixtures thereof.

### 6.7. Quantitative Analysis of Multiple Target Species

In the previous section, PCA method was used to classify the analyte in the sample solution using the 2-dimensional (2-D) mapping without considering the concentration of each analyte. In this section, a PCA-based 2-D mapping technique is further investigated to determine whether quantitative information can be obtained from the map. Although PCA is primarily done for classification purposes, it has been reported that it can also be used to extract some level of quantitative information [167]. To simplify the analysis, detection and quantification of a mixture of two analyte is examined.

As illustrated in Figure 2.1Figure 0.10, the responses of dopamine (DA) and hydrogen peroxide ($H_2O_2$) show a visible trend, although not linear, as concentrations are varied. Hence, a mixture of DA and $H_2O_2$ is first considered. In addition to the data set shown in Table 0.2 and Table 0.4, a few more combinations of concentrations for the DA and $H_2O_2$ were tested and included into the PCA algorithm. Table 0.5 summarizes all the tested concentrations and the measured responses from the sensor array for the quantification of DA and $H_2O_2$.

Table 0.5. Various combinations of concentrations for DA and $H_2O_2$ and the resulting sensor responses.

| Concentration (mM) | | Blank | $Mn_2O_3$ | CuO | Ag |
|---|---|---|---|---|---|
| DA | $H_2O_2$ | | | | |
| 2 | 10 | 0.037 | -0.261 | -0.543 | -0.011 |
| 5 | 10 | 0.102 | -0.352 | -0.456 | 0.002 |
| 10 | 5 | 0.161 | -0.591 | -0.276 | 0.077 |
| 10 | 2 | 0.160 | -0.332 | -0.097 | 0.064 |
| 10 | 10 | 0.150 | -0.537 | -0.405 | 0.024 |

The PCA algorithm was performed on the entire data set including Table 0.2, Table 0.4, and Table 0.5, and each data point from the set was transformed onto the 2-dimensional domain as previously described. Figure 0.12 shows only the plot for DA and $H_2O_2$ measurement for closer examination of these two analyte. The numbers in the graph indicate the concentrations of the analyte in mM. The plot reveals that the data points for the mixture of two analyte (marked with green) are mapped onto the region that lies in between the two areas occupied by the single analyte (either DA or $H_2O_2$) mapping, shown in blue for DA and black for $H_2O_2$. One can observe that the data point approaches closer to either DA only region or the $H_2O_2$ only region depending on the composition of the sample. For instance, the data points for (2, 10) and (10, 2) are positioned close to the data points for 10 mM of $H_2O_2$ and 10 mM of DA, respectively, whereas (10, 10) are located approximately equidistant from the two groups (i.e. the black and

the blue data points). Although the data mapping is not perfectly linear and seems to contain some degree of distortion, this result does demonstrate the possibility for quantitative analysis of analyte using this technique.

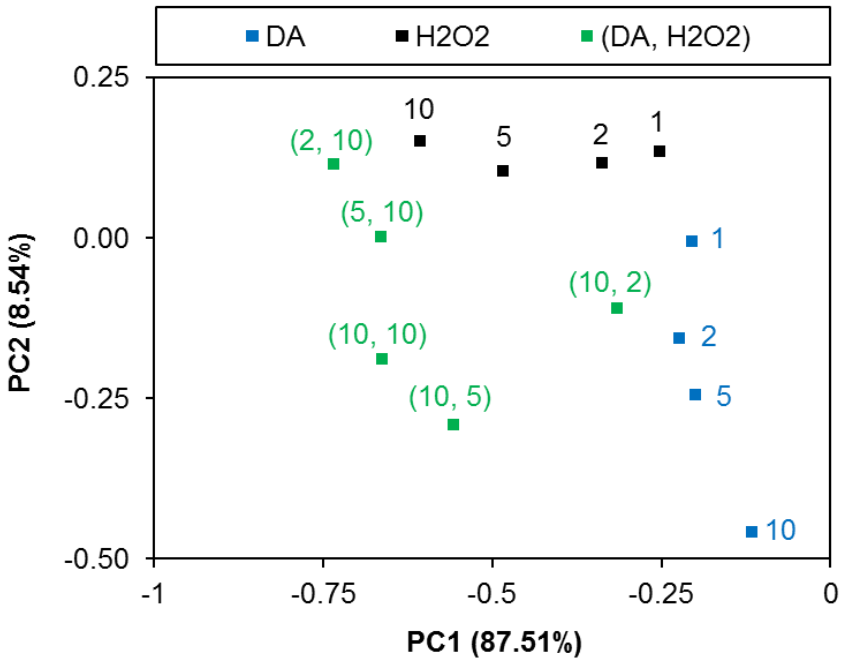


Figure 0.12. Two-dimensional mapping of a mixture of two analyte: dopamine (DA) and hydrogen peroxide ($H_2O_2$). The concentration is marked with the number next to each data point. The numbers inside the bracket indicate the concentration of DA and $H_2O_2$ in mM, respectively.

Similar approach can be taken for the mapping of the other two cases of the mixed analyte: ascorbic acid (AA) mixed with DA, and AA mixed with $H_2O_2$. Figure 0.13 shows the mapping of the entire data set under study. As can be seen from the graph, the bottom left corner of the plot covering the black, blue and green data points is identical to Figure 0.12. The data points for (AA, $H_2O_2$) combination is mapped on the top left corner of the graph (marked in orange) whereas the (AA, DA) combination is located on the bottom right corner of the plot (marked in purple). The results show that as the concentration of AA is increased, the position of the (AA, $H_2O_2$) data moves in the bottom right direction where pure AA sample points are

located. For the case of (AA, DA) couple, an increased concentration of AA leads to the shifting of data to the right due to the contribution from both DA and AA.

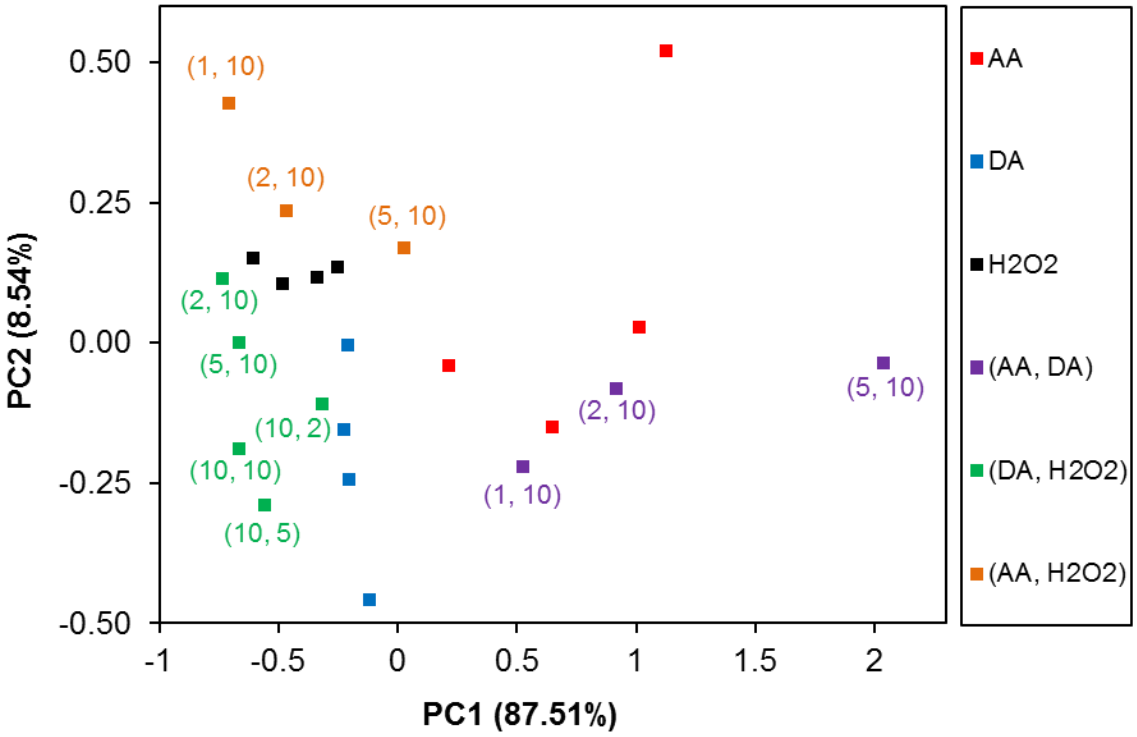


Figure 0.13. Quantification of the mixture of two species: (AA, DA), (DA, $H_2O_2$), and (AA, $H_2O_2$). The numbers in the bracket indicate the concentration of each species of the mixture in their respective order.

### 6.8. Discussion

Since the sensing elements in the array are relatively closely positioned (with a distance between the two neighboring sensing elements being approximately 4 mm), there is a possibility that some catalytic byproducts produced from one sensing element could migrate to the adjacent sensor to affect its response. This apparent "cross-talk" among the sensing elements could potentially generate adverse effect on the sensing performances. To minimize this cross-talk, the diffusion of the byproducts must be minimized. One possible solution would be to implement a

multi-channel microfluidic system which separates the fluid that each sensor is exposed to, thereby avoiding the interference caused by the mixing of the byproducts from different sensing components.

As the dimensions of each sensing element are further reduced, for example down to the nanoscale, the dynamics for the diffusion of species in the solution is much different from that in macroscale. In a nanoscale environment, the rate of diffusion of species is much faster which means that any byproducts generated by the catalytic reaction will immediately diffuse out rendering it difficult to establish a local pH gradient. Therefore, in order to develop a highly sensitive nanoscale catalyst-based chemical sensor, a method to capture the pH-altering byproducts near the polyaniline nanowires and to prevent them from diffusing away from the sensing area is needed.

Although the PCA-based quantitative analysis shows some promising results, at this point the ability to obtain quantitative information about multiple analyte from the two-dimensional mapping and from pattern recognition is limited for the following reasons. First, the data points mapped on Figure 0.13 do not always show a clear trend especially when different species are mixed together. This could be in part due to the instability or the lack of reproducibility of the polyaniline-based chemiresistor. Another possible source of measurement uncertainty is the inconsistency in the number of catalysts that are deposited on each sensor component. It was observed that some catalysts such as $Mn_2O_3$ were consumed as a result of the catalysis which lead to the decrease in the catalytic activity. Another point to note is that PCA is based on a linear transformation method of the data matrix and therefore works under the assumption that the data obtained from each sensing component behaves in a linear fashion. In other words, PCA will be most accurate if each sensing component has a linear calibration curve. As described in

section 6.5, not all calibration curves of the developed sensor array were linear which may have contributed to the nonlinearity of the patterns in the data mapping.

As the number of analytes in the sample increases, more complex algorithm will be necessary to analyze the data. Possible alternatives to the linear techniques such as PCA for dealing with complex nonlinear data set is to use artificial neural networks (ANN) or cluster analysis (CA) [168]. These techniques are not based on statistical methods but can be used to model nonlinearity that may exist in the data by optimizing the parameters in the algorithm with a large number of training data set.

## 6.9. Conclusions

In this chapter, a simultaneous multi-analyte detection was implemented and characterized by utilizing a chemiresistive sensor array based on polyaniline nanowires. Various types of catalysts were incorporated into the sensing area to promote selectivity and cross-reactivity of the chemical species. Ascorbic acid, dopamine, and hydrogen peroxide were selected as the target analyte, and the sensor array comprising four sensing elements was used to identify the solution composition. Classification of the analyte was performed using the principal component analysis (PCA) technique which was effective in reducing the dimensionality of the data space as well as in maximizing the separation of the data samples. PCA method was further expanded for quantification of multi-analyte samples. While some level of quantification can be done by the mapping of data points on two-dimensional space and pattern recognition, full quantification is premature at this point and needs further investigation and development of the technique. For accurate quantification, the chemiresistor must be better optimized to provide reliable signal responses while more advanced multivariate algorithm such as artificial neural network is to be employed for handling large number of analytes with nonlinear data set.

# 7. Conclusions and Future Work

## 7.1. Summary

The main objective of this work is the development of a chemiresistive sensor array for multi-analyte detection based on conducting polymer nanowires. Among the family of conducting polymers, polyaniline nanowires have many advantages for chemiresistive sensing applications such as large conductivity change, easy synthesis and environmental stability. However, the two most critical limitations associated with polyaniline-based chemiresistive sensors are the lack of reproducibility and the lack of chemical selectivity in sensing. To overcome such limitations, this work was done to suggest possible solutions for these problems. This work also demonstrates the possibility of a polyaniline-based sensor array that is capable of multiple species detection. The following is the summary of the three main contributions from this thesis:

1. Development of the self-calibration mechanism of the polyaniline-based chemiresistive sensor for reproducible measurements with minimum hysteresis.
2. Selective detection of chemical species by modifying the polyaniline nanowires with metal- and oxide-based nanoparticles to induce catalytic reactions that cause resistivity change in polyaniline.
3. Implementation and characterization of a polyaniline-based chemiresistive sensor array for simultaneous detection of multiple species.

In the following subsections, the achievements and conclusions from each chapter are given in detail.

### 7.1.1. Polyaniline Nanowire Fabrication and Characterization

In chapter 3, the growth condition for producing one-dimensional polyaniline nanowires using an electrochemical synthesis method was investigated. In order to synthesize polyaniline nanowires, fast polymerization rate is required. Therefore, a potentiostatic growth method, which promotes fast polymerization rate, was chosen in this research. If the monomer concentration was too high, larger diameter fibers were formed. On the other hand, if the monomer concentration was too low, the rate of polymerization was reduced preventing the formation of elongated nanowires.

The electrochemical potential vs. the conduction current relationship of polyaniline nanowires showed a bell-shaped curve with maximum conduction current occurring at approximately half-oxidized state. As the pH of the environment increased, the maximum conductivity was reduced and, at the same time, the potential window within which the polyaniline exhibited conductivity was also narrowed.

The hysteresis in the conductivity was characterized by sweeping the potential in the positive and negative direction which resulted in different I-V curves depending on the direction of the sweep which suggested that the conductivity of polyaniline is highly dependent upon the previous redox state of the polymer.

The conductivity degradation was also examined by repeatedly sweeping the potential and measuring the maximum conductivity for each sweep cycle. As the potential is repeatedly cycled, conductivity degradation became apparent. Possible causes for this degradation are structural damages of the polymer, irreversible oxidation, and hydrolysis of the polymer.

### 7.1.2. Self-Calibration of the Polyaniline-Based Chemiresistive Sensor

Due to the inherent hysteresis and degradation problem associated with the nature of polyaniline, obtaining repeatable sensing measurements from a polyaniline-based chemiresistor had been a challenge. Therefore in chapter 4, new a strategy to produce a repeatable and low-hysteresis current response from the sensor was investigated and proposed. In a self-calibration technique, two approaches were suggested: one is measuring the rate of peak current decay over repeated potential cycling, and the other is measuring the position of the second redox potential of the cyclic voltammetry which is pH-dependent.

Utilizing the ratio of the peak currents of the consecutive potential cycling turned out to be effective only in weak acid solutions (pH > 4) since the decay of the peak conduction current was not significant in the strong acidic environment. On the contrary, making use of the potential for the second redox couple in the CV curve was effective only in low pH environment (pH < 4) since the second redox couple is virtually nonexistent in high pH environment. Therefore the operating regions for the two self-calibration mechanisms complement each other, and therefore the combination of the two methods can provide a wider detection range.

### 7.1.3. Selective Detection of the Chemical Species with the Use of Catalysts

To solve the lack of selectivity issue with polyaniline nanowire-based chemiresistors, a novel concept of catalyst-assisted selective detection of chemicals has been suggested. It was proposed that the catalytic reaction between the target species and the catalysts could cause a local pH change near the polyaniline nanowires which could be detected by measuring the resistance change of the nanowire network. To demonstrate this concept, various nanoparticles such as silver and iron oxide were used as catalysts for the selective detection of hydrogen peroxide. The results confirmed that silver nanoparticles were effective in the selective detection

of hydrogen peroxide which generated catalytic activity with the nanoparticles resulting in a reduced conduction current of the polyaniline nanowires. It was further demonstrated that the rate of the catalysis was proportional to the number of nanoparticles, and given sufficient number of catalysts, the reaction rate was dictated by the concentration of the hydrogen peroxide species.

### 7.1.4. Polyaniline-based Generic Sensor Array for Multi-Analyte Sensing

Once it was confirmed from chapter 5 that selectivity can be enhanced by utilizing catalysts, a natural extension to this work was to develop an array of polyaniline-based sensing elements with each element modified with different types of catalysts to achieve cross-reactive sensing. Three types of catalysts were investigated, namely copper oxide, manganese oxide, and silver nanoparticles, whose catalytic reactions were used for the detection of ascorbic acid, dopamine, and hydrogen peroxide. A sensor array with four sensing components was tested to see whether the responses from each component could be used to detect multiple species simultaneously. Principal component analysis (PCA), which is a pattern recognition tool based on statistical methods, was adopted to process the data and to visualize the patterns in the measured data. PCA is also useful in reducing the dimensionality and removing redundancy in the data set especially when the number of analytes is large. The results show that PCA was effective in classifying the analyte, whether single species or mixed species. The data set obtained from the array of sensors was mapped onto the 2-dimensional space spanned by the first two principal components which provided sufficient information about the variance in the data set with minimum loss of information. Although PCA is mainly used for classification, to a certain extent, quantification can also be done by observing the pattern and the trends in the data points on the mapping. However, true quantification of the multi-species analyte was not achieved with this technique. Developing a more reliable chemiresistive sensor with a larger

array and an advanced nonlinear multivariate algorithm such as artificial neural networks could be used to solve this challenge.

## 7.2. Future Work

For future improvements of this research, the following areas could be further investigated to advance this concept as a viable choice for future sensing technology.

### 7.2.1. Improving the Sensing Performance of the Polyaniline-based Chemiresistor

Although polyaniline-based chemiresistive sensing shows promising results, presently the sensing performance is not impressive. In particular, the limit of detection (LOD) is on the order of a millimolar (mM) range. Reducing the LOD down to the micromolar (μM) range could make this sensor attractive in many applications. Possible solutions to achieving low LOD include: (1) fabrication of a narrower and a thinner polyaniline nanowire network with a more accurate current measurement system, (2) increasing the surface area of the catalysts by uniformly dispersing the nanoparticles throughout the nanowire network in order to maximize the catalytic activity, (3) extending the conductive pH range of polyaniline to the neutral and alkaline pH, and (4) developing a catalytic byproduct capturing mechanism to prevent or minimize the pH-changing species from quickly diffusing away from the polyaniline nanowires.

### 7.2.2. Developing Advanced Algorithm for Multi-Analyte Sensing

Using principal component analysis (PCA) as a pattern recognition algorithm for classification and semi-quantification of multiple species, was a first step toward developing a generic cross-reactive sensor array. However, for the realization of the true quantification capability in multi-analyte sensing, in addition to increasing the number of sensing components in the array, a more complex and nonlinear algorithm is necessary. Artificial neural networks and

cluster analysis are the two main examples that seem to be promising in this regard. These techniques could be used to process a high-dimensional data set containing a large number of target species and sensing components.

### 7.2.3. Inkjet Printing of Polyaniline Nanowires and Nanoparticles

Inkjet printing of nanomaterials have recently emerged as a viable alternative to the conventional fabrication methods for sensor development especially for disposable sensors. Disposable sensors have many advantages especially in biosensors due to their low cost, mass producibility, and portability. Inkjet printing can provide an easy solution to develop disposable sensors [Tortorich_nanomaterials]. Inkjet printing of polyaniline nanoparticles have been previously reported [Crowley_Analyst] however, particles or grains do not form good conducting path for electron transport**.** Therefore, interweaved nanowire network is the desired solution for applications in resistive sensing. Inkjet printing can also be used in developing the polyaniline-based array sensors where each material can be printed individually. The main benefit of this approach in this case is that polyaniline nanowires and the catalysts can be printed in the alternating order so that the two materials can be evenly distributed for optimized catalytic reaction. Moreover, customization of the array can be done relatively easily by choosing the printer cartridge that contains the proper catalysts and by designing the printing pattern to assign which sensing elements are printed with the particular catalysts. If proven successful, this technology may have potential applications in disposable chemical and biological sensors which can easily be printed from home for point-of-care diagnostics.

# References


[1] F. Patolsky, G. Zheng, and C. M. Lieber, "Nanowire-based biosensors," *Anal. Chem.*, vol. 78, no. 13, pp. 4260–4269, Jul. 2006.

[2] M. A. Bangar, D. J. Shirale, H. J. Purohit, W. Chen, N. V. Myung, and A. Mulchandani, "Single conducting polymer nanowire chemiresistive label-free immunosensor for cancer biomarker," *Anal. Chem.*, vol. 81, no. 6, pp. 2168–2175, Mar. 2009.

[3] S. Iijima, "Helical microtubules of graphitic carbon," *Nature*, vol. 354, no. 6348, pp. 56–58, Nov. 1991.

[4] J. Wang, "Carbon-nanotube based electrochemical biosensors: A review," *Electroanalysis*, vol. 17, no. 1, pp. 7–14, 2005.

[5] C. B. Jacobs, M. J. Peairs, and B. J. Venton, "Review: Carbon nanotube based electrochemical sensors for biomolecules," *Analytica Chimica Acta*, vol. 662, no. 2, pp. 105–127, Mar. 2010.

[6] Y. Cui, Q. Wei, H. Park, and C. M. Lieber, "Nanowire nanosensors for highly sensitive and selective detection of biological and chemical species," *Science*, vol. 293, no. 5533, pp. 1289–1292, Aug. 2001.

[7] F. Patolsky and C. M. Lieber, "Nanowire nanosensors," *Materials Today*, vol. 8, no. 4, pp. 20–28, Apr. 2005.

[8] U. Yogeswaran and S.-M. Chen, "A review on the electrochemical sensors and biosensors composed of nanowires as sensing material," *Sensors*, vol. 8, no. 1, pp. 290–313, Jan. 2008.

[9] M. A. Bangar, W. Chen, N. V. Myung, and A. Mulchandani, "Conducting polymer 1-dimensional nanostructures for FET sensors," *Thin Solid Films*, vol. 519, no. 3, pp. 964–973, Nov. 2010.

[10] S. Virji, R. B. Kaner, and B. H. Weiller, "Hydrogen sensors based on conductivity changes in polyaniline nanofibers," *J. Phys. Chem. B*, vol. 110, no. 44, pp. 22266–22270, Nov. 2006.

[11] J. Wang, Y. L. Bunimovich, G. Sui, S. Savvas, J. Wang, Y. Guo, J. R. Heath, and H.-R. Tseng, "Electrochemical fabrication of conducting polymer nanowires in an integrated microfluidic system," *Chemical Communications*, no. 29, pp. 3075–3077, 2006.

[12] J. Wang, S. Chan, R. R. Carlson, Y. Luo, G. Ge, R. S. Ries, J. R. Heath, and H.-R. Tseng, "Electrochemically fabricated polyaniline nanoframework electrode junctions that function as resistive sensors," *Nano Lett.*, vol. 4, no. 9, pp. 1693–1697, Sep. 2004.

[13] P. Kuhn, J. Puigmartí-Luis, I. Imaz, D. Maspoch, and P. S. Dittrich, "Controlling the length and location of in situ formed nanowires by means of microfluidic tools," *Lab on a Chip*, vol. 11, no. 4, p. 753, 2011.

[14] S. Hou, S. Wang, Z. T. F. Yu, N. Q. M. Zhu, K. Liu, J. Sun, W.-Y. Lin, C. K.-F. Shen, X. Fang, and H.-R. Tseng, "A hydrodynamically focused stream as a dynamic template for site-specific electrochemical micropatterning of conducting polymers," *Angewandte Chemie*, vol. 120, no. 6, pp. 1088–1091, 2008.

[15] J. Puigmartí-Luis, D. Schaffhauser, B. R. Burg, and P. S. Dittrich, "A microfluidic approach for the formation of conductive nanowires and hollow hybrid structures," *Advanced Materials*, vol. 22, no. 20, pp. 2255–2259, 2010.

[16] H. Shirakawa, E. J. Louis, A. G. MacDiarmid, C. K. Chiang, and A. J. Heeger, "Synthesis of electrically conducting organic polymers: Halogen derivatives of polyacetylene, (CH)x," *J. Chem. Soc., Chem. Commun.*, no. 16, pp. 578–580, 1977.

[17] A. G. Macdiarmid, J. C. Chiang, A. F. Richter, and A. J. Epstein, "Polyaniline: A new concept in conducting polymers," *Synthetic Metals*, vol. 18, no. 1–3, pp. 285–290, Feb. 1987.

[18] T. A. Sergeyeva, N. V. Lavrik, S. A. Piletsky, A. E. Rachkov, and A. V. El'skaya, "Polyaniline label-based conductometric sensor for IgG detection," *Sensors and Actuators B: Chemical*, vol. 34, no. 1–3, pp. 283–288, Aug. 1996.

[19] M. Gerard, A. Chaubey, and B. D. Malhotra, "Application of conducting polymers to biosensors," *Biosensors and Bioelectronics*, vol. 17, no. 5, pp. 345–359, May 2002.

[20] C. Dhand, M. Das, M. Datta, and B. D. Malhotra, "Recent advances in polyaniline based biosensors," *Biosensors and Bioelectronics*, vol. 26, no. 6, pp. 2811–2821, Feb. 2011.

[21] U. Lange, N. V. Roznyatovskaya, and V. M. Mirsky, "Conducting polymers in chemical sensors and arrays," *Analytica Chimica Acta*, vol. 614, no. 1, pp. 1–26, Apr. 2008.

[22] T. Kobayashi, H. Yoneyama, and H. Tamura, "Oxidative degradation pathway of polyaniline film electrodes," *Journal of Electroanalytical Chemistry and Interfacial Electrochemistry*, vol. 177, no. 1–2, pp. 293–297, Oct. 1984.

[23] E. Song and J.-W. Choi, "Conducting Polyaniline Nanowire and Its Applications in Chemiresistive Sensing," *Nanomaterials*, vol. 3, no. 3, pp. 498–523, Aug. 2013.

[24] J. Reddinger and J. Reynolds, "Molecular Engineering of π-Conjugated Polymers," in *Radical Polymerisation Polyelectrolytes*, vol. 145, Springer Berlin / Heidelberg, 1999, pp. 57–122.

[25] A. G. MacDiarmid and A. J. Epstein, "Polyanilines: a novel class of conducting polymers," *Faraday Discussions of the Chemical Society*, vol. 88, pp. 317–332, 1989.

[26] A. A. Syed and M. K. Dinesan, “Review: Polyaniline—A novel polymeric material,” *Talanta*, vol. 38, no. 8, pp. 815–837, Aug. 1991.

[27] E. M. Geniès, A. Boyle, M. Lapkowski, and C. Tsintavis, “Polyaniline: A historical survey,” *Synthetic Metals*, vol. 36, no. 2, pp. 139–182, Jun. 1990.

[28] W.-S. Huang, B. D. Humphrey, and A. G. MacDiarmid, “Polyaniline, a novel conducting polymer. Morphology and chemistry of its oxidation and reduction in aqueous electrolytes,” *Journal of the Chemical Society, Faraday Transactions 1*, vol. 82, no. 8, pp. 2385–2400, 1986.

[29] S. Bhadra, D. Khastgir, N. K. Singha, and J. H. Lee, “Progress in preparation, processing and applications of polyaniline,” *Progress in Polymer Science*, vol. 34, no. 8, pp. 783–810, Aug. 2009.

[30] J. Stejskal, I. Sapurina, and M. Trchová, “Polyaniline nanostructures and the role of aniline oligomers in their formation,” *Progress in Polymer Science*, vol. 35, no. 12, pp. 1420–1481, Dec. 2010.

[31] H. D. Tran, Y. Wang, J. M. D’Arcy, and R. B. Kaner, “Toward an Understanding of the Formation of Conducting Polymer Nanofibers,” *ACS Nano*, vol. 2, no. 9, pp. 1841–1848, Sep. 2008.

[32] D. Zhang and Y. Wang, “Synthesis and applications of one-dimensional nano-structured polyaniline: An overview,” *Materials Science and Engineering: B*, vol. 134, no. 1, pp. 9–19, Sep. 2006.

[33] A. G. Macdiarmid, S.-L. Mu, N. L. D. Somasiri, and W. Wu, “Electrochemical Characteristics of ‘Polyaniline’ Cathodes and Anodes in Aqueous Electrolytes,” *Molecular Crystals and Liquid Crystals*, vol. 121, no. 1–4, pp. 187–190, 1985.

[34] V. Gupta and N. Miura, “High performance electrochemical supercapacitor from electrochemically synthesized nanostructured polyaniline,” *Materials Letters*, vol. 60, no. 12, pp. 1466–1469, Jun. 2006.

[35] M. Zhiani, H. Gharibi, and K. Kakaei, “Performing of novel nanostructure MEA based on polyaniline modified anode in direct methanol fuel cell,” *Journal of Power Sources*, vol. 210, pp. 42–46, Jul. 2012.

[36] F. M. Kelly, L. Meunier, C. Cochrane, and V. Koncar, “Polyaniline: application as solid state electrochromic in a flexible textile display,” *Displays*, vol. 34, no. 1, pp. 1–7, Jan. 2013.

[37] M. R. Anderson, B. R. Mattes, H. Reiss, and R. B. Kaner, “Conjugated Polymer Films for Gas Separations,” *Science*, vol. 252, no. 5011, pp. 1412–1415, Jun. 1991.

[38] C.-H. Chang, T.-C. Huang, C.-W. Peng, T.-C. Yeh, H.-I. Lu, W.-I. Hung, C.-J. Weng, T.-I. Yang, and J.-M. Yeh, "Novel anticorrosion coatings prepared from polyaniline/graphene composites," *Carbon*, vol. 50, no. 14, pp. 5044–5051, Nov. 2012.

[39] S. Stafström, J. L. Brédas, A. J. Epstein, H. S. Woo, D. B. Tanner, W. S. Huang, and A. G. MacDiarmid, "Polaron lattice in highly conducting polyaniline: Theoretical and optical studies," *Phys. Rev. Lett.*, vol. 59, no. 13, pp. 1464–1467, Sep. 1987.

[40] A. J. Heeger, "Semiconducting and Metallic Polymers: The Fourth Generation of Polymeric Materials†," *J. Phys. Chem. B*, vol. 105, no. 36, pp. 8475–8491, Sep. 2001.

[41] E. M. Genies and C. Tsintavis, "Redox mechanism and electrochemical behaviour or polyaniline deposits," *Journal of Electroanalytical Chemistry and Interfacial Electrochemistry*, vol. 195, no. 1, pp. 109–128, Nov. 1985.

[42] E. M. Geniès, M. Lapkowski, and J. F. Penneau, "Cyclic voltammetry of polyaniline: interpretation of the middle peak," *Journal of Electroanalytical Chemistry and Interfacial Electrochemistry*, vol. 249, no. 1–2, pp. 97–107, Jul. 1988.

[43] P. Nunziante and G. Pistoia, "Factors affecting the growth of thick polyaniline films by the cyclic voltammetry technique," *Electrochimica Acta*, vol. 34, no. 2, pp. 223–228, Feb. 1989.

[44] W. W. Focke, G. E. Wnek, and Y. Wei, "Influence of oxidation state, pH, and counterion on the conductivity of polyaniline," *J. Phys. Chem.*, vol. 91, no. 22, pp. 5813–5818, Oct. 1987.

[45] A. G. MacDiarmid, "'Synthetic Metals': A Novel Role for Organic Polymers (Nobel Lecture)," *Angewandte Chemie International Edition*, vol. 40, no. 14, pp. 2581–2590, 2001.

[46] W. W. Focke and G. E. Wnek, "Conduction mechanisms in polyaniline (emeraldine salt)," *Journal of Electroanalytical Chemistry and Interfacial Electrochemistry*, vol. 256, no. 2, pp. 343–352, Dec. 1988.

[47] A. H. Saheb and S. S. Seo, "UV-Vis and Raman Spectral Analysis of Polyaniline/Gold Thin Films as a Function of Applied Potential," *Analytical Letters*, vol. 44, no. 7, pp. 1206–1216, 2011.

[48] Y.-F. Lin, C.-H. Chen, W.-J. Xie, S.-H. Yang, C.-S. Hsu, M.-T. Lin, and W.-B. Jian, "Nano Approach Investigation of the Conduction Mechanism in Polyaniline Nanofibers," *ACS Nano*, vol. 5, no. 2, pp. 1541–1548, Feb. 2011.

[49] Q. Li, L. Cruz, and P. Phillips, "Granular-rod model for electronic conduction in polyaniline," *Phys. Rev. B*, vol. 47, no. 4, pp. 1840–1845, Jan. 1993.

[50] W. Li and M. Wan, "Porous polyaniline films with high conductivity," *Synthetic Metals*, vol. 92, no. 2, pp. 121–126, Jan. 1998.

[51] N. F. Mott and E. A. Davis, *Electronic Processes in Non-Crystalline Materials*. Oxford University Press, 2012.

[52] J. Joo, S. M. Long, J. P. Pouget, E. J. Oh, A. G. MacDiarmid, and A. J. Epstein, "Charge transport of the mesoscopic metallic state in partially crystalline polyanilines," *Phys. Rev. B*, vol. 57, no. 16, pp. 9567–9580, Apr. 1998.

[53] M. Ghosh, A. Barman, S. K. De, and S. Chatterjee, "Crossover from Mott to Efros-Shklovskii variable-range-hopping conductivity in conducting polyaniline," *Synthetic Metals*, vol. 97, no. 1, pp. 23–29, Aug. 1998.

[54] P. Sheng, B. Abeles, and Y. Arie, "Hopping Conductivity in Granular Metals," *Phys. Rev. Lett.*, vol. 31, no. 1, pp. 44–47, Jul. 1973.

[55] Y. Zhou, M. Freitag, J. Hone, C. Staii, A. T. Johnson, N. J. Pinto, and A. G. MacDiarmid, "Fabrication and electrical characterization of polyaniline-based nanofibers with diameter below 30 nm," *Applied Physics Letters*, vol. 83, no. 18, pp. 3800–3802, 2003.

[56] W. Liu, J. Kumar, S. Tripathy, K. J. Senecal, and L. Samuelson, "Enzymatically Synthesized Conducting Polyaniline," *J. Am. Chem. Soc.*, vol. 121, no. 1, pp. 71–78, Jan. 1999.

[57] Y. Ma, J. Zhang, G. Zhang, and H. He, "Polyaniline Nanowires on Si Surfaces Fabricated with DNA Templates," *J. Am. Chem. Soc.*, vol. 126, no. 22, pp. 7097–7101, Jun. 2004.

[58] M. Trchová, I. Šeděnková, E. N. Konyushenko, J. Stejskal, P. Holler, and G. Ćirić-Marjanović, "Evolution of Polyaniline Nanotubes: The Oxidation of Aniline in Water," *J. Phys. Chem. B*, vol. 110, no. 19, pp. 9461–9468, May 2006.

[59] L. Zhang, Z. D. Zujovic, H. Peng, G. A. Bowmaker, P. A. Kilmartin, and J. Travas-Sejdic, "Structural Characteristics of Polyaniline Nanotubes Synthesized from Different Buffer Solutions," *Macromolecules*, vol. 41, no. 22, pp. 8877–8884, Nov. 2008.

[60] N.-R. Chiou and A. J. Epstein, "Polyaniline Nanofibers Prepared by Dilute Polymerization," *Advanced Materials*, vol. 17, no. 13, pp. 1679–1683, 2005.

[61] Y. Wei, X. Tang, Y. Sun, and W. W. Focke, "A study of the mechanism of aniline polymerization," *Journal of Polymer Science Part A: Polymer Chemistry*, vol. 27, no. 7, pp. 2385–2396, 1989.

[62] H. Yang and A. J. Bard, "The application of fast scan cyclic voltammetry. Mechanistic study of the initial stage of electropolymerization of aniline in aqueous solutions," *Journal of Electroanalytical Chemistry*, vol. 339, no. 1–2, pp. 423–449, Nov. 1992.

[63] D. Li, J. Huang, and R. B. Kaner, "Polyaniline Nanofibers: A Unique Polymer Nanostructure for Versatile Applications," *Acc. Chem. Res.*, vol. 42, no. 1, pp. 135–145, Jan. 2009.

[64] J. Huang and R. B. Kaner, “Nanofiber Formation in the Chemical Polymerization of Aniline: A Mechanistic Study,” *Angewandte Chemie*, vol. 116, no. 43, pp. 5941–5945, 2004.

[65] H. V. R. Dias, X. Wang, R. M. G. Rajapakse, and R. L. Elsenbaumer, “A mild, copper catalyzed route to conducting polyaniline,” *Chemical Communications*, no. 9, p. 976, 2006.

[66] J. Huang and R. B. Kaner, “A General Chemical Route to Polyaniline Nanofibers,” *J. Am. Chem. Soc.*, vol. 126, no. 3, pp. 851–855, Jan. 2004.

[67] J. Huang, S. Virji, B. H. Weiller, and R. B. Kaner, “Polyaniline Nanofibers: Facile Synthesis and Chemical Sensors,” *J. Am. Chem. Soc.*, vol. 125, no. 2, pp. 314–315, Jan. 2003.

[68] J. Qiang, Z. Yu, H. Wu, and D. Yun, “Polyaniline nanofibers synthesized by rapid mixing polymerization,” *Synthetic Metals*, vol. 158, no. 13, pp. 544–547, Aug. 2008.

[69] C. R. Martin, “Template Synthesis of Electronically Conductive Polymer Nanostructures,” *Acc. Chem. Res.*, vol. 28, no. 2, pp. 61–68, Feb. 1995.

[70] C. R. Martin, “Nanomaterials: A Membrane-Based Synthetic Approach,” *Science*, vol. 266, no. 5193, pp. 1961–1966, Dec. 1994.

[71] V. Gupta and N. Miura, “Large-area network of polyaniline nanowires prepared by potentiostatic deposition process,” *Electrochemistry Communications*, vol. 7, no. 10, pp. 995–999, Oct. 2005.

[72] A. Kitani, M. Kaya, J. Yano, K. Yoshikawa, and K. Sasaki, “‘Polyaniline’: Formation reaction and structure,” *Synthetic Metals*, vol. 18, no. 1–3, pp. 341–346, Feb. 1987.

[73] L. Liang, J. Liu, C. F. Windisch, Jr., G. J. Exarhos, and Y. Lin, “Direct Assembly of Large Arrays of Oriented Conducting Polymer Nanowires,” *Angewandte Chemie International Edition*, vol. 41, no. 19, pp. 3665–3668, 2002.

[74] S.-J. Choi and S.-M. Park, “Electrochemical Growth of Nanosized Conducting Polymer Wires on Gold Using Molecular Templates,” *Advanced Materials*, vol. 12, no. 20, pp. 1547–1549, 2000.

[75] D. E. Stilwell and S.-M. Park, “Electrochemistry of Conductive Polymers IV Electrochemical Studies on Polyaniline Degradation — Product Identification and Coulometric Studies,” *J. Electrochem. Soc.*, vol. 135, no. 10, pp. 2497–2502, Oct. 1988.

[76] L. Huang, Z. Wang, H. Wang, X. Cheng, A. Mitra, and Y. Yan, “Polyaniline nanowires by electropolymerization from liquid crystalline phases,” *Journal of Materials Chemistry*, vol. 12, no. 2, pp. 388–391, Jan. 2002.

[77] S. Mu and Y. Yang, “Spectral Characteristics of Polyaniline Nanostructures Synthesized by Using Cyclic Voltammetry at Different Scan Rates,” *J. Phys. Chem. B*, vol. 112, no. 37, pp. 11558–11563, Sep. 2008.

[78] A. F. Diaz and J. A. Logan, “Electroactive polyaniline films,” *Journal of Electroanalytical Chemistry and Interfacial Electrochemistry*, vol. 111, no. 1, pp. 111–114, Jul. 1980.

[79] G. Li, C. Martinez, J. Janata, J. A. Smith, M. Josowicz, and S. Semancik, “Effect of Morphology on the Response of Polyaniline-based Conductometric Gas Sensors: Nanofibers vs. Thin Films,” *Electrochem. Solid-State Lett.*, vol. 7, no. 10, pp. H44–H47, Oct. 2004.

[80] S. Virji, J. Huang, R. B. Kaner, and B. H. Weiller, “Polyaniline nanofiber gas sensors: Examination of response mechanisms,” *Nano Lett.*, vol. 4, no. 3, pp. 491–496, Mar. 2004.

[81] A. Z. Sadek, W. Wlodarski, K. Kalantar-Zadeh, C. Baker, and R. B. Kaner, “Doped and dedoped polyaniline nanofiber based conductometric hydrogen gas sensors,” *Sensors and Actuators A: Physical*, vol. 139, no. 1–2, pp. 53–57, Sep. 2007.

[82] F.-W. Zeng, X.-X. Liu, D. Diamond, and K. T. Lau, “Humidity sensors based on polyaniline nanofibres,” *Sensors and Actuators B: Chemical*, vol. 143, no. 2, pp. 530–534, Jan. 2010.

[83] Q. Lin, Y. Li, and M. Yang, “Polyaniline nanofiber humidity sensor prepared by electrospinning,” *Sensors and Actuators B: Chemical*, vol. 161, no. 1, pp. 967–972, Jan. 2012.

[84] Y. Liao, C. Zhang, Y. Zhang, V. Strong, J. Tang, X.-G. Li, K. Kalantar-zadeh, E. M. V. Hoek, K. L. Wang, and R. B. Kaner, “Carbon Nanotube/Polyaniline Composite Nanofibers: Facile Synthesis and Chemosensors,” *Nano Lett.*, vol. 11, no. 3, pp. 954–959, Mar. 2011.

[85] M. D. Shirsat, M. A. Bangar, M. A. Deshusses, N. V. Myung, and A. Mulchandani, “Polyaniline nanowires-gold nanoparticles hybrid network based chemiresistive hydrogen sulfide sensor,” *Applied Physics Letters*, vol. 94, no. 8, pp. 083502–083502–3, 2009.

[86] L. C. Clark and C. Lyons, “Electrode Systems for Continuous Monitoring in Cardiovascular Surgery,” *Annals of the New York Academy of Sciences*, vol. 102, no. 1, pp. 29–45, 1962.

[87] J. Wang, “Electrochemical Glucose Biosensors,” *Chem. Rev.*, vol. 108, no. 2, pp. 814–825, Feb. 2008.

[88] P. N. Bartlett and Y. Astier, “Microelectrochemical enzyme transistors,” *Chem. Commun.*, no. 2, pp. 105–112, Jan. 2000.

[89] H. S. White, G. P. Kittlesen, and M. S. Wrighton, “Chemical derivatization of an array of three gold microelectrodes with polypyrrole: fabrication of a molecule-based transistor,” *J. Am. Chem. Soc.*, vol. 106, no. 18, pp. 5375–5377, Sep. 1984.

[90] D. Ofer, R. M. Crooks, and M. S. Wrighton, “Potential dependence of the conductivity of highly oxidized polythiophenes, polypyrroles, and polyaniline: finite windows of high conductivity,” *J. Am. Chem. Soc.*, vol. 112, no. 22, pp. 7869–7879, Oct. 1990.

[91] A. Mulchandani and N. V. Myung, “Conducting polymer nanowires-based label-free biosensors,” *Current Opinion in Biotechnology*, vol. 22, no. 4, pp. 502–508, Aug. 2011.

[92] P. N. Bartlett and P. R. Birkin, “A Microelectrochemical Enzyme Transistor Responsive to Glucose,” *Anal. Chem.*, vol. 66, no. 9, pp. 1552–1559, May 1994.

[93] P. N. Bartlett, P. R. Birkin, J. H. Wang, F. Palmisano, and G. De Benedetto, “An Enzyme Switch Employing Direct Electrochemical Communication between Horseradish Peroxidase and a Poly(aniline) Film,” *Anal. Chem.*, vol. 70, no. 17, pp. 3685–3694, Sep. 1998.

[94] F. Battaglini, P. N. Bartlett, and J. H. Wang, “Covalent Attachment of Osmium Complexes to Glucose Oxidase and the Application of the Resulting Modified Enzyme in an Enzyme Switch Responsive to Glucose,” *Anal. Chem.*, vol. 72, no. 3, pp. 502–509, Feb. 2000.

[95] E. S. Forzani, H. Zhang, L. A. Nagahara, I. Amlani, R. Tsui, and N. Tao, “A Conducting Polymer Nanojunction Sensor for Glucose Detection,” *Nano Lett.*, vol. 4, no. 9, pp. 1785–1788, Sep. 2004.

[96] S. Pal, E. C. Alocilja, and F. P. Downes, “Nanowire labeled direct-charge transfer biosensor for detecting Bacillus species,” *Biosensors and Bioelectronics*, vol. 22, no. 9–10, pp. 2329–2336, Apr. 2007.

[97] J. S. Yuk, J.-H. Jin, E. C. Alocilja, and J. B. Rose, “Performance enhancement of polyaniline-based polymeric wire biosensor,” *Biosensors and Bioelectronics*, vol. 24, no. 5, pp. 1348–1352, Jan. 2009.

[98] Z. Muhammad-Tahir and E. C. Alocilja, “A conductometric biosensor for biosecurity,” *Biosensors and Bioelectronics*, vol. 18, no. 5–6, pp. 813–819, May 2003.

[99] Z. M. Tahir, E. C. Alocilja, and D. L. Grooms, “Polyaniline synthesis and its biosensor application,” *Biosensors and Bioelectronics*, vol. 20, no. 8, pp. 1690–1695, Feb. 2005.

[100] E. S. Forzani, X. Li, and N. Tao, “Hybrid Amperometric and Conductometric Chemical Sensor Based on Conducting Polymer Nanojunctions,” *Anal. Chem.*, vol. 79, no. 14, pp. 5217–5224, Jul. 2007.

[101] Y. Fan, X. Chen, A. D. Trigg, C. Tung, J. Kong, and Z. Gao, “Detection of MicroRNAs Using Target-Guided Formation of Conducting Polymer Nanowires in Nanogaps,” *J. Am. Chem. Soc.*, vol. 129, no. 17, pp. 5437–5443, May 2007.

[102] Z. Q. Gao, S. Rafea, and L. H. Lim, “Detection of Nucleic Acids Using Enzyme-Catalyzed Template-Guided Deposition of Polyaniline,” *Advanced Materials*, vol. 19, no. 4, pp. 602–606, 2007.

[103] H. Chang, Y. Yuan, N. Shi, and Y. Guan, “Electrochemical DNA Biosensor Based on Conducting Polyaniline Nanotube Array,” *Anal. Chem.*, vol. 79, no. 13, pp. 5111–5115, Jul. 2007.

[104] M. M. Castillo-Ortega, D. E. Rodriguez, J. C. Encinas, M. Plascencia, F. A. Méndez-Velarde, and R. Olayo, “Conductometric uric acid and urea biosensor prepared from electroconductive polyaniline–poly(n-butyl methacrylate) composites,” *Sensors and Actuators B: Chemical*, vol. 85, no. 1–2, pp. 19–25, Jun. 2002.

[105] H. Sangodkar, S. Sukeerthi, R. S. Srinivasa, R. Lal, and A. Q. Contractor, “A Biosensor Array Based on Polyaniline,” *Anal. Chem.*, vol. 68, no. 5, pp. 779–783, Mar. 1996.

[106] Z. Muhammad-Tahir and E. C. Alocilja, “Fabrication of a disposable biosensor for Escherichia Coli O157:H7 detection,” *IEEE Sensors Journal*, vol. 3, no. 4, pp. 345–351, 2003.

[107] D. Raffa, K. T. Leung, and F. Battaglini, “A Microelectrochemical Enzyme Transistor Based on an N-Alkylated Poly(Aniline) and Its Application to Determine Hydrogen Peroxide at Neutral pH,” *Anal. Chem.*, vol. 75, no. 19, pp. 4983–4987, Oct. 2003.

[108] J. Yue and A. J. Epstein, “Synthesis of self-doped conducting polyaniline,” *J. Am. Chem. Soc.*, vol. 112, no. 7, pp. 2800–2801, Mar. 1990.

[109] J. Yue, Z. H. Wang, K. R. Cromack, A. J. Epstein, and A. G. MacDiarmid, “Effect of sulfonic acid group on polyaniline backbone,” *J. Am. Chem. Soc.*, vol. 113, no. 7, pp. 2665–2671, Mar. 1991.

[110] J. Yue, A. J. Epstein, and A. G. Macdiarmid, “Sulfonic Acid Ring-Substituted Polyaniline, A Self-Doped Conducting Polymer,” *Molecular Crystals and Liquid Crystals Incorporating Nonlinear Optics*, vol. 189, no. 1, pp. 255–261, 1990.

[111] C. Thiemann and C. M. . Brett, “Electrosynthesis and properties of conducting polymers derived from aminobenzoic acids and from aminobenzoic acids and aniline,” *Synthetic Metals*, vol. 123, no. 1, pp. 1–9, Aug. 2001.

[112] C. Thiemann and C. M. . Brett, “Electropolymerisation and properties of conducting polymers derived from aminobenzenesulphonic acids and from mixtures with aniline,” *Synthetic Metals*, vol. 125, no. 3, pp. 445–451, Dec. 2001.

[113] L. V. Lukachova, E. A. Shkerin, E. A. Puganova, E. E. Karyakina, S. G. Kiseleva, A. V. Orlov, G. P. Karpacheva, and A. A. Karyakin, "Electroactivity of chemically synthesized polyaniline in neutral and alkaline aqueous solutions: Role of self-doping and external doping," *Journal of Electroanalytical Chemistry*, vol. 544, pp. 59–63, Mar. 2003.

[114] L. Zhang and S. Dong, "The electrocatalytic oxidation of ascorbic acid on polyaniline film synthesized in the presence of camphorsulfonic acid," *Journal of Electroanalytical Chemistry*, vol. 568, pp. 189–194, Jul. 2004.

[115] M. Reghu, Y. Cao, D. Moses, and A. J. Heeger, "Counterion-induced processibility of polyaniline: Transport at the metal-insulator boundary," *Phys. Rev. B*, vol. 47, no. 4, pp. 1758–1764, Jan. 1993.

[116] X. Lu, H. Y. Ng, J. Xu, and C. He, "Electrical conductivity of polyaniline–dodecylbenzene sulphonic acid complex: thermal degradation and its mechanism," *Synthetic Metals*, vol. 128, no. 2, pp. 167–178, Apr. 2002.

[117] T. Del Castillo-Castro, M. M. Castillo-Ortega, I. Villarreal, F. Brown, H. Grijalva, M. Pérez-Tello, S. M. Nuño-Donlucas, and J. E. Puig, "Synthesis and characterization of composites of DBSA-doped polyaniline and polystyrene-based ionomers," *Composites Part A: Applied Science and Manufacturing*, vol. 38, no. 2, pp. 639–645, Feb. 2007.

[118] P. N. Bartlett and E. Simon, "Poly(aniline)–poly(acrylate) composite films as modified electrodes for the oxidation of NADH," *Physical Chemistry Chemical Physics*, vol. 2, no. 11, pp. 2599–2606, 2000.

[119] O. A. Raitman, E. Katz, A. F. Bückmann, and I. Willner, "Integration of Polyaniline/Poly(acrylic acid) Films and Redox Enzymes on Electrode Supports: An in Situ Electrochemical/Surface Plasmon Resonance Study of the Bioelectrocatalyzed Oxidation of Glucose or Lactate in the Integrated Bioelectrocatalytic Systems," *J. Am. Chem. Soc.*, vol. 124, no. 22, pp. 6487–6496, Jun. 2002.

[120] A. M. Bonastre, M. Sosna, and P. N. Bartlett, "An analysis of the kinetics of oxidation of ascorbate at poly(aniline)-poly(styrene sulfonate) modified microelectrodes," *Physical Chemistry Chemical Physics*, vol. 13, no. 12, p. 5365, 2011.

[121] P. N. Bartlett and J. H. Wang, "Electroactivity, stability and application in an enzyme switch at pH 7 of poly(aniline)-poly(styrenesulfonate) composite films," *Journal of the Chemical Society, Faraday Transactions*, vol. 92, no. 20, pp. 4137–4143, 1996.

[122] E. W. Paul, A. J. Ricco, and M. S. Wrighton, "Resistance of polyaniline films as a function of electrochemical potential and the fabrication of polyaniline-based microelectronic devices," *J. Phys. Chem.*, vol. 89, no. 8, pp. 1441–1447, Apr. 1985.

[123] M. Łapkowski and E. Vieil, "Control of polyaniline electroactivity by ion size exclusion," *Synthetic Metals*, vol. 109, no. 1–3, pp. 199–201, Mar. 2000.

[124] T. Kobayashi, H. Yoneyama, and H. Tamura, "Electrochemical reactions concerned with electrochromism of polyaniline film-coated electrodes," *Journal of Electroanalytical Chemistry and Interfacial Electrochemistry*, vol. 177, no. 1–2, pp. 281–291, Oct. 1984.

[125] D. E. Stilwell and S.-M. Park, "Electrochemistry of Conductive Polymers IV Electrochemical Studies on Polyaniline Degradation — Product Identification and Coulometric Studies," *J. Electrochem. Soc.*, vol. 135, no. 10, pp. 2497–2502, Oct. 1988.

[126] S.-Y. Lee, G.-R. Choi, H. Lim, K.-M. Lee, and S.-K. Lee, "Electronic transport characteristics of electrolyte-gated conducting polyaniline nanowire field-effect transistors," *Applied Physics Letters*, vol. 95, no. 1, pp. 013113–013113–3, Jul. 2009.

[127] S.-Y. Lee, S.-K. Lee, H. Lim, and G.-R. Choi, "Irreversible Degradation Behaviors of an Electrolyte-gated Polyaniline (PANI) Nanowire Field-effect Transistor," *Journal of the Korean Physical Society*, vol. 57, no. 6, pp. 1416–1420, Dec. 2010.

[128] M. Nechtschein, F. Genoud, C. Menardo, K. Mizoguchi, J. P. Travers, and B. Villeret, "On the nature of the conducting state of polyaniline," *Synthetic Metals*, vol. 29, no. 1, pp. 211–218, Mar. 1989.

[129] H. He, J. Zhu, N. J. Tao, L. A. Nagahara, I. Amlani, and R. Tsui, "A Conducting Polymer Nanojunction Switch," *J. Am. Chem. Soc.*, vol. 123, no. 31, pp. 7730–7731, Aug. 2001.

[130] N. T. Kemp, J. W. Cochrane, and R. Newbury, "Characteristics of the nucleation and growth of template-free polyaniline nanowires and fibrils," *Synthetic Metals*, vol. 159, no. 5–6, pp. 435–444, Mar. 2009.

[131] Z. Jin, Y. Su, and Y. Duan, "An improved optical pH sensor based on polyaniline," *Sensors and Actuators B: Chemical*, vol. 71, no. 1–2, pp. 118–122, Nov. 2000.

[132] C. M. Hangarter, N. Chartuprayoon, S. C. Hernández, Y. Choa, and N. V. Myung, "Hybridized conducting polymer chemiresistive nano-sensors," *Nano Today*, vol. 8, no. 1, pp. 39–55, Feb. 2013.

[133] Y. Tang, K. Pan, X. Wang, C. Liu, and S. Luo, "Electrochemical synthesis of polyaniline in surface-attached poly(acrylic acid) network, and its application to the electrocatalytic oxidation of ascorbic acid," *Microchim Acta*, vol. 168, no. 3–4, pp. 231–237, Mar. 2010.

[134] J. E. Yoo, J. L. Cross, T. L. Bucholz, K. S. Lee, M. P. Espe, and Y.-L. Loo, "Improving the electrical conductivity of polymer acid-doped polyaniline by controlling the template molecular weight," *Journal of Materials Chemistry*, vol. 17, no. 13, pp. 1268–1275, 2007.

[135] E. Song and J.-W. Choi, "Self-calibration of a polyaniline nanowire-based chemiresistive pH sensor," *Microelectronic Engineering*, vol. 116, pp. 26–32, Mar. 2014.

[136] K. M. Kost, D. E. Bartak, B. Kazee, and T. Kuwana, "Electrodeposition of platinum microparticles into polyaniline films with electrocatalytic applications," *Anal. Chem.*, vol. 60, no. 21, pp. 2379–2384, Nov. 1988.

[137] E. Song and J.-W. Choi, “A selective hydrogen peroxide sensor based on chemiresistive polyaniline nanowires modified with silver catalytic nanoparticles,” *Journal of Micromechanics and Microengineering*, vol. 24, no. 6, 065004, 2014.

[138] W. Chen, S. Cai, Q.-Q. Ren, W. Wen, and Y.-D. Zhao, “Recent advances in electrochemical sensing for hydrogen peroxide: a review,” *The Analyst*, vol. 137, no. 1, p. 49, 2012.

[139] C. M. Welch, C. E. Banks, A. O. Simm, and R. G. Compton, “Silver nanoparticle assemblies supported on glassy-carbon electrodes for the electro-analytical detection of hydrogen peroxide,” *Anal Bioanal Chem*, vol. 382, no. 1, pp. 12–21, May 2005.

[140] W. Zhao, H. Wang, X. Qin, X. Wang, Z. Zhao, Z. Miao, L. Chen, M. Shan, Y. Fang, and Q. Chen, “A novel nonenzymatic hydrogen peroxide sensor based on multi-wall carbon nanotube/silver nanoparticle nanohybrids modified gold electrode,” *Talanta*, vol. 80, no. 2, pp. 1029–1033, Dec. 2009.

[141] M. Kanungo, A. Kumar, and A. Q. Contractor, “Microtubule sensors and sensor array based on polyaniline synthesized in the presence of poly(styrene sulfonate),” *Anal. Chem.*, vol. 75, no. 21, pp. 5673–5679, Nov. 2003.

[142] R. D. Deegan, O. Bakajin, T. F. Dupont, G. Huber, S. R. Nagel, and T. A. Witten, “Capillary flow as the cause of ring stains from dried liquid drops,” *Nature*, vol. 389, no. 6653, pp. 827–829, Oct. 1997.

[143] K. J. Albert, N. S. Lewis, C. L. Schauer, G. A. Sotzing, S. E. Stitzel, T. P. Vaid, and D. R. Walt, “Cross-Reactive Chemical Sensor Arrays,” *Chem. Rev.*, vol. 100, no. 7, pp. 2595–2626, Jul. 2000.

[144] S. Stewart, M. A. Ivy, and E. V. Anslyn, “The use of principal component analysis and discriminant analysis in differential sensing routines,” *Chemical Society Reviews*, vol. 43, no. 1, p. 70, 2014.

[145] P. Anzenbacher, Jr., P. Lubal, P. Buček, M. A. Palacios, and M. E. Kozelkova, “A practical approach to optical cross-reactive sensor arrays,” *Chemical Society Reviews*, vol. 39, no. 10, p. 3954, 2010.

[146] A. T. Wright and E. V. Anslyn, “Differential receptor arrays and assays for solution-based molecular recognition,” *Chemical Society Reviews*, vol. 35, no. 1, p. 14, 2006.

[147] Y. Wu, N. Na, S. Zhang, X. Wang, D. Liu, and X. Zhang, “Discrimination and Identification of Flavors with Catalytic Nanomaterial-Based Optical Chemosensor Array,” *Anal. Chem.*, vol. 81, no. 3, pp. 961–966, Feb. 2009.

[148] X. Wang, Na, S. Zhang, Y. Wu, and X. Zhang, “Rapid Screening of Gold Catalysts by Chemiluminescence-Based Array Imaging,” *J. Am. Chem. Soc.*, vol. 129, no. 19, pp. 6062–6063, May 2007.

[149] M. S. Freund and N. S. Lewis, “A chemically diverse conducting polymer-based ‘electronic nose’.,” *PNAS*, vol. 92, no. 7, pp. 2652–2656, Mar. 1995.

[150] W.-D. Zhang, J. Chen, L.-C. Jiang, Y.-X. Yu, and J.-Q. Zhang, “A highly sensitive nonenzymatic glucose sensor based on NiO-modified multi-walled carbon nanotubes,” *Microchim Acta*, vol. 168, no. 3–4, pp. 259–265, Mar. 2010.

[151] L.-C. Jiang and W.-D. Zhang, “A highly sensitive nonenzymatic glucose sensor based on CuO nanoparticles-modified carbon nanotube electrode,” *Biosensors and Bioelectronics*, vol. 25, no. 6, pp. 1402–1407, Feb. 2010.

[152] Z. Zhuang, X. Su, H. Yuan, Q. Sun, D. Xiao, and M. M. F. Choi, “An improved sensitivity non-enzymatic glucose sensor based on a CuO nanowire modified Cu electrode,” *The Analyst*, vol. 133, no. 1, p. 126, 2008.

[153] R. P. Kalakodimi and M. Nookala, “Electrooxidation of Ascorbic Acid on a Polyaniline-Deposited Nickel Electrode: Surface Modification of a Non-Platinum Metal for an Electrooxidative Analysis,” *Anal. Chem.*, vol. 74, no. 21, pp. 5531–5537, Nov. 2002.

[154] X.-L. Luo, J.-J. Xu, W. Zhao, and H.-Y. Chen, “Ascorbic acid sensor based on ion-sensitive field-effect transistor modified with MnO2 nanoparticles,” *Analytica Chimica Acta*, vol. 512, no. 1, pp. 57–61, Jun. 2004.

[155] J. Tashkhourian, M. R. H. Nezhad, J. Khodavesi, and S. Javadi, “Silver nanoparticles modified carbon nanotube paste electrode for simultaneous determination of dopamine and ascorbic acid,” *Journal of Electroanalytical Chemistry*, vol. 633, no. 1, pp. 85–91, Aug. 2009.

[156] J. M. May, Z. Qu, and R. R. Whitesell, “Ascorbic Acid Recycling Enhances the Antioxidant Reserve of Human Erythrocytes,” *Biochemistry*, vol. 34, no. 39, pp. 12721–12728, Oct. 1995.

[157] E. Núñez-Delicado, A. Sánchez-Ferrer, and F. García-Carmona, “Cyclodextrins as Secondary Antioxidants: Synergism with Ascorbic Acid,” *J. Agric. Food Chem.*, vol. 45, no. 8, pp. 2830–2835, Aug. 1997.

[158] S. Mu and J. Kan, “The electrocatalytic oxidation of ascorbic acid on polyaniline film synthesized in the presence of ferrocenesulfonic acid,” *Synthetic Metals*, vol. 132, no. 1, pp. 29–33, Dec. 2002.

[159] A. S. Adekunle, B. O. Agboola, J. Pillay, and K. I. Ozoemena, “Electrocatalytic detection of dopamine at single-walled carbon nanotubes–iron (III) oxide nanoparticles platform,” *Sensors and Actuators B: Chemical*, vol. 148, no. 1, pp. 93–102, Jun. 2010.

[160] S. R. Ali, Y. Ma, R. R. Parajuli, Y. Balogun, W. Y.-C. Lai, and H. He, “A Nonoxidative Sensor Based on a Self-Doped Polyaniline/Carbon Nanotube Composite for Sensitive and Selective Detection of the Neurotransmitter Dopamine,” *Anal. Chem.*, vol. 79, no. 6, pp. 2583–2587, Mar. 2007.

[161] M. C. Janzen, J. B. Ponder, D. P. Bailey, C. K. Ingison, and K. S. Suslick, “Colorimetric Sensor Arrays for Volatile Organic Compounds,” *Anal. Chem.*, vol. 78, no. 11, pp. 3591–3600, Jun. 2006.

[162] B. Li, J. Liu, G. Shi, and J. Liu, “A research on detection and identification of volatile organic compounds utilizing cataluminescence-based sensor array,” *Sensors and Actuators B: Chemical*, vol. 177, pp. 1167–1172, Feb. 2013.

[163] L. G. Dias, A. M. Peres, T. P. Barcelos, J. Sá Morais, and A. A. S. C. Machado, “Semi-quantitative and quantitative analysis of soft drinks using an electronic tongue,” *Sensors and Actuators B: Chemical*, vol. 154, no. 2, pp. 111–118, Jun. 2011.

[164] X. Cetó, J. M. Gutiérrez, L. Moreno-Barón, S. Alegret, and M. del Valle, “Voltammetric Electronic Tongue in the Analysis of Cava Wines,” *Electroanalysis*, vol. 23, no. 1, pp. 72–78, Jan. 2011.

[165] W. P. Gardiner, *Statistical Analysis Methods for Chemists: A Software-based Approach*. Royal Society of Chemistry, 1997.

[166] A. K. Srivastava, “Detection of volatile organic compounds (VOCs) using SnO2 gas-sensor array and artificial neural network,” *Sensors and Actuators B: Chemical*, vol. 96, no. 1–2, pp. 24–37, Nov. 2003.

[167] H.-K. Hong, H. W. Shin, H. S. Park, D. H. Yun, C. H. Kwon, K. Lee, S.-T. Kim, and T. Moriizumi, “Gas identification using micro gas sensor array and neural-network pattern recognition,” *Sensors and Actuators B: Chemical*, vol. 33, no. 1–3, pp. 68–71, Jul. 1996.

[168] P. C. Jurs, G. A. Bakken, and H. E. McClelland, “Computational Methods for the Analysis of Chemical Sensor Array Data from Volatile Analytes,” *Chem. Rev.*, vol. 100, no. 7, pp. 2649–2678, Jul. 2000.

# Appendix A: Principal Component Analysis

## A.1. Introduction

The objective of this appendix is to provide more in-depth theory behind the Principal Component Analysis (PCA) technique from both a mathematical as well as a graphical perspective. The description of PCA in this appendix is based on [1] and [2].

## A.2. Mathematical Background

In mathematical terms, PCA is defined as an orthogonal linear transformation that maps the raw data to a new coordinate system such that the greatest variance by the projection of that data lies along the first coordinate, called the first principal component. The second largest variance is defined along the second coordinate and the process continues until all the principal components are defined in a given dimension. Therefore the main goal of the PCA algorithm is to determine the linear transformation, or the mapping, that achieves this requirement in terms of the directionality of the variances.

First, let's consider two $m \times n$ matrices $\mathbf{X}$ and $\mathbf{Y}$ related by a linear transformation $\mathbf{P}$.

$$\mathbf{PX} = \mathbf{Y}$$

$\mathbf{X}$ is the original data set obtained from $n$ number of observations (i.e. number of sensors in the array) and $m$ number of samples (i.e. number of measurements). $\mathbf{Y}$ is the representation of $\mathbf{X}$ in the new coordinate system. We wish to develop a transformation matrix $\mathbf{P}$ such that the individual variables of $\mathbf{Y}$ inherit the maximum possible variance from $\mathbf{X}$.

In order to maximize the variance in the data set during the coordinate transformation process, a covariance matrix is needed. A covariance matrix $\mathbf{S_X}$ is defined by the following:

$$\boldsymbol{S_X} \equiv \frac{1}{n-1}\boldsymbol{XX}^T$$

There are a few important properties about the covariance matrix:

1. $\mathbf{S_X}$ is a square symmetric $m \times m$ matrix.
2. The diagonal terms of $\mathbf{S_X}$ are the variance of the particular measurement variables (e.g., sensing element in an array).
3. The off-diagonal terms of $\mathbf{S_X}$ are the covariance between measurement variables.

In order to minimize redundancy in the dataset, we would like each variable to have as little correlation as possible with other variables. In other words, the covariance between two separate variables must be zero. Therefore, if the redundancy is to be minimized, it is required that the off-diagonal terms of the covariance matrix be zero. Here we re-iterate the objective of the PCA algorithm: find a transformation matrix $\mathbf{P}$ with $\mathbf{PX} = \mathbf{Y}$ such that $\mathbf{S_Y}$ is diagonalized. Then the rows of $\mathbf{P}$ are the principal components of $\mathbf{X}$. $\mathbf{S_Y}$ can be re-written in terms of the matrix $\mathbf{P}$:

$$\boldsymbol{S_Y} = \frac{1}{n-1}\boldsymbol{YY}^T = \frac{1}{n-1}(\boldsymbol{PX})(\boldsymbol{PX})^T = \frac{1}{n-1}\boldsymbol{PXX}^T\boldsymbol{P}^T = \frac{1}{n-1}\boldsymbol{P}(\boldsymbol{XX}^T)\boldsymbol{P}^T$$

Note that matrix $\mathbf{XX}^T$ is a symmetric matrix. It is also well known that a symmetric matrix can be diagonalized by an orthogonal matrix consisting of its eigenvectors.

$$\boldsymbol{XX}^T = \boldsymbol{EDE}^T$$

where $\mathbf{D}$ is a diagonal matrix with the eigenvalues along the diagonals, and $\mathbf{E}$ is a matrix with each column being the eigenvectors. Here, we choose the matrix $\mathbf{P}$ such that each row of $\mathbf{P}$ is an eigenvector of $\mathbf{XX}^T$. Therefore we define $\mathbf{P} \equiv \mathbf{E}^T$.

$$\boldsymbol{XX^T = P^T DP}$$

Therefore substituting the above relation into the equation for the covariance matrix $\mathbf{S_Y}$, we obtain the following:

$$\boldsymbol{S_Y = \frac{1}{n-1} P(XX^T)P^T = \frac{1}{n-1} P(P^T DP)P^T = \frac{1}{n-1} PP^{-1}DPP^{-1} = \frac{1}{n-1} D}$$

Note that $\mathbf{PP^{-1} = I}$ when **P** is an orthonormal matrix. Therefore, by choosing the appropriate orthonormal matrix **P**, The covariance matrix $\mathbf{S_Y}$ can be diagonalized. The following summarizes the key results from this derivation:

1. The principal components of the data matrix **X** are the eigenvectors of $\mathbf{XX}^T$ or the rows of the transformation matrix **P**.
2. The variance of the data **X** along the $i^{th}$ principal component is given by the $i^{th}$ diagonal entry of the covariance matrix $\mathbf{S_Y}$.

### A.3. Graphical Representation

In this section, a graphical description is given to provide an intuitive illustration of the PCA technique. Although the figures are drawn in a 3 dimensional space, it can be assumed that the dimension of the data space is arbitrary.

Consider a set of data points in an *m* dimensional space as shown in Figure A.1. Defining the first principal component: (a) the data obtained from the measurements is plotted on an arbitrary dimensional space, and (b) the first principal component vector is defined in a direction of maximum variance.Figure A.1(a). The PCA algorithm defines the first principal component ($PC_1$) in a direction that maximizes the variance of the data points as depicted in Figure A.1(b). Therefore $PC_1$ contains the most information about the distribution of the data set.

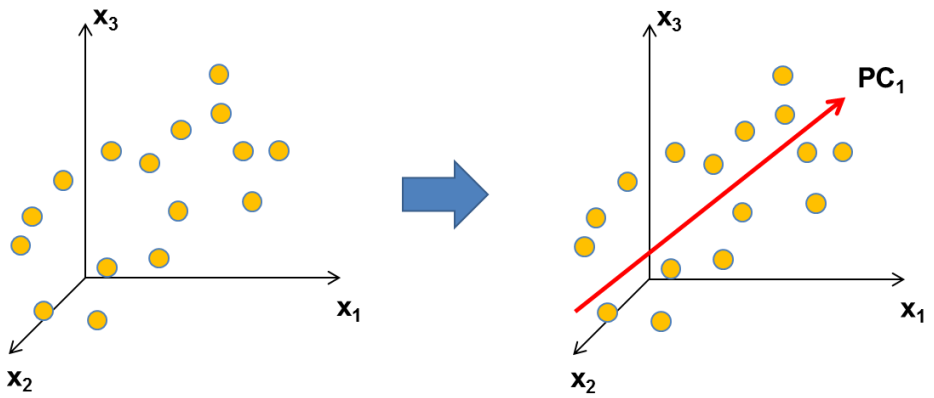


(a) (b)

Figure A.1. Defining the first principal component: (a) the data obtained from the measurements is plotted on an arbitrary dimensional space, and (b) the first principal component vector is defined in a direction of maximum variance.

Since all the principal component vectors are defined to be mutually orthogonal, $PC_2$ is aligned in a direction perpendicular to $PC_1$ while maximizing the variance of the data given the restriction on the directionality. This idea is illustrated in Figure A.2.

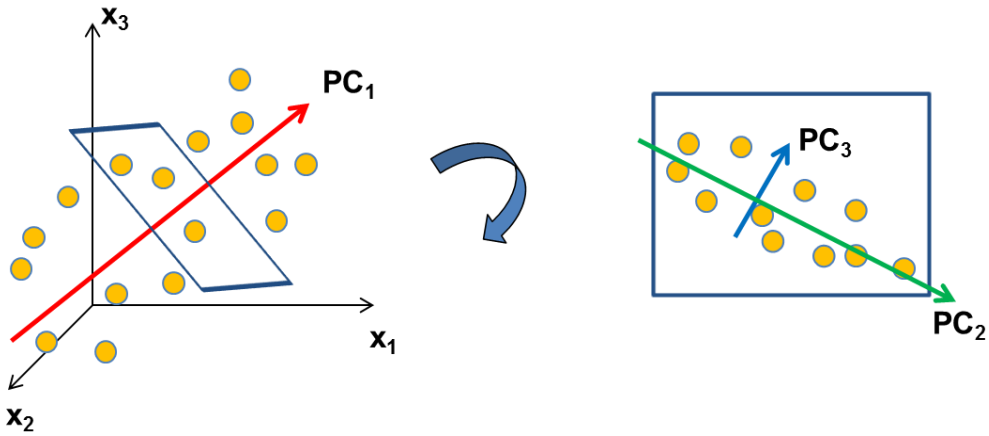


(a) (b)

Figure A.2. Defining the second and the third principal component vectors: (a) all the data points are projected on to a plane that is perpendicular to $PC_1$, (b) $PC_2$ is defined on the plane in the direction of maximum variance. $PC_3$ is fined such that it is perpendicular to both $PC_1$ and $PC_2$.

Imagine a plane that is perpendicular to $PC_1$, shown as a blue window in Figure A.2(a). Looking directly into the plane along the direction of $PC_1$, the data points may appear similar to that shown in Figure A.2(b). Another way to visualize this is to project all data points onto the imaginary plane that is perpendicular to $PC_1$. Now, $PC_2$ can be defined on this plane while aligning itself in a direction of maximum variance. Finally, $PC_3$ is defined in a direction perpendicular to both $PC_2$ and $PC_1$. For an arbitrary n dimensional space, this process of defining the principal components can be repeated n times until all the PC base vectors ($PC_1$ to $PC_n$) are defined. One important point to note is that the PCs are arranged in the following order:

$$\mathrm{Var}(PC_1) > \mathrm{Var}(PC_2) > \ldots > \mathrm{Var}(PC_n)$$

Therefore the first few PC vectors contain the majority of the information about the distribution of the sample data and by using the reduced number of PC, for example $PC_1$ and $PC_2$, the data points can be adequately described without much loss of information.

## A.4. References


[1] J. Shlens, "A tutorial on principal component analysis: derivation, discussion and singular value decomposition," 2005 (unpublished work).

[2] S. Stewart, M. A. Ivy, and E. V. Anslyn, "The use of principal component analysis and discriminant analysis in differential sensing routines," Chemical Society Reviews, vol. 43, no. 1, p. 70, 2014.

# Appendix B: List of Publications

Journal Publications

**E. Song** and J.-W. Choi, "A catalyst-based chemiresistive sensor array for multi-analyte detection," (in preparation).

**E. Song**, R. P. Tortorich, and J.-W. Choi, "Inkjet-printed polyaniline nanowire network patterns for sensing applications," (in preparation).

**E. Song** and J.-W. Choi, "A selective hydrogen peroxide sensor based on chemiresistive polyaniline nanowires modified with silver catalytic nanoparticles," *Journal of Micromechanics and Microengineering*, vol. 24, no. 6, 065004, 2014.

R. Tortorich, **E. Song**, and J.-W. Choi, "Inkjet-printed carbon nanotube electrodes with low sheet resistance for electrochemical sensor applications," *Journal of the Electrochemical Society*, vol. 161, no. 2, B3044-B3048, 2014.

**E. Song** and J.-W. Choi, "Self-calibration of a polyaniline nanowire-based chemiresistive pH sensor," *Microelectronic Engineering*, vol. 116, pp. 26-32, 2014.

**E. Song** and J.-W. Choi, "Conducting polyaniline nanowire and its applications in chemiresistive sensing," *Nanomaterials*, vol. 3, pp. 498-523, 2013.

Conference Proceedings

Y. Hu, S. Chen, L. Peng, **E. Song**, and J.-W. Choi, "Effective thermal control techniques for liquid-cooled 3d multi-core processors," in *Proceedings of the International Symposium on Quality Electronic Design (ISQED)*, Santa Clara, CA, March 4-6, 2013, pp. 8-15.

**E. Song** and J.-W. Choi, "An on-chip chemiresistive polyaniline nanowire-based pH sensor with self-calibration capability," in *Proceedings of the 34th Annual International Conferences of the IEEE Engineering in Medicine & Biology Society (IEEE EMBC 2012)*, San Diego, CA, August 28 – September 1, 2012, pp. 4018-4021.

**E. Song** and J.-W. Choi, "A patterned conducting polyaniline layer on a non-conducting polymer matrix," in *Materials Research Society (MRS) Symposium Proceedings*, vol. 1312, 2011, pp. 99-103.

Conference Abstracts

**E. Song** and J.-W. Choi, "A conducting polymer nanowire-based sensor array for simultaneous multi-analyte detection," *The 40th Micro and Nano Engineering (MNE)*, Lausanne, Switzerland, September 22 – 26, 2014 (submitted).

**E. Song**, R. P. Tortorich, and J.-W. Choi, "Inkjet Printed Conducting Polymer Nanowires for Flexible Electronics and Sensors," *The 40th Micro and Nano Engineering (MNE)*, Lausanne, Switzerland, September 22 – 26, 2014 (submitted).

**E. Song**, R. P. Tortorich, and J.-W. Choi, "Printing conductive polymer nanowire network and its application in chemical sensing," *The 18th International Conference on Miniaturized Systems for Chemistry and Life Sciences (μTAS)*, San Antonio, TX, October 26 – 30, 2014 (submitted).

R. P. Tortorich, **E. Song**, and J.-W. Choi, "A fully inkjet-printed carbon nanotube electrochemical sensor on paper," *The 18th International Conference on Miniaturized Systems for Chemistry and Life Sciences (μTAS)*, San Antonio, TX, October 26 – 30, 2014 (submitted).

R. P. Tortorich, T. H. da Costa, **E. Song**, and J.-W. Choi, "A printed carbon nanotube sensor on a flexible substrate," *The 226th ECS Meeting*, Cancun, Mexico, October 5-10, 2014 (submitted).

R. P. Tortorich, **E. Song**, and J.-W. Choi, "Inkjet-printed carbon nanotube electrodes for electrochemical sensor applications," *The 224th Electrochemical Society Meeting*, San Francisco, CA, October 27 – November 1, 2013.

**E. Song** and J.-W. Choi, "A polyaniline nanowire network with catalytic nanoparticles for chemical sensing," *The 224th Electrochemical Society Meeting*, San Francisco, CA, October 27 – November 1, 2013.

J.-W. Choi and **E. Song**, "A self-calibrating polymer nanowire-based chemical sensor," *2012 Nanotechnology for Defense Conference (NT4D 2012)*, Summerlin, NV, August 6-9, 2012.

**E. Song** and J.-W. Choi, "pH responsive polyaniline nanowires and its sensitivity on electrochemical potentials," *2012 International Conference on Electronics, Information and Communication (ICEIC 2012)*, Jeongseon, Korea, February 1-3, 2012.

# Vita

Edward Song was born in Edmonton, Alberta, Canada in 1981. He graduated from Henry Wise Wood High School in Calgary, Alberta, in 2000. He received a Bachelor of Science degree in Mathematics and Engineering at Queen's University in Kingston, Ontario, Canada in 2004, and received a Master of Science degree in Electrical and Computer Engineering at University of Alberta in Edmonton in 2007. In August 2007, he began pursuing his doctoral program in Electrical Engineering with a minor in Mechanical Engineering at Louisiana State University. In May 2014, he successfully defended his doctoral thesis. His current research interest include nanowire-based sensors, bioMEMS, Lab-on-a-chip, inkjet printing of nanomaterials, and microcarrier-based cell culturing systems.